KTH Electrical Engineering

Methods for Synchrophasor-Based Power System Instability Detection and HVDC Control

RUJIROJ LEELARUJI

Doctoral Thesis
Royal Institute of Technology
School of Electrical Engineering
Electric Power Systems
Stockholm, Sweden, 2012

School of Electrical Engineering
Electric Power Systems
Royal Institute of Technology
SE-100 44 Stockholm
Sweden

TRITA-EE 2012:49
ISSN 1653-5146
ISBN 978-91-7501-542-2

Akademisk avhandling som med tillstånd av Kungl Tekniska högskolan framlägges till offentlig granskning för avläggande av teknologie doktorsexamen i elektrotekniska system fredagen den 7 december 2012 kl 10.00 i E2, Kungl Tekniska Högskolan, Stockholm.

Tryck: Universitetsservice US-AB

Abstract

The recent availability Phasor Measurement Unit (PMU) functionalities in relay technology has opened up new opportunities for power system protection, allowing this microprocessor-based technology to be used beyond traditional protection purposes. This technology now also considers the computation and communication mechanisms that allow the transmission of synchronized phasor measurements. This makes possible the use of these features in protection applications. As a result, Wide-Area Monitoring, Protection and Control (WAMPAC) systems can expand by using protective relays built with synchrophasor capabilities which may facilitate many applications such as the synchronization distributed generation to large power grids or for the integration of renewable sources of energy.

This thesis rationalizes the need of coordination between protective relays with synchrophasor capabilities and High Voltage Direct Current (HVDC) controls to steer power systems away from instability conditions. The concept of coordination involves the use of feasible communication mechanisms which can be exploited by protection systems to send out synchornized voltage and current phasors to a mechanism which determines preventive, corrective, and protective actions particularly by taking advantage of the availability of HVDCs. Coordination refers to the ability of the protective systems and HVDCs to cooperate and to harmonize their actions so that voltage instability can be avoided. Synchrophasor processing capabilities allow for the exploitation of phasor measurements while satisfying protective relaying requirements.

The author addresses the challenge of mitigation of voltage instability through two sequential approaches. First, voltage sensitivities computed from synchrophasor data can be used for voltage stability monitoring and can be exploited for delivering wide-area early action signals. These signals can be used for activating controllable devices such as HVDCs which may also exploit phasor measurements for control. In order to provide reliable information, synchrophasor data must be pre-processed to extract only the useful features embedded in the measurements and to correct for errors. The methodology is derived by considering both positive-sequence simulations for methodology development purposes, and *real* phasor measurement data from a real-time (RT) hardware-in-the-loop (HIL) laboratory. The use of the RT-HIL laboratory allows to test the robustness of the developed approach in a more realistic environment, this will guarantee its performance for use in control rooms. The methodology has also been tested with *real* PMU data obtained from the Norwegian transmission system showing the validity and applicability

of the method.

The wide-area early action signals derived from the method are then used for voltage stability mitigation through HVDC control. The signals are used to trigger the operation of HVDCs or to change their control modes before they reach stringent operating conditions. In addition, synchrophasors are also exploited as feedback signals feeding supplementary stability controls. The proper selection of signals and activation of these special HVDC control is investigated.

The second approach is used to ensure that HVDCs will operate securely when their transfer is pushed towards the maximum transferable power level. It is shown that Classical HVDCs are prone to voltage instability when operating on weak AC grids. To cope with this delicate operation scenarios, the Automatic Voltage Stabilizer (AVS) and Automatic Power Order Reduction (APOR) controls are implemented for HVDC control to cope with these undesired conditions. The implementation is carried out both in off-line and real-time simulation environments.

Keywords. Wide-Area Monitoring Protection and Control Systems, Synchrophasor applications, Wide-Area Voltage Instability Detection, Wide-Area Early Warning Systems, Automatic Voltage Stabilizer.

Contents

Chapter 1

Introduction

1.1 Background and motivation

In the Nordic region, as well as the rest of Europe, there are plans for a large-scale integration of renewable energy sources into power systems, in order to replace old power plants (not CO2 emission free) and to meet increased energy demand in the years to come. Many of the new production sites are far away from the load-centers, which requires investments in new overhead lines and a significant extension of the existing main grid. A good example of the required installation of transmission lines is the "Three Gorges Dam" [1] hydro power plant in China which transmit power across the country.

On the other hand, relevant generation potential may be located close to large industrial loads or industrial parks, such as is the case in the Norwegian Grid. Proper management of these generation sources together with large industrial loads may facilitate a quicker integration of renewable sources and aid in coping with a decreasing security of supply. As an example, note that there are large amounts of renewable energy in the form of small hydro and wind generation in the Nordic Region, with a large untapped potential in Northern Norway [2]. At the same time, Northern Norway also is home to large industrial parks such as the Snøhvit Liquefied Natural Gas (LNG) project [3] at Hammerfest, where there are challenges for guaranteeing security of supply. A proper interaction of local and untapped generation resources may aid in increasing the reliability in this case. This might be possible to achieve in the short term as Statnett plans to bring these generation sources closer to these large industrial loads. Statnett's Grid Development Plan 2008-2025 proposed the installation of new stations and transformers to receive new wind and small-scale hydro power and new 420 kV lines that will increase the capacity in North Norway interconnecting Hammerfest with Balsfjord. These extensions will increase the capacity of the main grid, and will meet the requirements for integration of renewable energy and the increased load.

From an energy-relevance perspective, the current power transfer pattern depends on seasonal changes. This will be shifted due to "price differences" resulting from the integration of renewable energy, as shown in Fig. 1.1. This requires a larger focus on

operational planning and actual on-line operation. The uncertainty brought by these energy sources creates an increased need for balancing of production and demand, and drastically changes the power system dynamics hence requiring more real-time monitoring, control, and protection.

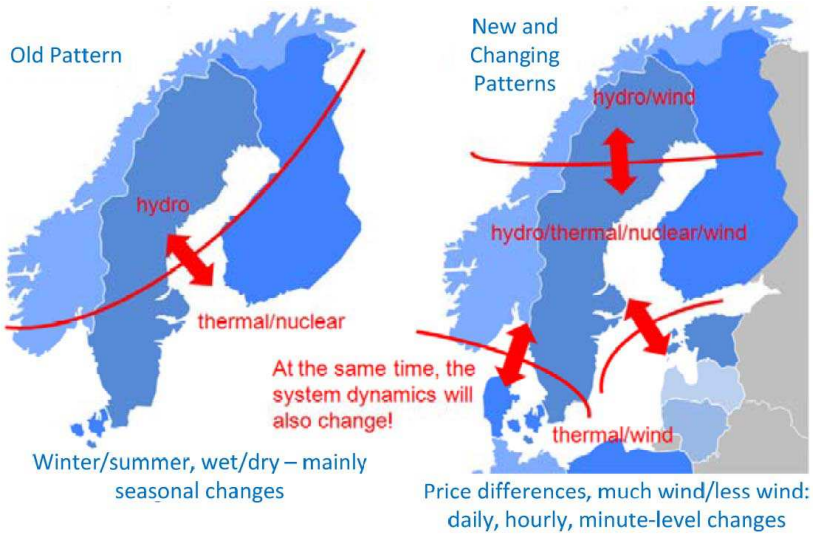

Figure 1.1: New and changing power transfer patterns in the Nordic Grid

To establish adequate monitoring systems, one potential approach is to develop wide-area monitoring systems (WAMS) [4, 5] or wide-area monitoring, protection and control systems (WAMPAC) [6] by using synchronized phasor measurements (PMUs). In order to implement such systems, synchronized phasor measurement may serve as an effective data source from which critical information about the system's condition can be extracted. Synchronized phasor measurement capabilities are now one of the features available in the most advanced protective relays commercially available, and the use of this feature is proliferating. In addition, these capabilities can also be utilized to complement the conventional (local and zonal) protection strategies which results to the improvement in wide protection and control. Indeed, early applications of this technology for the synchronization of distributed generation to large power grids [7] and for islanding management [8] show a promising opportunity for the use of this technology in combination of traditional protective devices for the integration of distributed renewable sources of energy [9, 10].

Simultaneously, the application of controllable devices to reinforce the transmission network and to increase transmission power flow control capability has been proposed. For instance, coordination of several controllable devices for stability enhancement as proposed either for FACTS devices [11–13]. The technological advances in Voltage Source Converters-based High Voltage Direct Current (VSC-HVDC) have allowed to prove this

technology's advantages for control, such as the ability to independently control active and reactive power [14] and voltage control. These controllable devices can improve the performance and reliability of power systems. Some applications which combines the WAMS and control of VSC-HVDC have been implemented, for instance WAMS with embedded VSC-HVDC control for oscillation damping [15]. This implies that controllable devices with properly designed controls exploiting synchrophasor data from protection systems can substantially enhance stability of power systems.

1.2 Objectives

Within the framework of blending PMU-based WAMS and utilizing existing controllable devices mentioned earlier, the main theme of this work is the development of methods that use synchrophasor measurements to determine detective and defensive actions that can aid in mitigating voltage instability. The detective actions should aid in performing a system wide stability assessment while the defensive actions exploit the presence of controllable devices to relief stressed conditions, consequently system voltage collapse can be avoided. Moreover, the proposed methods must secure the operation controllable devices in all operating conditions. The ultimate goal of the project is to assure that the developed methods are suitable for their adoption in the control room, thus it should not only simple to comprehend but also consider some practical issues regarding real-time performance. Therefore, real-time hardware-in-the loop simulations using physical protective devices with PMU capabilities are carried out to validate the methods.

The objectives of this thesis are the following:

1. To give readers a comprehensive overview of the state-of-the-art in implementation of protective functions and synchrophasor capabilities available in today's relays.
2. To give a comprehensive and detailed overview of the communication mechanisms used for power system relaying and synchrophasor data transfer.
3. To identify the importance of modeling details of each power system component which will be used as a basis prior to any proposed methodology.
4. To develop a synchrophasor-based voltage stability monitoring method.
5. To develop and demonstrate wide-area voltage stability monitoring tools with displays that are simple to comprehend.
6. To develop methods for utilizing sensitivities to adapt HVDC control modes for mitigating voltage instability.
7. To investigate the use of synchrophasor measurements as HVDC controller input signals for stabilizing controls.
8. Development of additional controller on HVDCs to steer away from voltage and angle instabilities.

Therefore with the above objectives, this thesis content is organized as shown in the following flowchart:

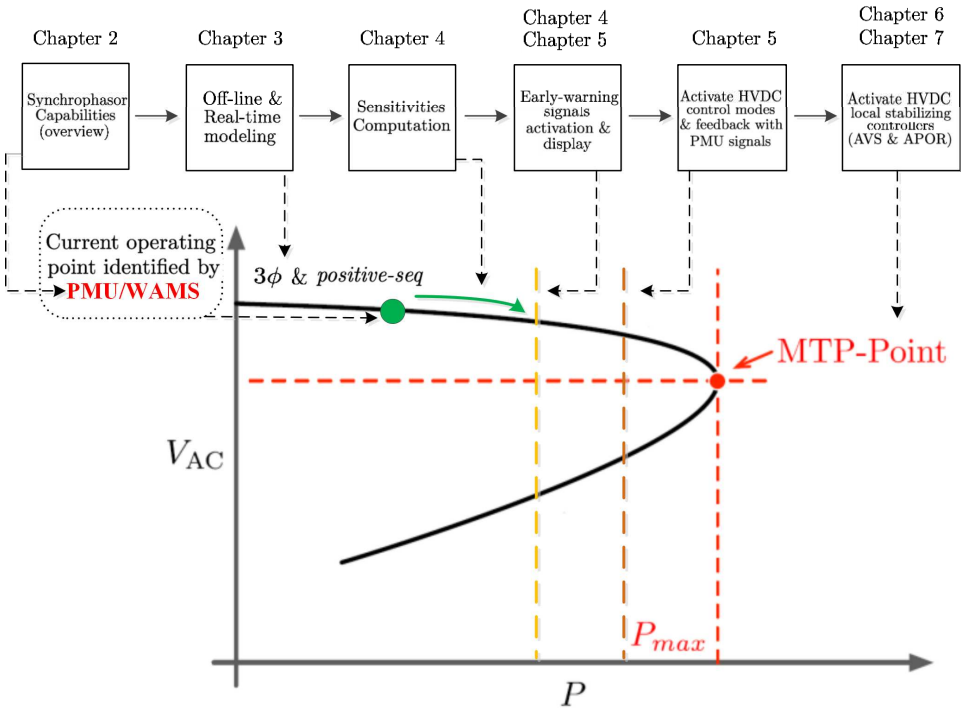

Figure 1.2: Thesis Content

1.3 Outline of the Thesis

The thesis is organized in eight chapters:

Chapter 2 presents an overview of state-of-the-art in the industrial implementation of protective relay functions, communication mechanism and synchronized phasor capabilities for electric power systems monitoring, control, and protection.

Chapter 3 describes experimental and simulation set-ups that were used for the development of the methodologies presented in this thesis.

Chapter 4 elaborates on the first approach to mitigate voltage instability. This approach utilizes sensitivities computed from synchronized phasor measurement data in wide-area early warning systems. Then these sensitivities are used to derive control signals for the activation of HVDCs, and synchrophasors are used as input signals for stabilizing controls so that voltage instability can be avoided.

Chapter 5 presents examples of how voltage sensitivities can be used to detect voltage instability and a visualization approach is also given. Then, results of voltage instability mitigation by coordinating the use of synchrophasor-based sensitivities and VSC-HVDC controls is illustrated.

Chapter 6 presents the implementation of the Automatic Voltage Stabilizer (AVS) and Automatic Power Order Reduction (APOR) controls which form the basis for the second approach used to prevent instabilities on HVDCs when they operate under stringent operating conditions.

Chapter 7 presents examples of how the AVS and APOR can prevent voltage and angle instabilities suffered by HVDC transmission.

Chapter 8 summarizes the results of this project and suggests some possible extensions based on the present work.

1.4 Main contributions

The main contributions of the thesis are:

- **An overview of state-of-the-art in industrial power systems protection and its synchrophasor capabilities.** Protective relaying and its associated communications technology used in today's power transmission systems has been reviewed. The capabilities of these devices are highlighted to show the possibility of going beyond their traditional application, especially with the provision of synchrophasor capabilities. This part can be found in Chapter 2.

- **Modeling of a test system for methodology development.** Accurate modeling of integral power systems is essential for studying instabilities. This thesis provides theoretical explanations and implementation in different simulators in order to identify specific modeling needs for generating instabilities in power system simulations. This part can be found in Chapter 3.

- **Voltage Stability Monitoring, Visualization, and Instability Mitigation.** A methodology to use voltage sensitivities computed from synchrophasor data for voltage stability monitoring, and a visualization approach that can be implemented in wide-area early warning systems is proposed. Then, an approach for utilizing an early warning signal to activate HVDCs so that voltage instability can be avoided. This includes the use of PMU measurements as input signals to the HVDC controllers. This part can be found in Chapter 4.

- **Controllable power transmission methods.** Control methods to ensure that HVDCs will operate securely when their transfer is pushed towards the maximum transferable power level are introduced. These methods are also validated in a real-time platform. This part can be found in Chapter 6

1.5 List of Publications

The following articles were published during the project:

- R. Leelaruji and L. Vanfretti, "Utilizing the Synchrophasor-based Protection Systems with VSC-HVDC to mitigate Voltage Instability", *Power System Technology International Conference (POWERCON)*, Auckland, New Zealand, November 2012.
- R. Leelaruji, L. Vanfretti, K. Uhlen, and J. O. Gjerde, "Computing Sensitivities from Synchrophasor Data for Voltage Stability Monitoring and Visualization", *Submitted to European Transactions on electrical power*, 2012.
- M.S. Almas, R. Leelaruji, and L. Vanfretti, "Over-Current Relay Model Implementation for Real-Time Simulation and Hardware-in-the-Loop Validation", **Invited Paper**, IEEE IECON, Montréal, Canada, October 2012.
- K. Weyrich, R. Leelaruji, W. Kühn, and L. Vanfretti, "Real-Time Implementation of an Automatic Voltage Stabilizer for HVDC Control", *IEEE PES Innovative Smart Grid Technologies (ISGT) Europe Conference*, Berlin, Germany, October 2012.
- R. Leelaruji and L. Vanfretti, "State-of-the-Art in the Industrial Implementation of Protective Relay Functions, Communication Mechanisms and Synchronized Phasor Capabilities for Electric Power Systems Protection", Elsevier, *Journal in Renewable and Sustainable Energy*, Volume 16, September 2012, page 4385–4395.
- R. Leelaruji and L. Vanfretti, "Power System Protective Relaying: Basic Concepts, Industrial-Grade Devices, and Communication Mechanisms", **Book Chapter** in *Standard Handbook for Electrical Engineers*, 16th Edition, 2012
- R. Leelaruji, L. Vanfretti, and M.S. Almas, "Voltage Stability Monitoring using Sensitivities Computed from Synchronized Phasor Measurement Data", **Invited Paper**, *IEEE PES General Meeting*, San Diego, CA, USA, July 2012.
- L. Vanfretti, M. Chenine, M.S. Almas, R. Leelaruji, and L. Nordström, "SmarTS Lab: A Laboratory for Developing Applications for WAMPAC Systems", *IEEE PES General Meeting*, San Diego, CA, USA, July 2012.
- A. Al-Hammouri, L. Nordström, M. Chenine, L. Vanfretti, N. Honeth, and R. Leelaruji, "Virtualization of Synchronized Phasor Measurement Units Within Real-Time Simulators for Smart Grid Applications", *IEEE PES General Meeting*, San Diego, CA, USA, July 2012.
- R. Leelaruji and L. Vanfretti, "Detailed modelling, implementation and simulation of an "all-in-one" stability test system including power system protective devices", Elsevier, *Journal in Simulation Modelling Practice and Theory*, Volume 23, April 2012, page 36–59.

- K. Weyrich, R. Leelaruji, W. Kühn, and L. Vanfretti, "Mitigating System's Voltage Instability through Wide-Area Early Warning Signals and Real-Time HVDC Control", **Invited Paper**, *IEEE Workshop on Complexity in Engineering*, Aachen, Germany, April 2012.

- R. Leelaruji and L. Vanfretti, "All-in-one test system modelling and simulation for multiple instability scenarios, *Internal Report*, April 2011. available from: `https://eeweb01.ee.kth.se/upload/publications/reports/2011/Smarts-Lab-2011-002.pdf`.

- R. Leelaruji, L. Vanfretti, M. Ghandhari and L. Söder, "Coordination of Protection system and HVDC link for Mitigating Cascading Failures", *Power System Technology International Conference (POWERCON)*, Hangzhou, China, March 2010.

- R. Leelaruji and V. Knazkins, "The use of voltage stability indices and proposed instability prediction to coordinate with protection systems", *International Conference on Electric Power and Energy Systems Conference*, Tokyo, Japan, May 2009.

- R. Leelaruji and V. Knazkins, "Modeling Adequacy for Cascading Failure Analysis", *Australasian Universities Power Engineering Conference*, Sydney, Australia, December 2008.

Chapter 2

Synchronized Phasor Capabilities in Protective Relays

Protective systems in electricity delivery networks have a major role to play in facilitating the increase of renewable energy, and a broad understanding of their current and future application can aid into better taking them into account for developing future energy networks that adapt for the integration of renewable energy generation sources. This chapter provides a survey in the state of the art of protective relaying, PMU functionalities and associated communications mechanisms used in today's power transmission systems including those used for PMU data transfer. The aim of this chapter is to briefly describe the fundamental knowledge concerned with power system relaying communications and synchrophasor data transmission. The unifying theme is to highlight that the future potential of these devices lies in realizing the possibility of going beyond their traditional application as stand-alone equipments with the single role of acting "the last line of defense", this can be acheived by exploting PMU functionalities and communication mechanisms for PMU data transfer.

2.1 Impact of renewable generation on power system dynamics and stability

The growth of renewable energy integration has increased gradually in the last decade seeking to replace conventional generation methods. The connection between renewable energy sources and main power systems can be categorized into two types; which are remote and local connections. Renewable energy sources that are located far away from the load-centers require an investment in new overhead lines and significant extension of the existing main grid. A good example of the required transmission lines installation is the "Three Gorges dam" hydro power plant in China which transmits power across the country. Recent research has focused on developing concepts for improving grid integration for this type of sources such as wind turbines [16, 17] or photovoltic [18, 19] plants. Meanwhile, the second type of connection is where renewable energy plants are installed locally, al-

lowing local consumers to generate electricity for their own. This type of connection is growing rapidly, especially in distribution networks due to no long-distance transmission requirements. In other words, having renewable sources close to the load location reduces transmission losses and prevents network congestions.

In spite of many economic and technical advantages, high penetration of renewable sources could cause some negative impacts on network operation. That is because the power systems are traditionally designed and operated assuming uni-directional power flow, particularly in distribution network. Once a set of protective devices has been co-ordinated under this paradigm, reversing or allowing multi-directional power flow in some particular operation scenarios, according to the infeed from renewable energy resources, can cause serious protective device maloperations. This problem has occurred in many countries, for example in Germany [20], UK [21], and South Korea [22]. This implies that and increasing amount of renewable energy resources (with intermitted energy production) requires a larger focus on the operational planning and the actual on-line operation of power networks due to: increased need for balancing of production and demand, more adequate monitoring, storage capability, etc. In addition, more challenges brought by the impact of distributed resources on distribution relay protection are summarized by IEEE-Power System Relay Committee, which can be found in [23].

In order to address undesirable consequences (regarding integration of renewable sources) on protection systems, new functions are required in protective relays when compared to traditional devices. As describe in [24] here is where the use of PMU data can have new applications to cope with the challenges listed above. New, PMU data based functions would allow relays to change predefined-settings to ensure that the entire power system is protected at all times. Technical requirements for new protection system paradigms consist of [25] :

- Relays that satisfy the selectivity requirement. This is because the current time-graded protection schemes used at MV and LV networks are inapplicable to handle bidirectional flows.
- Relays which allow using programmable or different tripping characteristics that can be parameterized remotely or locally, either automatically or manually [26].
- Using new/existing communication infrastructures and/or standard communication protocols (for example, IEEE C37.118.2, IEC 61850 or ModBus) that allows individual relays to exchange information (e.g. PMU measurements at different locations) with a control room or among relays to guarantee a required application performance.

Some practical implementations of protective relays with programmable tripping characteristics can be found in [27], the software tools for setting these characteristics of different relay vendors are summarized in Table 2.1. Meanwhile, the adoption of communications processors with relays can be found in [28], more details regarding communication mechanism will be provide in Section 2.3.

The unifying theme of this chapter tries to highlight that the future potential of these devices lies in the possibility of going beyond the common view which catalogs them as stand-alone equipments with the single role of protection which should act as “the last line of defense”. Here is where PMU functionalities can be a major aid by realizing that they play a vital role in improving the system awareness, improving system stability and security [29, 30]. For example, the combination of protective functions and synchronized phasors in protective relays could aid in coordinating better with power system controllers to mitigate outages [31], and to enable the smooth integration of distributed renewable sources of energy [9]. To this end, the following sections are provided to emphasize the aspects of the communication mechanisms used for protective relaying and PMU data transfer, and the requirements that they should meet.

2.2 Comparison of relay characteristic among vendors in PMU functionalities

The IEEE defines protective relays as: “relays whose function is to detect defective lines or apparatus or other power system conditions of an abnormal or dangerous nature and to initiate appropriate control circuit action ” [32]. Relays detect and locate faults by measuring electrical quantities in the power system which are different during normal and intolerable conditions. The most important role of protective relays is to first protect personal, and second to protect equipment. In the second case, their task is to minimize the damage and expense caused by insulation breakdowns which (above overloads) are called “faults” by relay engineers. These faults could occur as a result from insulation deterioration or unforeseen events, for example, lighting strikes or trips due to contact with trees and foliage.

The intention of this section is not to indicate the strengths and weaknesses of relays from different vendors. Instead, the important characteristics of different vendors’ relays are summarized, thus readers might be able to select the one that is most best suited for their particular application. The characteristics of relays such as available measurements, PMU functionalities, operating times and communication protocols, from different vendors are summarized in Table 2.1. These relays’ characteristics are obtained from several manufacture product manuals General Electric (GE) [33–37], Schweitzer Engineering Laboratories (SEL) [38–42], Areva-Alstom [43–47], and ABB [48–52].

Table 2.1: Comparison of relay characteristics between different vendors

Comparison of Relay Characteristics between Different Vendors					
Characteristic	**Protection Relay**	**Vendors**			
		GE	**ABB**	**SEL**	**ALSTOM**
Units from Manufacturer	Generator Protection	G60	REG 670	SEL-700G	P-345
	Differential Protection	T60	RET 545	SEL-487E	P-645
	Over-current Protection	MIFII	REF 545	SEL-551C	P-145
	Distance Protection	D60	REL 512	SEL-311A	P-441
	Over/Under Voltage Protection	MIV	REM 545	SEL-387E	P-923
Available Measurements	Generator Protection	RMS and Phasors (magnitude and angle) for currents and voltages; current harmonics and THD; symmetrical components; frequency, power; power factor; energy	Voltage; current; apparent power; reactive power; real power; frequency; power factor; the primary and secondary phasors	RMS and Phasors for currents and voltages; positive, negative and zero-sequence voltages and currents; system frequency; power; energy; power factor; V/Hz; generator thermal capacity	Current; voltage; power; energy; frequency; phase differential quantities; V/Hz; rate of change of frequency; CTs current magnitude and phase
	Differential Protection			RMS and Phasors for currents and voltages; power; energy; differential harmonic quantities	Phase and neutral currents; frequency; power factor; maximum demand; power; differential currents
	Distance Protection	RMS and Phasors for currents, and voltages, and power metering	RMS and Phasors for currents, and voltages, and power metering	RMS and Phasors for currents and voltages; power; energy; power factor; frequency; demand and peak current; demand and peak power; sequence components	RMS and Phasors for currents, and voltages, and power metering
	Over-current Protection	Phase and ground currents; thermal image	Phase currents; line and phase voltages; frequency; power factor; energy; power; THD	Currents; residual ground current; negative-sequence current; demand metering values	Current; voltages; power; power factor; frequency; energy
	Over/Under Voltage Protection	Phase, ground and phase-to-phase voltages; frequency	Phase currents; line and phase voltages; frequency; power factor; energy; power	RMS and Phasors for currents, and voltages; power; frequency; V/Hz; harmonics; differential currents	Phase, ground and phase-to-phase voltages; frequency

Comparison of Relay Characteristics between Different Vendors *(Cont.)*

Characteristic	Protection Relay	Vendors			
		GE	**ABB**	**SEL**	**ALSTOM**
Diagnostic Features	Generator Protection	Event Recorder (1024 time-tagged events, Oscillography for up to 64 records	1000 events time tagged, 100 disturbances	Event Recorder (1024 time-tagged events)	512 events, 5 fault records, 10 maintenance records
	Differential Protection		100 events each time tagged	Event recorder (1000 time-tagged events)	
	Distance Protection		Fault records 20 (each 16 cycle),	Event recorder (512 time-tagged events)	500 events , 28 disturbance records each time-tag
	Over-current Protection	Event recorder (32 events each time-tag), one oscillography record	Disturbance record for 16 waveforms and 16 digital signals(total 32)	Event recorder (20 time-tagged events)	512 events , 50 disturbance records each time-tag, 5 fault records
	Over/Under Voltage Protection	Event recorder (24 events each time-tag), one oscillography record		Event recorder (512 time-tagged events)	Event records 75, fault records 5, disturbance records 5 of 2.5s each
Operation Time	Generator Protection	5 to 30 ms	About 15 ms	< 20 ms	<30 ms
	Differential Protection		< 35 ms		< 33 ms
	Over-current Protection	20 to 30ms	< 30 ms	<25 ms	<30 ms
	Distance Protection	10 to 30 ms	< 30 ms	<30 ms	17 to 30 ms
	Over/Under Voltage Protection	< 30 ms	< 30 ms	<25 ms	< 30 ms
Programming and Software Features	Generator Protection	GE ENERVISTA UR	Protection and control IED Manager PCM 600	ACSELERATOR QuickSet SEL-5030 Software	S1 Studio Software for editing and extracting setting files, extracting events and disturbance records
	Differential Protection		CAP 505 Tools		
	Distance Protection		RELTOOLS		
	Over-current Protection	ENERVISTA MII	CAP 505 Tools		
	Over/Under Voltage Protection				

Comparison of Relay Characteristics From Different Vendors *(Cont.)*

Characteristic	Protection Relay	Vendors			
		GE	**ABB**	**SEL**	**ALSTOM**
Additional Functions	Generator Protection	Loss of excitation; generator unbalance; accidental energization; power swing detection; rate of change of frequency	Loss of/ under excitation; restricted earth fault; over/under frequency; directional power; pole slip; thermal overload; breaker failure; rate of change of frequency	Over-current; restricted earth fault; over excitation; loss of field protection; over/under voltage; system backup; rate of change of frequency; thermal overload	Over/under voltage; over/under frequency; rate of change of frequency; loss of field; over fluxing; thermal overload
	Differential Protection	Volts per hertz; over/under current; over voltage; over/under frequency; thermal overload; synchrocheck	Over-current; under impedance; earth fault; over load; over/under frequency; over/under voltage; over excitation	Over/under voltage; breaker failure; restricted earth fault; Volts/Hz; current imbalance	Restricted earth fault; thermal overload; V/Hz, over-fluxing; breaker failure; over/under frequency; CT/VT supervision
	Over-current Protection	Thermal Overload; cold load pickup; breaker failure to open	Earth fault; over/under voltage; thermal overload; breaker failure, auto reclosure	Auto reclosure; demand current overload; CT saturation	Auto reclosure; CT/VT supervision; overload; frequency protection; over/ under voltage; cold load pick up
	Distance Protection	Automatic reclosure; power swing blocking; breaker failure; current disturbance; over current; under/over voltage; directional elements	Breaker failure; Auto reclosure; over/under voltage	Over-current; loss of potential; load encroachment	Over-current; power swing; thermal overload; auto reclosure; over/under frequency; breaker failure
	Over/Under Voltage Protection	Voltage unbalance; under/over frequency; ground over-voltage	Over-current; earth fault; differential; under excitation; thermal overload; frequency	Over-current; differential; Volts/Hz; over/under frequency	Over/under frequency; trip circuit supervision; rate of change of frequency
Communication Method	Generator Protection	RS232; RS485; IEC 61850; ModBus TCP/IP; DNP 3.0; IEC 60870-5-104	RS232; RS485; IEC 61850-8-1; IEC 60870-5-103; LON; SPA; DNP 3.0; ModBus RTU/ASCII	SEL; ModBus TCP/IP; DNP; FTP; IEC 61850; MIRROR BITS; EVMSG; C37.118 (synchrophasors)	RS232; RS485; Courier/K-BUS ModBus; IEC 60870-5-103; DNP 3.0; IEC 61850
	Differential Protection				
	Distance Protection		RS232; RS485; DNP 3.0; ModBus RTU/ASCII		
	Over/Under Voltage Protection	RS232; RS485; IEC 61850; ModBus TCP/IP; IEC 60870-5-103	RS232; RS485; DNP 3.0 ; ModBus RTU/ASCII; IEC 61850-8-1; IEC 60870-5-103	EIA 485; ModBus RTU; EIA 232	
	Over-current Protection				

Short description of programming and software features from different vendors

This section provides the short description of softwares' functionalities and features for the user interface. They are categorized by the different manufactures as follow.

- **GE:**
  - *ENERVISTA UR and ENERVISTA MII* are Windows-based softwares that allow users to communicate with relays for data review and retrieval, oscillography, I/O configurations and logic programming.
- **SEL:**
  - *ACSELERATOR QuickSet Software* provides analysis support for SEL-relays. It creates, tests, and manages relay settings with a Windows interface.
  - *SEL-5077 SYNCHROWAVE Server* provides phasor data concentration (PDC) for synchrophasor information, and transmit data to a display software in IEEE C37.118.2 format.
- **ALSTOM:**
  - *MICOM S1 Studio* provides user with global access to all IED's data by sending and extracting relay settings. It is also used for analysis of events and disturbance records which acts as IEC 61850 IED configurator.
- **ABB:**
  - *IED Manager PCM 600* is the toolbox for control and protection IEDs. It covers the process steps of the IED's life cycle, testing, operation and maintenance, to the support for function analysis after primary system faults.
  - *CAP 505 Relay Product Engineering Tool* is a graphical programming tool for control and protection units. It can be used both as a local system near the relay and as a central system connected to several relays.
  - *RELTOOLS* is management tool for controlling relays of the ABB-family. It allows the user to edit settings and to modify control logics.

Nevertheless, these tools support limited range of different protection and control products. For instance, the *PCM 600* tool supports the REG 670 relay (generator protection) but the software does not patronize to the REL 512 (distance protection) [53]. Another example is the *CAP 500* supports the RE_545 relay-family, this group of relays are differential, over-current, and over/under voltage protections (see Table 2.1), but this software is not available for the REG 670 relay [54]. This can imply that there is no interface between different tools. Moreover, only relays manufactured by SEL have implemented and support the IEEE C37.118.2 protocols [55] which is a standard for communicating synchrophasor measurements in real-time

from a PMU to a Phasor Data Concentrator (PDC). This protocol is used to guarantee the data streams quality when aggregating them from different monitored power system regions. This feature would allow for a further exploitation of a transmission system operator's assets through the development of Wide-Area Monitoring System (WAMS), Wide-Area Control Systems (WACS), and Wide-Area Protection System (WAPS).

In practical terms SEL and Alstom provide a more consistent software interface to the IEDs by using 1 single configuration and programming software, while GE and ABB require 2 and 3, respectively. It is apparent that there is a large practical disadvantage in learning and maintaining more than 1 software for IED configuration.

In addition, as mentioned in Chapter 1, in order to implement WAMS, WACS and WAPS, local measurements such as bus frequencies, voltage phasors, current phasors, and breaker status need to be transferred from different geographical locations, for example at distant substations and power plants. Most electromechanical relays (which are not designed to handle actual engineering analysis information in complex network topologies) are intentionally being replaced by the modern relays with communications channels, this opens an opportunity to actively incorporate them within WAMS, WACS and WAPS. However, to fully exploit the benefit of replacing these relays, the most advantageous options from both the practical[1] and future-looking perspective[2] are those providing consistency in the software used for management and that implement the latest IEC 61850 and IEEE C37.118 protocols. These channels can be utilized to support an analysis system capable of evaluating protection operation against unexpected and expected behaviors, pinpointing possible malfunctions and indicating problems that may rise in the future.

2.3 Communications mediums and networks

A communication system consists of a transmitter, a receiver and communication channels. Type of mediums and network topologies in communications provide different opportunities to advance the speed, security, dependability, and sensitivity of protection relays. There are several types of communication medium such as micro wave, radio system, fiber optic, etc. The advantages and disadvantages in communication mediums which are currently in operation (both analog and digital) and different network topologies are summarized in Table 2.2 and Table 2.3 [56], respectively.

[1] A common and transparent software platform to manage All protective relays.
[2] Those supporting the IEEE C37.118.2 protocol.
[3] Transmitting back and forth the signal 36,000 km between the earth and the satellite.

Table 2.2: Comparison of communication mediums

Medium	Advantages	Disadvantage
Transmission Power Line Carrier	Economical, suitable for station to station communication. Equipment installed in utility owned area	Limited distance of coverage, low bandwidth, inherently few channels available, exposed to public access
Microwave	Cost effective, reliable, suitable for establishing back bone communication infrastructure, high channel capacity, high data rates	Line of sight clearance required, high maintenance cost, specialized test equipment and need for skilled technicians, signal fading and multipath propagation
Radio System	Mobile applications, suitable for communication with areas that are otherwise inaccessible	Noise, adjacent channel interference, changes in channel speed, overall speed, channel switching during data transfer, power limitations, and lack of security
Satellite System	Wide area coverage, suitable to communicate with inaccessible areas, cost independent of distance, low error rates	Total dependency to remote locations, less control over transmission, continual leasing cost, subject to eavesdropping (tapping). End to end delays[3] in order of 250 ms rule out most protective relay applications [57].
Spread Spectrum Radio	Affordable solution using unlicensed services	Yet to be examined to satisfy relaying requirement
Leased Phone	Effective if solid link is required to site served by telephone service	Expensive in longer term, not good solution for multi channel application
Fiber Optic	Cost effective, high bandwidth, high data rates, immune to electromagnetic interference. Already implemented in telecommunication, SCADA, video, data, voice transfer etc.	Expensive test equipment, failures may be difficult to pin-point, can be subject to breakage

Table 2.3: Comparison of different communication network topologies

Topology	Graphical Model	Advantages	Disadvantages
Point-to-Point network is the simplest configuration with channel available only between two nodes	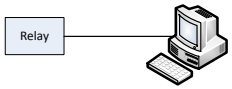	Suitable for systems that require high exchange rate of communication between two nodes	Communication can only be transferred between two nodes, disconnection of the communication channel will lead to a total loss of information exchange
Star network consists of multiple point-to-point systems with one common data collector	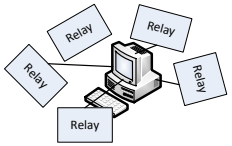	Easy to add and remove nodes, simple in managing and monitoring, node breakdown does not affect rest of the system	The reliability of entire network depends only on single hub failure
Bus network has single communication path which runs throughout the system to connect nodes	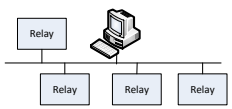	Bus network is not dependent on a single machine (hub). This provides high flexibility in configuration (easy to remove or add nodes and node to node can be directly connected).	High information load might delay the communication traffic speed. Also, it is sometime inefficient to utilize communication channels since the information cannot be exchanged directly between the desired relay and hub without passing through relays along the communication path. In other words, some relays may receive information packets which are unnecessary for them. Thus, it is also hard to troubleshoot the root cause of problem when needed.
Linear Drop and Insert network consists of multiple paths for relays to communicate with each other. Information between two non-adjacent nodes can be transferred directly passes through intervening node(s).	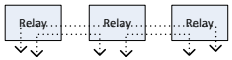	When a certain communication channel drops, its bandwidth can be balanced by other channels	Lack of channel backup against fiber or equipment failure
SONET Path Switched Ring comprises of two separate optical fiber links connecting all the nodes in counter rotating configuration. In normal case, the information is transferred from A to C through outer ring (via B) which is the primary route (left figure). However if channel failure occurs, the information is transferred through inner ring which is secondary route (right figure)	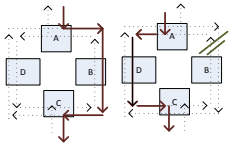	This type of network is redundant which means that channel failures will not affect the communication process	An unequal time delay between transmitter and receiver might cause the false operation of protective relays when there is a switch to from primary to secondary route in the case of channel failure
SONET Line Switched Ring has the same structure as SONET Path type however one path is active and other is a reserved one. Under normal condition, the active path transfers information via outer ring (left figure). However in case of channel failure, the inner ring is activated to reverse and transmit information through another direction (right figure)	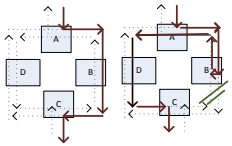	More efficient use of fiber communications for some applications	This communication type is not suitable for teleprotection applications since it requires complex handshaking (Synchronizing) that causes a delay of 60 ms.

2.4 Communication protocols

Communications protocols are sets of rules by which communication over a network is achieved. Communications protocols are responsible for enabling and controlling network communication. Protocols set the rules for the representation of data, the signals used in communications, the detection of errors, and the authentication of computing devices on the network. It is not mandatory for relay manufacturers to follow the same protocols as shown in Table 2.1. Communication protocols can be categorized into two groups which are (*i*) Physical-based protocols and (*ii*) Layered-based protocols. Both types of protocol are briefly discussed in this section.

Physical-based protocol

Physical-based protocols have been developed to ensure compatibility between units provided by different manufacturers, and to allow for a reasonable success in transferring data over specified distances and/or data rates. The Electronics Industry Association (EIA) has produced protocols such as RS232, RS422, RS423 and RS485 that deal with data communications. In addition, these physical-based protocols are also included in the "Physical layer" of the Open Systems Interconnection (OSI) model that will be explained in Layered-based protocols, section below.

- **RS232 Protocols**

  The RS232 Protocol is the most basic communication protocol which specifies the criteria for communication between two devices. This type of communication can be simplex (one device acts as transmitter and other acts as receiver and there is only one way traffic i.e. from transmitter to receiver), half duplex (any of the device can act as a transmitter or receiver but not at the same time) or full duplex (any of the device can transmit or receive data at the same time). A single twisted pair connection is required between the two devices. Figure 2.1 shows the RS232 protocol configuration.

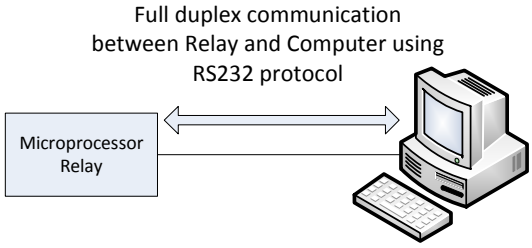

Figure 2.1: RS232 Protocol configuration

- **RS485 Protocol**

  This protocol is similar to the RS232 protocol which allows multiple relays (up to 32) to communicate at half-duplex. This half duplex scheme authorizes one relay either to transmit or receive command information. This means that the information is handled by polling/ responding. The communication is always initiated by the "Master unit" (host) and the "Slave units" (relays) will neither transmit data without receiving a request from the "Master unit" nor communicate with each other. There are two communication modes in RS485 protocol *(i) Unicast mode* and *(ii) Broadcast mode*. In the unicast mode, the "Master unit" sends polling commands, and only one "Slave unit" (assigned by an unique address) responds to its command accordingly. The "Master unit" will wait until it obtains a response from a "Slave unit"or abandon a response in case a pre-defined period expires. In the broadcast mode, the "Master unit" broadcasts message to all "Slave units". Figure 2.2 and 2.3 show a simple RS485 protocol configuration in the unicast and the broadcast mode, respectively.

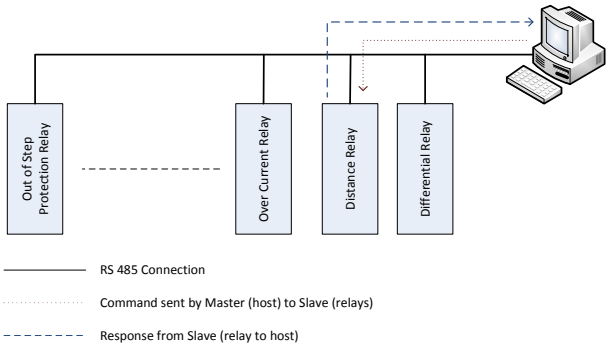

Figure 2.2: RS485 Protocol configuration: Unicast mode

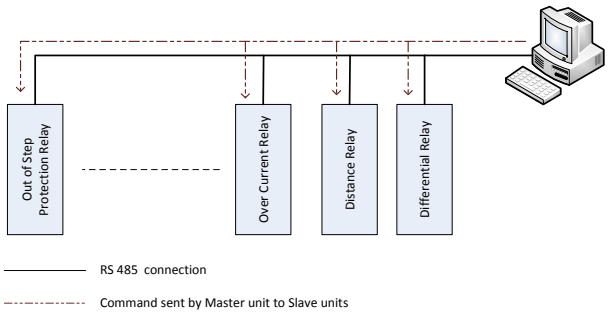

Figure 2.3: RS485 Protocol configuration: Broadcast mode

Layered-based protocols

Other protocols mentioned in Table 2.1 are developed by the Open Systems Interconnection (OSI) model [58]. This model is a product of the Open Systems Interconnection effort at the International Organization for Standardization. The model sub-divides a communication system into several layers. A layer is a collection of similar functions that provide services to the layer above it and receives services from the one below. On each layer, an instance provides services to the instances at the layer above and requests service from the layer below. When data is transferred from one device to another, each layer would add the specific information to the "headers" and the information will be decrypted at the destination end. Figure 2.4 demonstrates data communication using OSI model where "H" represents "headers". Table 2.4 describes function of each layer.

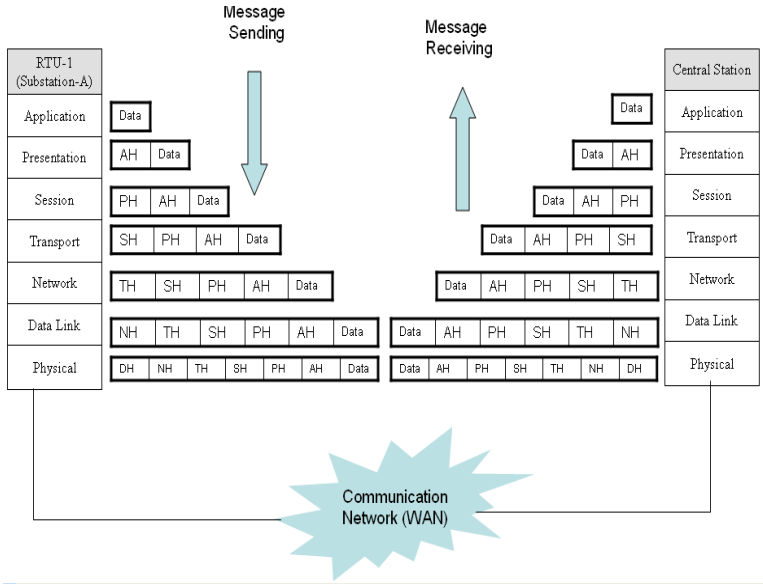

Figure 2.4: OSI model

Table 2.4: Functions of OSI model

Layers	Function
Application (**A**)	Offers direct interaction of user with the software application. Adds an application header to the data which defines which type of application has been requested. This forms an application data unit. There are several standards for this layer e.g. HTTP, FTP, etc.
Presentation (**P**)	Handles format conversion to common representation data and compresses and decompresses the data received and sent over the network. It adds a presentation header to the application data unit having information about the format of data and the encryption used.
Session (**S**)	Establishes a dialogue and logical connection with the end user and provides functions like fault handling and crash recovery. It adds a session header to the presentation data unit and forms a session data unit.
Transport (**T**)	Manages the packet to the destination and divides a larger amount of data into smaller packages. There are two transport protocols, Transmission Control Protocol (TCP) and User Datagram Protocol (UDP), in this layer. Reliability and speed are the primary difference between these two protocols. TCP establishes connections between two hosts on the network through packages which are determined by the IP address and port number. TCP keeps track of the packages delivery order and check of those that must be resent. Maintaining this information for each connection makes TCP a stateful protocol. On the other hand, UDP provides a low overhead transmission service, but with less error checking.
Network (**N**)	Controls the routing and addressing of the packages between the networks and conveys the packet through the shortest and fastest route in the network. Adds a network header to the Transport Data Unit which includes the Network Address.
Data Link (**D**)	Specifies Physical Address (MAC Address) and provides functions like error detection, resending etc. This layer adds a Data Link Header to the Network Data Unit which includes the Physical Address. This makes a data link data unit
Physical	Determines electrical, mechanical, functional and procedural properties of the physical medium.

Some of protocols, mentioned in Table 2.1, that are derived from OSI model are described below:

- **DNP 3.0** [59]

  The Distributed Network Protocol (DNP) 3.0 is a protocol developed to achieve interoperability standard between substation computers. This protocol adopts layers 1, 2 and 7 from the OSI model for basic implementation. A fourth layer (a pseudo-transport layer) can be added to allow for the message segmentation. This DNP 3.0 protocol with a pseudo-transport layer is called the Enhanced Performance Architecture (EPA) model. It is primarily used for communications between master stations in Supervisory Control and Data Acquisition (SCADA) systems, Remote Terminal Units (RTUs), and Intelligent Electronic Devices (IEDs) for the electric utility industry. This protocol does not wait for data as TCP/IP. If a packet is delayed, after a while, it will be dropped. This is because the protocol consists of embedded time synchronization (timetag) associated with messages. This timetag's accuracy is on the order of milliseconds. It is feasible to exchange messages asynchronously which is shown in a function of the polling/ response rate. The typical processing throughput rate is 20 milliseconds [60].

- **ModBus** [61]

  ModBus is also a three-layer protocol that communicates using a "master-slave" technique in which only one device (the master) can initiate transactions (called queries). The other devices (slaves) respond by supplying the requested data to the master, or by taking the action requested in the query. This protocol does not consist of embedded time synchronization as in case of DNP 3.0 that each message is stored in an internal buffer. However, time synchronization can be implemented either using the external time synchronization source, such as Global Positioning System (GPS) or using the external timing mechanism, such as Inter-Range Instrumentation Group (IRIG) to keep Intelligent Electronic Devices (IEDs) in synchronism. In general, IRIG provides accuracy in the 100 microsecond range [62] but it requires dedicated coaxial cable to transport the timing signals which can be limitation for the number of connected devices (depending on cable length and device load). On the other hand, GPS provides higher accuracy (in the range of 1 microsecond [62]) compare to IRIG but cost and complications of antennas installation to every device are the restriction for the GPS deployment. Nevertheless, the choice of time synchronization protocol is usually dictated by the number and type of power system devices as well as the physical arrangement of the equipment. The typical processing throughput rate of ModBus protocol is 8 milliseconds [60].

  The protocol can be categorized into three frame formats which are American Standard Code for Information Interchange (ASCII), Remote Terminal Unit (RTU), and Transfer Control Protocol and Internet Protocol (TCP/IP) format. The ModBus ASCII and ModBus RTU are both used in serial communication. The difference between these ASCII and RTU frames is the format of communication message. In

the ASCII format, two ASCII characters are used in each 8 bit byte message whereas two 4 bit hexadecimal characters (or 8-bit binary) are used in case of the RTU format. The advantage of ASCII format is that it allows time intervals of up to one second to occur between characters without causing an error. On the other hand, the greater character density in the RTU allows better data throughput compare with the ASCII for the same baud (modulation) rate however each message must be transmitted in a continuous stream. Figure. 2.5 shows the Protocol Data Unit (PDU) for ASCII and RTU frame formats.

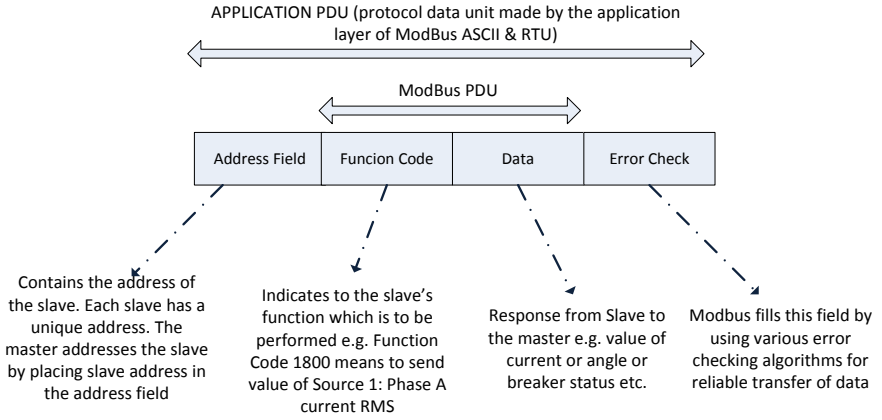

Figure 2.5: ModBus ASCII & RTU Protocol Data Unit (PDU)

Meanwhile, the ModBus TCP/IP is modified from the PDU frame with the Ethernet-TCP/IP as an additional data transmission technology for the ModBus Protocol. First, an "Error Check" algorithm at the end of frame is removed and the Address Field (address of slave) is replaced by a new header called the ModBus APplication (MBAP) Header. This header consists of (*i*) Transaction Identifier, (*ii*) Protocol Identifier, (*iii*) Length Field, and (*iv*) Unit Identifier. Figure. 2.6 shows the Application Data Unit (ADU) for TCP/IP frame format (compare with PDU message). In addition, details such as message format or function codes for all three frames format can be found in [63].

The difference between ModBus and DNP 3.0 is the communication purpose. ModBus is suitable for communication within substations that are used for communicating with devices meant for protection control and metering. Meanwhile DNP 3.0 is suitable for communicate outside the substations (communication of data from substation to master control centers). This is because the ModBus protocol has limited function codes while the DNP 3.0 supports the specific data objects that provide more flexibility, reliability and security. For example, the DNP 3.0 has 'Control Function Code' to perform specific function. The comparison between ModBus and DNP 3.0 can be found in [64]. In addition, the ModBus protocol is

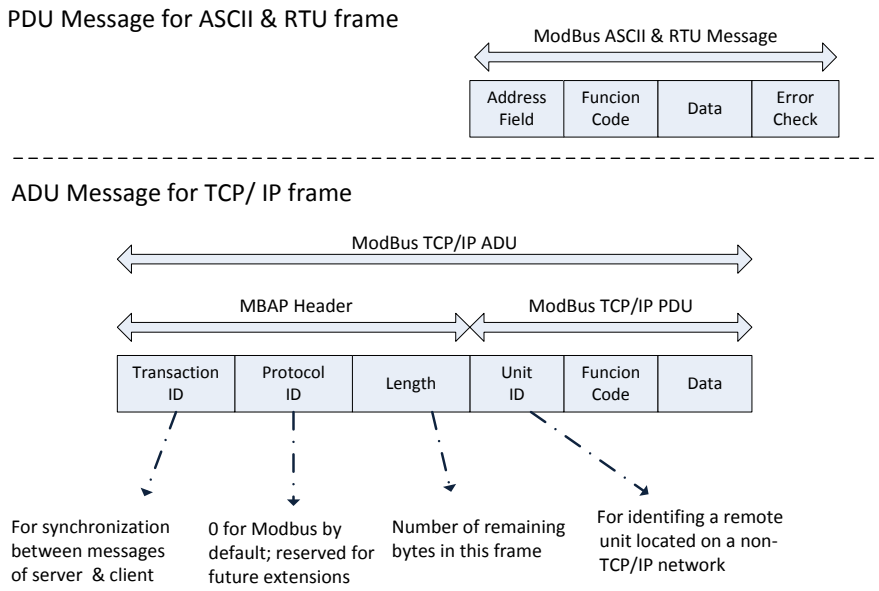

Figure 2.6: Message frame comparison between ModBus PDU and ADU

a prototype for proprietary protocols such as **K-BUS** [65] and **SPA** [66] protocols which are of Areva-Alstom and ABB, respectively.

- **IEC 61850** [61]

  IEC 61850 is an electrical substation standard promoted by the International Electrotechnical Commission (IEC). The data models defined in IEC 61850 protocol can be mapped to various protocols, for example to Generic Object Oriented Substation Events (GOOSE) that allows for both analog and digital peer-to-peer data exchange. The protocol includes time tags and also messages that can be exchanged asynchronously. The typical processing throughput rate is 12 milliseconds [60]. IEC 61850 provides many advantage over other protocols such as programming can be done independent of wiring, higher performance with more data exchange, or data is transmitted multiple times to avoid missing information. More advantages can be found in [67] and [68].

- **LON** [69]

  The Local Operating Network (LON) protocol equates all seven layers of the OSI Model. It is capable of establishing network communications not only for power system applications, but also for factory automation, process control, building networks, vehicle networks, etc. This may be considered as a drawback in relay communication perspective since the LON protocol occupies seven layers in order

to transfer information, thus it provides lower data exchange rates compare to the EPA model such as DNP 3.0.

Communication delays in data delivery for synchrophasor applications

The communication infrastructure is an essential element for protective relays and especially for WAMS, WACS and WAPS. PMU devices are used in order to transmit data from several parts of the system to a control center, therefore the communication network has a potential to be a bottleneck that could impacts the achievable wide area system's performance. Delay due to the use of PMUs depends on many components such as transducers that are involved starting from the initial sampling instant. The processing time required for converting transducer data, into phasor information depends on the selected Discrete Fourier Transform's (DFT) time frame or the specific phasor computation algorithm. Moreover, the overall delay also caused by PMU's data size, multiplexing and transitions, and type of communication medium. A Phasor Data Concentrator (PDC) receives data streams from PMUs, then correlates them into a single data stream that is transmitted to a PC via an Ethernet port, both PMUs and PDCs use the IEEE C37.118.2 protocol to achieve this. The propagation delays associated with the communication is dependent on the medium and physical distance while the delay associated with transducers used, phasor computation algorithm, data concentration, and multiplexing are not fixed. The associated delays for various communication mediums when using PMUs are summarized in Table 2.5 [70]. However, the time duration of different delays has

Table 2.5: Associated delays with various communication mediums

Communication link	Associated delay one way [ms]
Fiber Optic	100 - 150
Microwave	100 - 150
Power Line	150 - 350
Telephone line	200 - 300
Satellite System	500 - 700

been ambiguous, particular for communication timing. Reference [70] describes that the delay caused by processing time (data concentrating, multiplexing and delay associated with transducers) is fixed and estimated to be around 75 ms. This is questionable, as the IEEE C37.118 standard does not specify how processing time must be implemented and therefore each manufacturer differs. As a consequence, processing time is not consistent between each manufacturer. Meanwhile this processing time delay is stated only 5 ms in [71] (see Table 2.6) and it is doubtfully cited in certain number of publications as in [72–74]. Hence, there is not actual consensus on the time delays involved in each stage of the process between measurement and concentration of synchrophasors. Experimental studies

are necessary to establish these important characteristics and to clarify these contradictions.

Table 2.6: Time estimates for steps in wide-area protection [72]

Activity	Time [ms]
Sensor Processing time	5
Transmission time of information	10
Processing incoming message queue	10
Computing time for decision	100
Transmission of control signal	10
Operating time of local device	50

Chapter 3

Experimental and Simulation Set-Ups

This chapter describes experimental and simulation set-ups which are required prior to the development of algorithms for voltage stability monitoring, visualization, and instability mitigation. These set-ups are comprised of both software and hardware implementations. Regarding the simulation set-up, a test system that can generate different instability scenarios is implemented in both a positive-sequence-based (PSB) simulator and a Real-time Hardware-In-Loop (RT-HIL) platform. The detailed modeling of each device with their required initialization settings are provided to show the need of accurate system models' implementation. For the experimental hardware set-up, the purpose of the SmarTS-Lab at KTH and its components is explained. This "test-bench" provides an environment that allows to carry out experiments as close as possible to real existing power networks.

3.1 The system modelling in DIgSILENT software

The commercial and proprietary DIgSILENT PowerFactory simulation software offers a Graphical User Interface (GUI) to implement power system models for stability analysis purposes. The software is complemented with a library that contains built-in IEEE models and it also allows users to create their own models if needed. The models can be implemented by either building block diagrams or programming in the DIgSILENT Simulation Language (DSL) block definitions; allowing for the representation of transfer functions, or differential equations for complex dynamic models. This section presents a test power system and the detailed models of each individual device implemented in PowerFactory by using block diagrams and DSL programming.

3.1.1 Test System

A one-line diagram of the "all-in-one" test system is shown in Fig. 3.1. This test system is an alteration of the Bonneville Power Administration test system initially developed by

Prof. T. Van Cutsem in [75], constructed to capture transient (angle), frequency and voltage instability phenomena, resulting in system collapse, within one system.

The system consists of a local area connected to a strong grid (Thevenin Equivalent) by two 380 kV transmission lines. A motor load (rated 750 MVA, 15 kV) is connected at Bus 4 and supplied via a 380/15 ratio transformer. A load with constant power characteristics and load tap changer (LTC) dynamics at the distribution side are explicitly modelled at Bus 5. A local generator (rated 450 MVA, 20 kV) is connected at Bus 2 to supply the loads through a 20/380 ratio transformer.

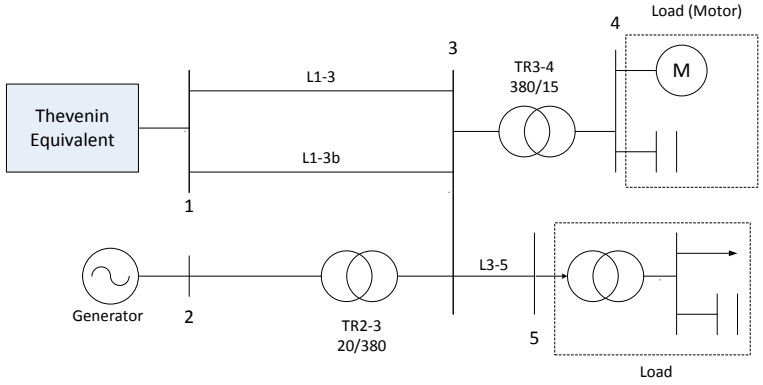

Figure 3.1: "All-in-one" test system

From the power system viewpoint, excitation systems should be capable of responding rapidly to a disturbance so that proper voltage support is provided through excitation control. Thus, excitation systems should be designed to have a fast acting response to enhance transient stability. This fast response requirement has been taken into consideration by manufactures which have developed excitation control systems, such as the GE EX2100 [76], Westinghouse's static excitation system [77], and others, that can be modelled through the IEEE Type ST excitation models recommended by the IEEE Standard 421.5 [78]. In this study, the ST1A model (shown in Fig. 3.2) is implemented by setting model parameters to appropriate values, then simplifications are made.

3.1.2 Adapting built-in models

This section describes an approach to adapt built-in models that are available in DIgSILENT software.

- The *simplified ST1A excitation system* is implemented by setting time constants T_B, T_{B1}, T_C and T_{C1} in the forward path of the original ST1A Excitation system to zero. The internal excitation control system stabilization is represented in the feedback path with the gain K_F (internal limits on V_I and the internal feedback stabilization time constant (T_F) are neglected in this thesis). This is a suitable practice in many

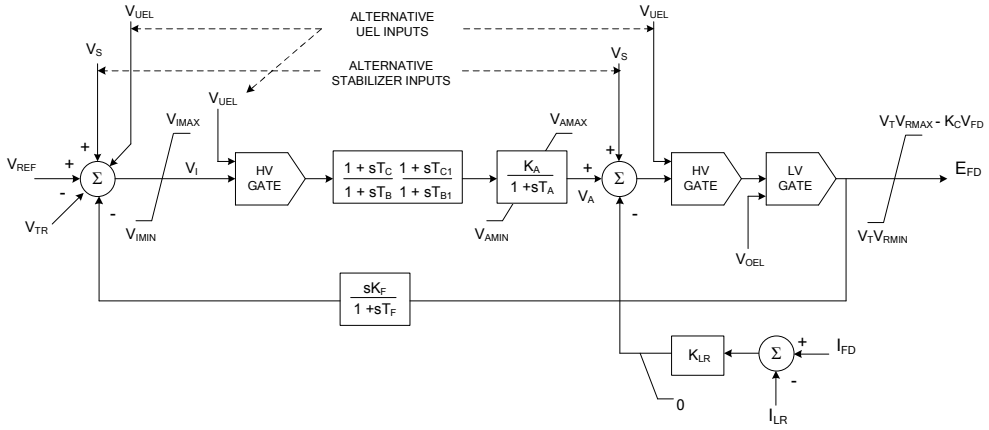

Figure 3.2: ST1A Excitation system block diagram showing major functional blocks (adapted from [78])

cases as stated in Ref. [78]. Moreover, the current limit (I_{LR}) and gain K_{LR} of the field current limiter are set to zero. An underexcitation limiter (V_{UEL}) input voltage is also ignored, nevertheless an overexcitation limiter (V_{OEL}) is added at the first summation junction instead of the low voltage gate.

Figure 3.3 depicts the excitation system obtained from the simplifications above, and used in this study. The input signal of the excitation system is the output of the voltage transducer, V_{TR}. This voltage is compared with the voltage regulator reference, V_{REF}. Thus, the difference between these two voltages is the error signal which drives the excitation system. An additional signal from overexcitation limiter (OEL) output, V_{OEL}, becomes non-zero only in the case of unusual conditions.

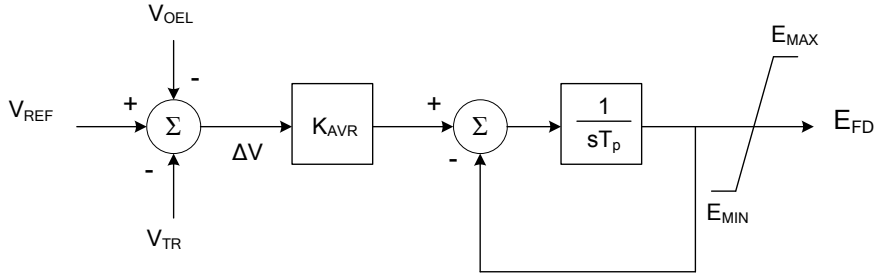

Figure 3.3: Simplified Excitation system model obtained by simplifying the IEEE ST1A excitation model

- A typical *speed-governing system* consists of a speed governor, a speed relay, hydraulic servomotors, and controlled valves, which are represented in the functional

block diagram in Fig. 3.4

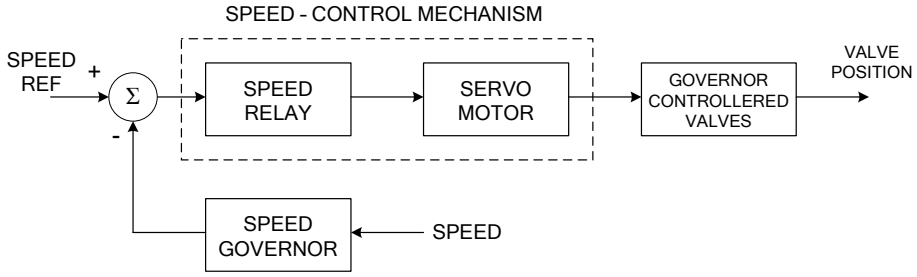

Figure 3.4: Functional block diagram of a typical speed-governing system

The speed-governor regulates the speed of a generator by comparing its output with a predefined speed reference, the resulting error signal is sent to and amplified by a speed relay (a shaft speed is transformed into a valve position). The servomotor is necessary to move steam values (especially, in case of large turbines) and can be considered as an amplification. A standard model that can be used to represent a mechanical-hydraulic system as shown in Fig. 3.5, can be found in an IEEE Working Grouping Report [79]. This model is altered by many manufacturers, such as GE and Westinghouse, by applying different governor time constant (T_1), governor derivative time constant (T_2), and servo time constant (T_3). In this study, the Westinghouse EH Without Steam Feedback [79] is considered. To implement this model in DIgSILENT; T_1, T_2, and T_3 are set to 0, 0, and 0.1, respectively. The valve speed (open or close) is determined by maximum and minimum rate of change of the valve position (Z'_{MAX} and Z'_{MIN}, respectively) where the the gate position is limited by maximum and minimum gate position (P_{MAX} and P_{MIN}, respectively).

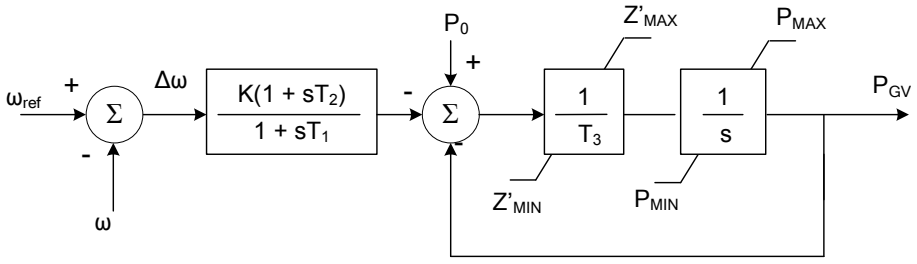

Figure 3.5: Model for the speed-governing steam turbine system

- A *steam turbine* converts stored energy from high pressure and temperature steam into rotating energy, which in turn is converted into electrical energy by a generator.

The general model used for representing steam turbines is provided in [79]. This model is applicable for common steam turbine system configurations which can be characterized by an appropriate choice of model parameters. A steam system, tandem compound single reheat turbine, was selected for this study (shown in Fig. 3.6). This turbine is represented by a simplified linear model [79], which is shown in Fig. 3.7.

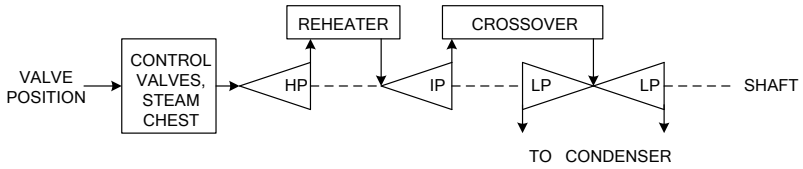

Figure 3.6: Steam turbine configuration

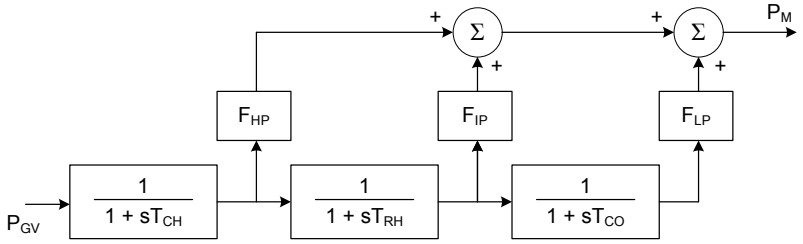

Figure 3.7: Approximate linear model representing the turbine in Fig. 3.6

From Fig. 3.6, steam enters the high pressure (HP) stage through the control valves and the inlet piping. The housing for the control valves is called “steam chest”. Then, the HP exhaust steam is passed through a reheater. Physically, this steam returns to the boiler to be reheated for improving efficiency before flowing into the intermediate pressure (IP) stage and the inlet piping. Subsequently, the crossover piping provides a path for the steam from the IP section to the low pressure (LP) inlet. In this thesis, Fig. 3.8 shows the models implementation in PowerFactory. It depicts the steam turbine with speed governor where the left-block and right-block represent speed governing system and steam turbine, respectively. This model was implemented by modifying DIgSILENT’s “gov_ IEESGO_ mod_ new: IEEE Standard Governor” model, where the speed governing system did not reflect the recommendation in [79]. Hence the speed-governing system was modified by replacing the lead-lag and the first-order delay filter with gain blocks by a constant block. Moreover, the limiter block in the original built-in model is replaced by the constant with limiter and the limited non-windup integrator blocks. Finally, the output signal from integrator block is added at the second summation junction. Figure 3.9 shows a comparison between the speed-governing system before and after being modified.

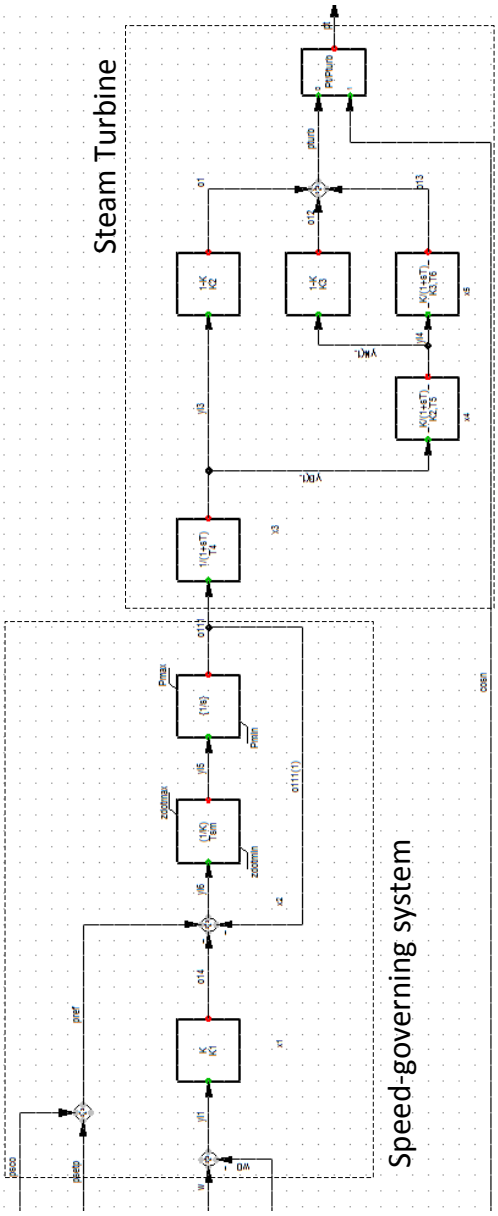

Figure 3.8: Steam turbine with speed governor modelled in DIgSILENT

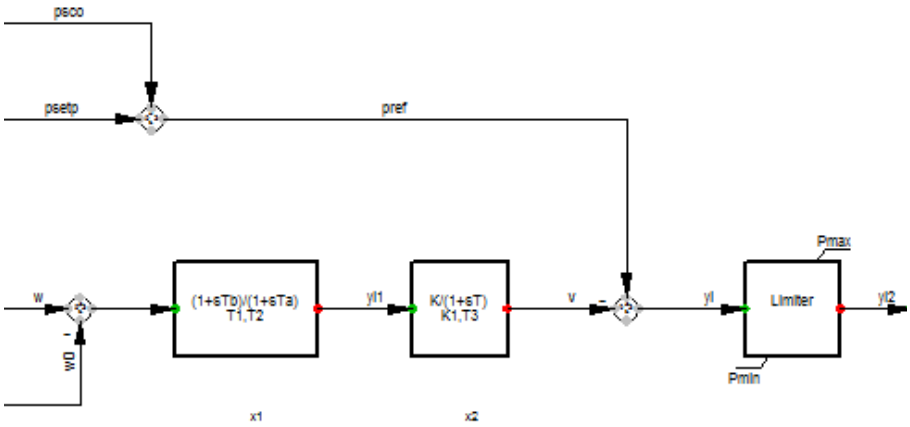

(a) Speed-governing system before modified

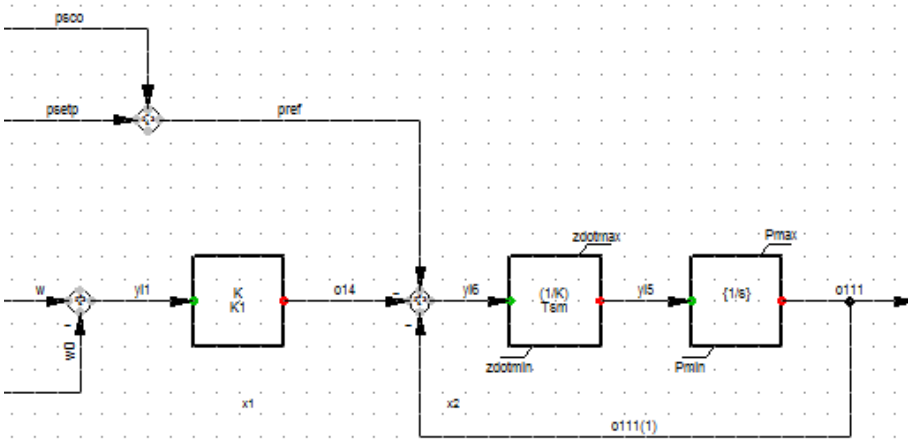

(b) Speed-governing system after modified

Figure 3.9: Comparison of speed-governing system before and after modification

3.1.3 Custom models

This section describes some devices that are necessary for producing instability scenarios. For example, an overexcitation limiter, a load tap changer, and a load restoration model are required to illustrate voltage instability phenomena. Since they were not available in DIgSILENT, they were implemented by using the DSL programming and block diagrams.

- An *overexcitation limiter (OEL)* model is necessary to capture slow acting phenomena, such as voltage collapse, which may force machines to operate at high excitation levels over ling periods. According to the IEEE recommended practice 421.5 [78], OELs are required in excitation systems to capture slow

changing dynamics associated with long-term phenomena. The OEL's purpose is to protect generators from overheating due to persistent and larger field currents beyond the design limits. This can be caused either by the failure of a component inside the voltage regulator, or an abnormal system condition. In other words, it allows machines to operate for a defined time period in overload conditions, and then reduces the excitation to a safe level. A standard model that can be used to implement most OELs can be found in [80]. In this study, an OEL is modelled and implemented following the block diagram shown in Fig. 3.10.

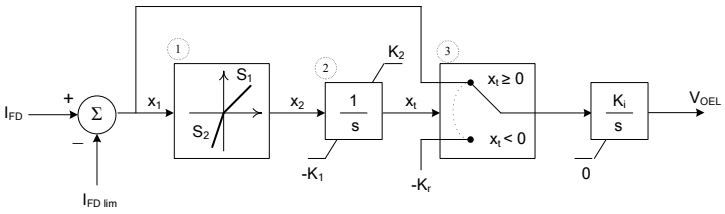

Figure 3.10: Overexcitation limiter (adapted from [81])

The OEL detects high field currents (I_{FD}) and outputs a voltage signal (V_{OEL}), which is sent to the excitation system summing junction. This signal is equal to zero in normal operation conditions. In other words, V_{OEL} is zero if I_{FD} is less than I_{FDlim}. As a result the error signal (ΔV) is altered so that the field current is decreased below overexcitation limits (forces I_{FD} to I_{FDlim}). As shown in Fig. 3.10, Block 1 is a two-slope gain obeying the following expressions.

$$x_2 = S_1 x_1 \quad \text{if } x_1 \geq 0, \tag{3.1}$$
$$= S_2 x_1 \quad \text{otherwise} \tag{3.2}$$

With S_1 and S_1 greater than zero, Block 2, the non-windup limited integrator block reacts as the following expressions.

$$\dot{x}_t = 0 \quad \text{if } (x_t = K_2 \text{ and } \dot{x}_2 \geq 0) \text{ or } (x_t = -K_1 \text{ and } \dot{x}_2 < 0), \tag{3.3}$$
$$= x_2 \quad \text{otherwise} \tag{3.4}$$

Assume that I_{FD} becomes larger than I_{FDlim}, this means that x_t is also greater than zero. Thus, Block 3 switches as indicated in Fig. 3.10 and the signal is sent to the wind-down limited integrator to produce V_{OEL}. Large values of S_2 and K_r cause V_{OEL} to return to zero when I_{FD} is less than I_{FDlim}. The OEL model implemented in the PowerFactory software is shown in Fig. 3.11 where block number 1, 2, and 3 represent the two-slope gain, the non-windup limited integrator, and the

switching blocks which behave similarly as an OEL presentation shown in Fig. 3.10, respectively.

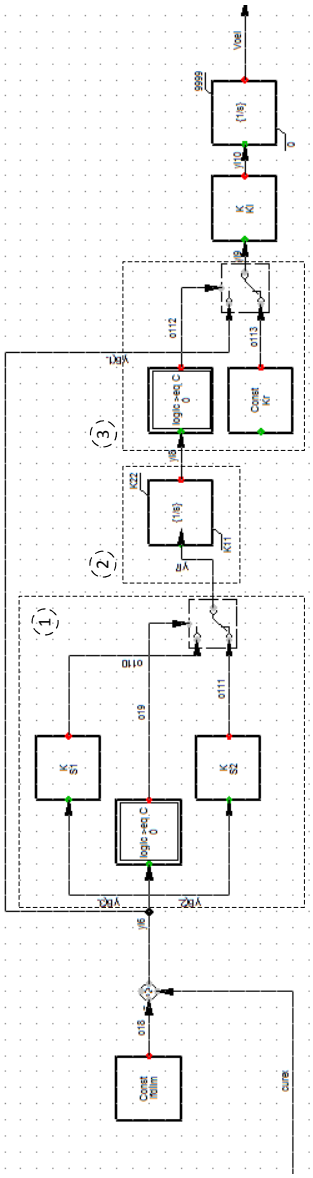

Figure 3.11: Overexcitation limiter implementation in the DIgSILENT software

- A *Load Tap Changer (LTC)* transformer which automatically operates to maintain voltages at the load within desired limits, especially when the system is under disturbances. In other words, LTCs act to restore voltages by adjusting transformer taps. As a result the voltage level will progressively increase to its pre-disturbance level. Dynamic characteristics of the LTC's logic can be modelled in different ways, as described in CIGRE Task Force 38-02-10 [82]. In this thesis, a discrete LTC model is chosen, its function is to raise or lower the transformer ratio by one tap step. The tap changing logic at a given time instant is modeled by [81]:

$$r_{k+1} = \begin{cases} r_k + \Delta r & \text{if } V > V^0 + d \text{ and } r_k < r^{max} \\ r_k - \Delta r & \text{if } V < V^0 - d \text{ and } r_k > r^{min} \\ r_k & \text{otherwise} \end{cases} \tag{3.5}$$

where Δr is the size of each tap step, k is the tap position, and r^{max}, r^{min} are the upper and lower tap limits, respectively.

The LTC is activated when the voltage error increases beyond one half of the LTC deadband limits (d). To this aim, a comparison between the controlled voltage (V) and the reference voltage (V^0) is performed by the LTC's logic:

$$k = 0 \quad \text{if} \quad \left|V(t_0^+) - V^0\right| > d \quad \text{and} \quad \left|V(t_0^-) - V^0\right| \leq d \tag{3.6}$$

Moreover, the tap movement can be categorized into two modes which are: *sequential*, and *non-sequential* [83]. In this study, the sequential mode is adopted. Here the first tap position changes after an initial time delay and continues to change at constant time intervals. If the transformer ratio limits are not met, the LTC will bring the error back inside into the deadband. The LTC can be modelled in DIgSILENT software by using the DIgSILENT Simulation Language (DSL) code that offers some flexibility for implementing user-specific models need for stability analysis purposes [84]. The DSL code for LTC modelling is given as follows.

```
1-  t=time()
2-  ! Initial value
3- inc(v0)=u
4- inc(nntap0)=nntapin
5- inc(tchangedown)=0
6- inc(tchangeup)=0
7- ! Definition of tap steps
8- tapdown     = nntap0 - 1
9- tapup       = nntap0 + 1
10- tapstop     = 0
11- changeup   = picdro({(u*nntap0/nntapin)>(v0+d)},0.0,0.0)
12- changedown = picdro({(u*nntap0/nntapin)<(v0-d)},0.0,0.0)
13- ! First step Delay
```

```
14- up1st   = select(changeup=1,1.0,0.0)
15- down1st = select(changedown=1,1.0,0.0)
16- cond    = select(picdro(up1st.or.down1st,15,0.0), 1, 0)
17- act     = select(cond=1, 1, 0)
18- later   = act+1
19- clear   = select(picdro(later=2, 0, 1000), 1, 0)
20- clear1st = select(clear=1, 1, 0)
22- event(1,clear1st, 'create=
       EvtParam Target=this name=Deactivate_1st_change value=0 variable=act')
23- ! command to change Tap position = triggering
24- tchangedown = picdro({later>1.and.nntap0>=
       Tmin.and.changedown.and. .not.delay(tchangedown,tdelay/15)},tdelay,0.0)
25- tchangeup   = picdro({later>1.and.nntap0<=
       Tmax.and.changeup.and. .not.delay(tchangeup,tdelay/15)  },tdelay,0.0)
26- ! force event signal zero crossing
27- evtdown     = tchangedown -0.5
28- evtup       = tchangeup  -0.5
29- nntapin     = nntap0
30- lim(select(evtdown,nntap0 - 1,select(evtup,nntap0 + 1,nntap0)),Tmin,Tmax)
31- ! set event
32- event(0,evtdown,'name=this dtime=0. value=tapdown  variable=nntap0')
33- event(0,evtup  ,'name=this dtime=0. value=tapup    variable=nntap0')
34- ! Check the difference
35- tstop  = picdro({abs((u*nntap0/nntapin)-v0) < 0.01},3.0,0.0)
36- evtstop  = picdro(evtstop>0.and.t>20,0.0,0.0)
37- event(0,evtstop,'name=stoptap dtime=0. value=nntap0  variable=nntapin')
38- check=(u*nntap0/nntapin)
39- vardef(Tmin)='p.u.';'Min Tap Position'
40- vardef(Tmax)='p.u.';'Max Tap Position'
41- vardef(d)='%';'LTC half volt deadband'
42- vardef(tdelay)='s';'Delay between 2 subsequent stap change'
43- vardef(umin)='pu';'Min Voltage'
44- vardef(umax)='pu';'Max Voltage'
```

The DSL code can be mapped to the example in Fig. 3.12 provided to illustrate how the LTC's tap position can be controlled.

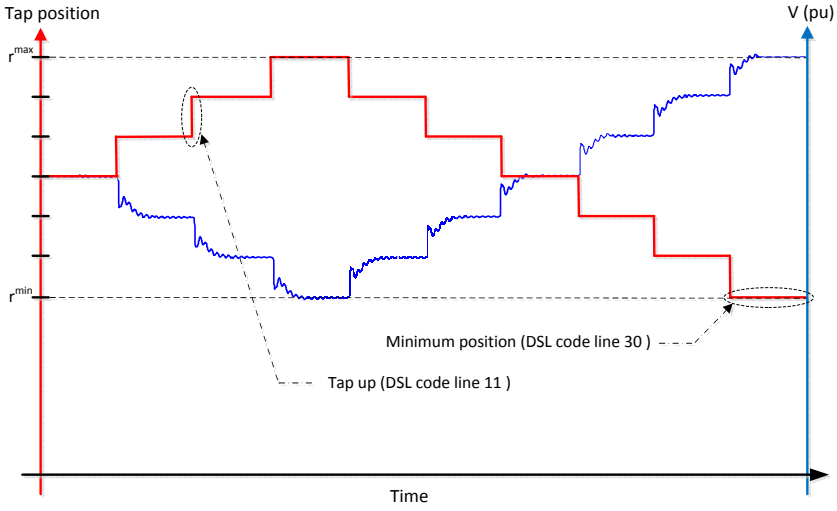

Figure 3.12: Example of LTC's tap position movement

From the code shown above, lines 1 - 6 indicate the initial settings for voltage level and transformer's tap position. Lines 8 - 12 represent the movement of tap position. The example shows, in Fig. 3.12, that the code in line 11 implements the first condition described in (3.5). Next, the code in line 14 - 22 represent the first tap movement. The code in lines 24 -25 describes how the subsequent taps are performed at a constant time where lines 27 - 28 represent the DSL programming requirement in order to move tap up or down. Code in line 30 is implemented to check the tap position reaches the minimum limit as shown in Fig. 3.12. The comparison between the controlled voltage and reference voltage described in (3.5) is performed by the DSL code in lines 35 - 38. Meanwhile, code in lines 39 -44 is for setting parameter values such as minimum tap position or LTC's half deadband.

- A *load restoration model* in this thesis is a generic type self-restoring load in which load dependencies on terminal voltages exhibit power restoration characteristics. Generic load models can be categorized into two types which are *multiplicative* and *additive*, in these models the load state variable is multiplied and added to a transient characteristic. In this study, a multiplicative generic load model is selected, the load power is given by [81]:

$$P = z_P P_0 \left(\frac{V}{V_0}\right)^{\alpha_t} \tag{3.7}$$

$$Q = z_Q Q_0 \left(\frac{V}{V_0}\right)^{\beta_t} \tag{3.8}$$

where z_P and z_Q are dimensionless state variables associated with load dynamics and $z_P = z_Q = 1$ in steady state.

Moreover, the dynamics of the multiplicative model are described by:

$$T_p \dot{z_P} = \left(\frac{V}{V_0}\right)^{\alpha_s} - z_P \left(\frac{V}{V_0}\right)^{\alpha_t} \tag{3.9}$$

$$T_Q \dot{z_Q} = \left(\frac{V}{V_0}\right)^{\beta_s} - z_P \left(\frac{V}{V_0}\right)^{\beta_t} \tag{3.10}$$

where T_P and T_Q are restoration time constants for active and reactive load, respectively. The steady state active and reactive load-voltage dependencies are characterized by α_s and β_s, respective. Meanwhile, the transient active and reactive load-voltage dependencies are characterized by α_t and β_t, respectively. The load restoration model implemented in DIgSILENT for this study is shown in Fig. 3.13. In this figure (for active load), Block 1 and 2 represent the first and second term on the right-handed side of (3.9), respectively. The voltage V_0 is set to the voltage bus at initial condition (see Appendix) and the voltage V is the measured bus voltage. Other parameters such as α_s, α_t, and T_P (in Block 3) are defined by DSL programming as described in LTC section. The equation for reactive power load follows the same form.

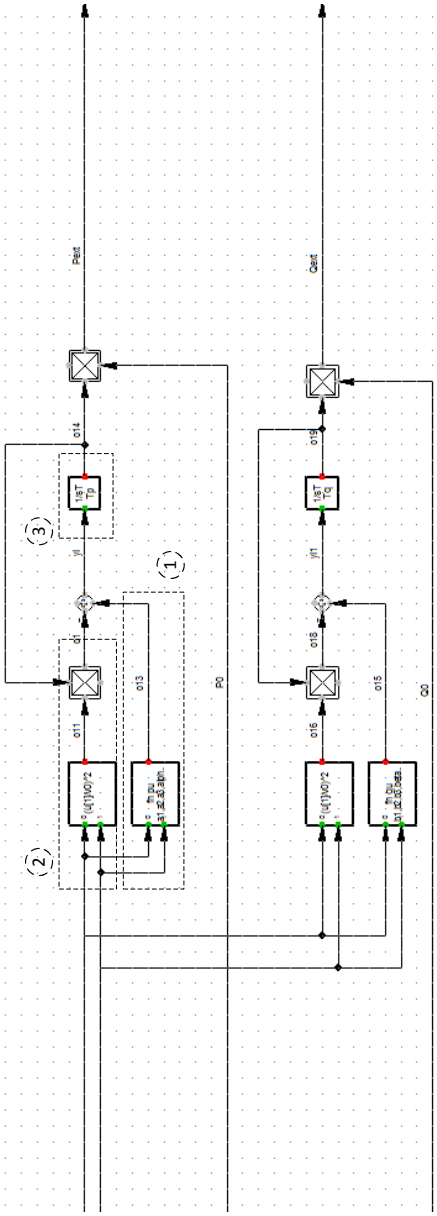

Figure 3.13: Load restoration model implemented in the DIgSILENT software

3.2 Simulation of voltage instability scenarios

As mentioned in Section 3.1.1, the "all-in-one" system can be used for simulating different instability scenarios by setting different parameters and initial (power flow) conditions. All possible instability scenarios can be generated with this test system. However, this thesis focuses only voltage instability scenarios, other types of instability such as frequency and dynamic instabilities are throughly documented in [85, 86].

Voltage stability is defined by the IEEE/CIGRÉ Joint Task Force on Stability Terms and Definitions [87] as *"the ability of a power system to maintain steady voltages at all buses in the system after being subjected to a disturbance from a given initial operating condition. It depends on the ability to maintain/restore equilibrium between load demand and load supply from the power system. Instability that may result occurs in the form of a progressive fall or rise of voltages of some buses"*. In the same document, voltage stability is categorized in two groups depending on the time frame in which the phenomena takes place, these are: *(i)* short-term voltage stability and *(ii)* long-term voltage stability. In this thesis, examples of short-term and long-term voltage instability are presented. In order to simulate these phenomena, some initialization settings must be fulfilled as shown in Appendix A.1.

3.2.1 Short-term voltage instability

In this system, there are several cases where short-term voltage instability conditions can be observed.

Case 1: One of the transmission line between Bus 1 and 3, and the generator at Bus 2, are disconnected at t = 1 sec

The voltage at Bus 3 drops to acceptable levels as well as the motor speed, if there is only one line trip (see Fig. 3.14a and Fig. 3.15a). However, the disturbance is too severe for the system to remain stable when both components are tripped. This leads to a dramatic drop in the motor voltage and speed (see Fig. 3.14b and Fig. 3.15b). In addition, Fig. 3.16 shows the power consumed by the motor for both situations.

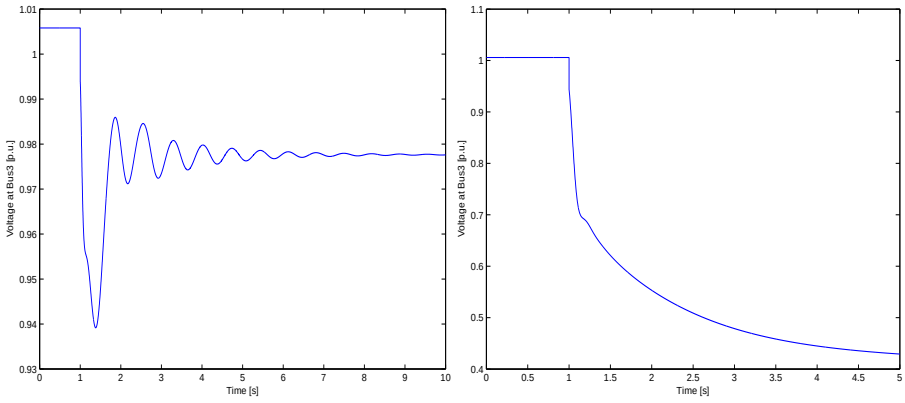

(a) Only L1-3 is tripped (b) Both L1-3 and Generator are tripped

Figure 3.14: Voltage at Bus 3

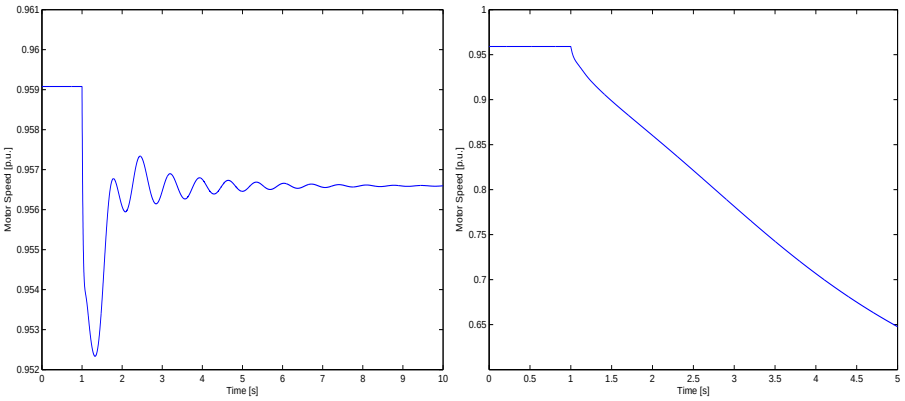

(a) Only L1-3 is tripped (b) Both L1-3 and Generator are tripped

Figure 3.15: Motor speed

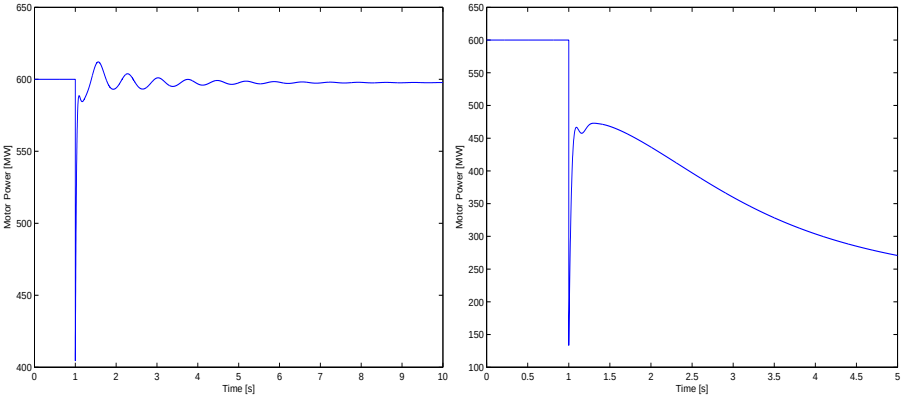

(a) Only L1-3 is tripped (b) Both L1-3 and Generator are tripped

Figure 3.16: Motor Power consumption

Case 2: Three-phase fault at t = 1 sec near Bus 3 and clearing by the trip of Line L1-3

A fault is cleared at different times: *(i)* t = 1.36 sec and *(ii)* t = 1.37 sec. For clearing time t = 1.36 sec, the fault lasts for 0.26 sec, which is short enough to preserve stability and hence the system returns to a new equilibrium. Meanwhile, for clearing time t = 1.37 sec, the fault lasts too long and the motor (load at Bus 4) stalls, causing voltage collapse. Figure 3.17 and 3.18 show a comparison of the voltage at Bus 3 and the motor speed for the two fault clearing time cases, t = 1.36 sec and t = 1.37 sec, respectively.

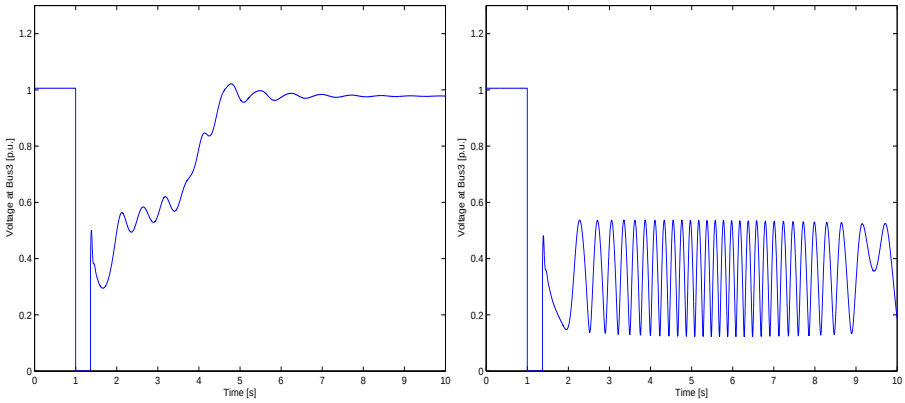

(a) t = 1.36 sec (b) t = 1.37 sec

Figure 3.17: Voltage at Bus 3

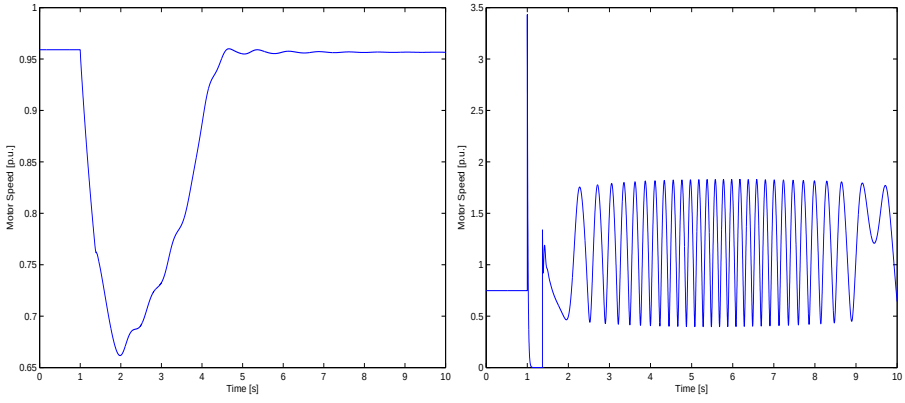

(a) t = 1.36 sec (b) t = 1.37 sec

Figure 3.18: Motor speed

3.2.2 Long-term voltage instability

Similar to short-term voltage instability, there are several ways to observe long-term voltage instability conditions in this system.

Case 1: Higher load consumption at Bus 5

In this case, one of the transmission lines between Bus 1 and 3 is tripped at $t = 1$ sec. The overexcitation limiter (OEL) at the generator is triggered, thus generator's voltage is no longer controlled. Consequently, the LTC unsuccessfully attemps to restore the load bus voltage, until reaches its lower limit. Figure 3.19a shows the load bus voltage decreases stepwise accordingly. This is a long-term voltage instability scenario compared to a case when load is decreased from 1500 MW and 150 MVAR to 1200 MW and 0 MVAR, shown in Fig. 3.19b. The load tap changer (LTC) is capable of restoring the voltage at the load bus within its deadband (see Fig. 3.19b). This forces the power system to operate at a new equilibrium point. In addition, Fig. 3.20 and 3.21 show the transformer tap position and field current of the generator at different load levels.

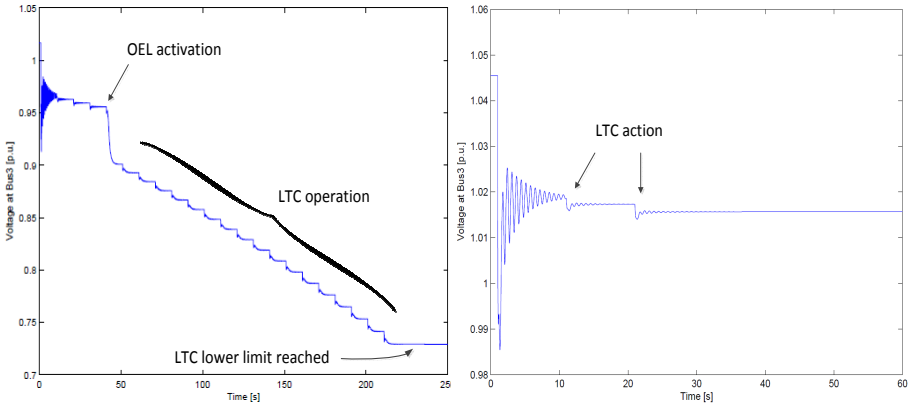

(a) Load = 1500 MW and 150 MVAR (b) Load = 1200 MW and 0 MVAR

Figure 3.19: Voltage at Bus 3

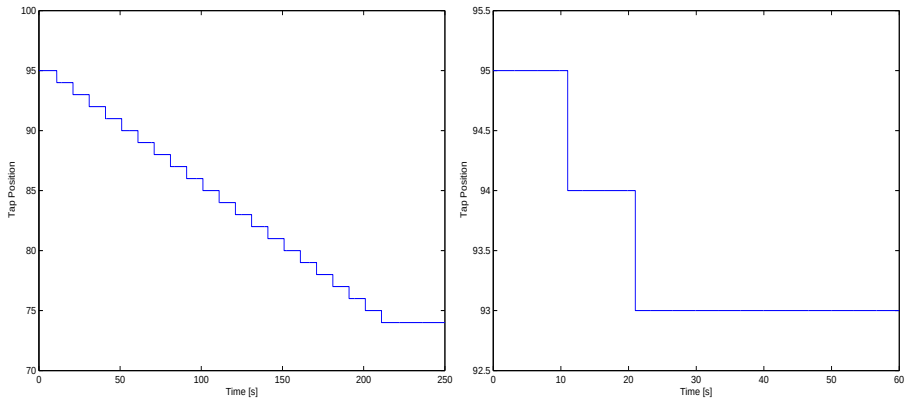

(a) Load = 1500 MW and 150 MVAR (b) Load = 1200 MW and 0 MVAR

Figure 3.20: LTC Transformer tap position

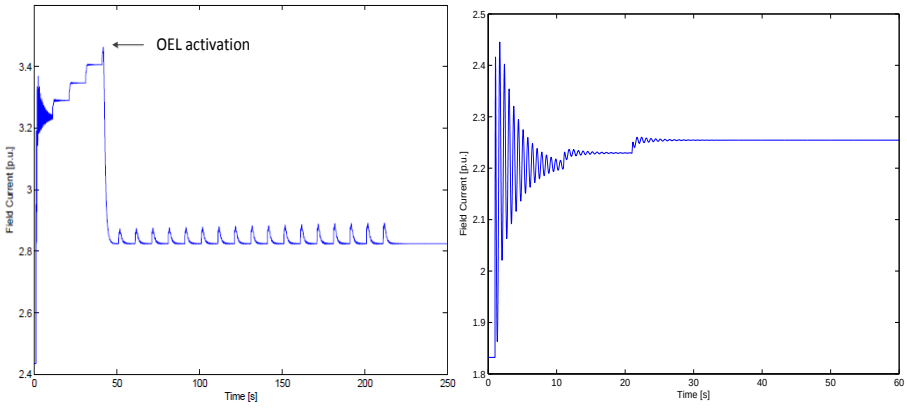

(a) Load = 1500 MW and 150 MVAR (b) Load = 1200 MW and 0 MVAR

Figure 3.21: Generator field current

Case 2: Higher power generation

This case is similar to Case 1 (which is a line trip at t = 1 sec) however, here power generation is changed from 300 MW to 450 MW. In this case, long-term voltage instability triggers an instability of the short-term dynamics in the form of a loss of the generator's synchronism. Figure 3.22 shows the dynamic response of the system from which it can be observed that the generator looses synchronism at t = 110 sec. Short-term dynamics are triggered about t = 100 sec when the machine is forced out of equilibrium.

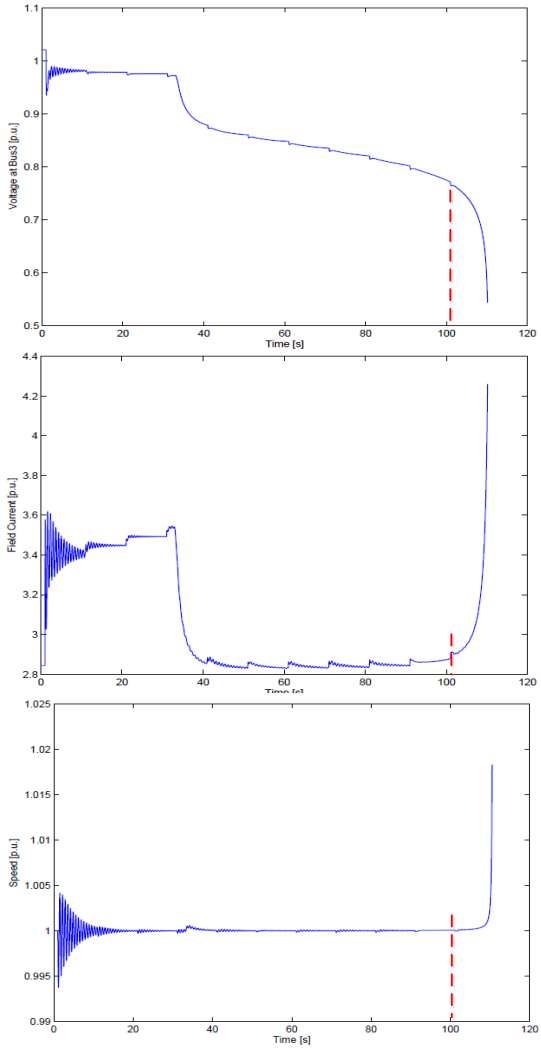

Figure 3.22: Voltage at Bus 3 (top), Field current (middle), Gen-Speed (bottom)

Case 3: Higher motor load

This case is similar to Case 2, however, part of the load at Bus 5 is shared with the motor load at Bus 4 while power generation is kept at 300 MW. In this case, long-term voltage instability triggers an instability of the short-term dynamics resulting in both loss of generator's synchronism and motor stalling at t = 47 sec. Short-term dynamics are initiated about t = 27 sec when the OEL is activated. This results in an uncontrolled field voltage which is not able to restore the voltage at Bus 3. Finally, the lack of reactive support prompts short-term angular instability at t = 35 sec which initiates the final system collapse.

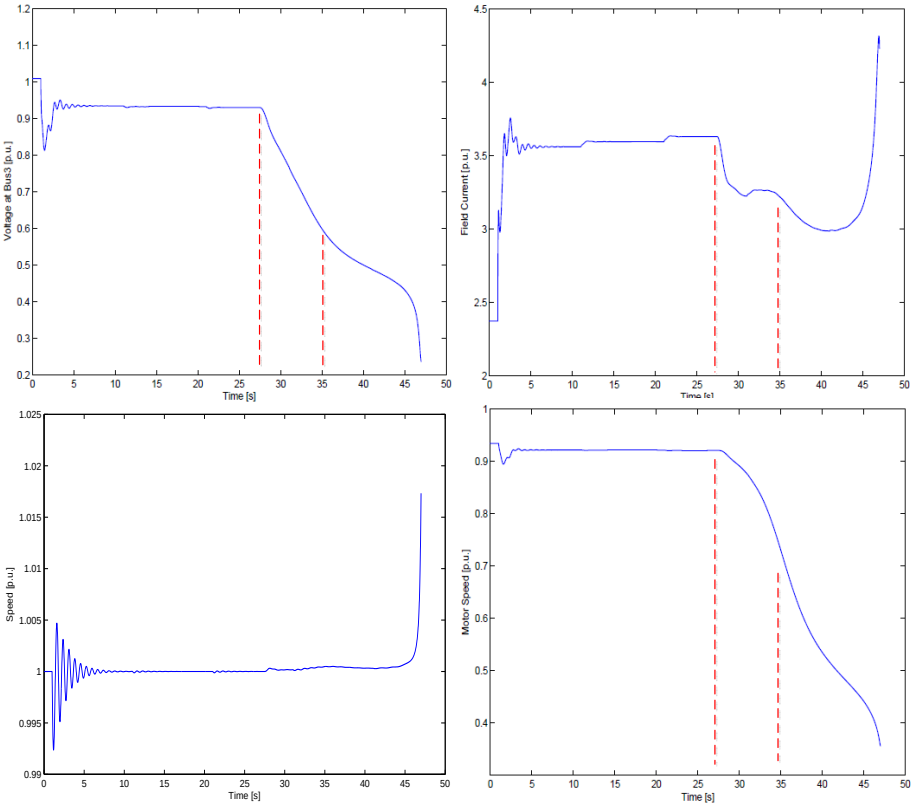

Figure 3.23: Voltage at Bus 3 (top-left), Field current (top-right), Gen-Speed (bottom-left) and Motor-Speed (bottom-left)

3.3 Architecture and components of the SmartTS-Lab

This section describes the real-time hardware-in-the-loop platform used to carry out experiments in this thesis. The main architecture hardware and software implementation are described.

3.3.1 Overall architecture

The purpose of SmarTS-Lab is to develop different wide area measurement, protection and control applications which exploit PMU data, that can be utilized by transmission system operators and utilities for safe, efficient and reliable operation of power systems. This includes the design and validation of real-time applications involving deterministic computers that can be used to implement wide-area controllers [88], in particular for wide-area power oscillation damping [89], and the coordination of real-time controllers with protective relays [31], which requires the implementation of synchrophasor, station and process bus for data exchange. With such aim it becomes necessary to include in the architecture design and implementation, the use of actual physical devices, and *ad hoc* communication networks and application software development hosts. This section describes the conceptual architecture, implementation, and major components used in the laboratory.

Figure 6.1 depicts the overall architecture of SmarTS Lab. Measurement and data streams are indicated, non-exclusively, as follows: blue for WAMS, red for WAPS, and green for WACS applications. Solid lines indicate measurement streams, while dotted lines indicate digital data streams over Ethernet. An RT simulator is used to emulate the power system and to interfacing with physical devices. Data for WAMS applications is streamed from PMUs into an *ad hoc* communication network, where it is sent to a WAMPAC application host platform which includes PDCs. WACS applications stream data either directly to the simulator over Ethernet or to external controllers that can drive models in the RT simulator or low-powered physical devices. As for WAPS applications, the simulator streams data using IEC 61850, using sampled values to communicate with the process bus or GOOSE for the Station Bus, these in turn communicate with the protective relays and the WAPS applications.

3.3.2 Hardware and software implementation

The SmarTS-Lab currently deployed at KTH is comprised of several components. These include hardware components and software components, which are different PDCs and application host platforms that allow users to develop applications for wide area measurement based on the data acquired from these hardware components.

The current laboratory set-up consists of both software and hardware components, as shown in Figure 3.25, where the current implementation as of December 2011 is shown[1]. (1) The power system is simulated using the eMegaSim Real-Time Simulator from Opal-RT [90], capable of providing real-time analog and digital I/Os for its interfacing with

[1] Refer to Fig.3.25 in the following description to map to the numbers listed to the photograph.

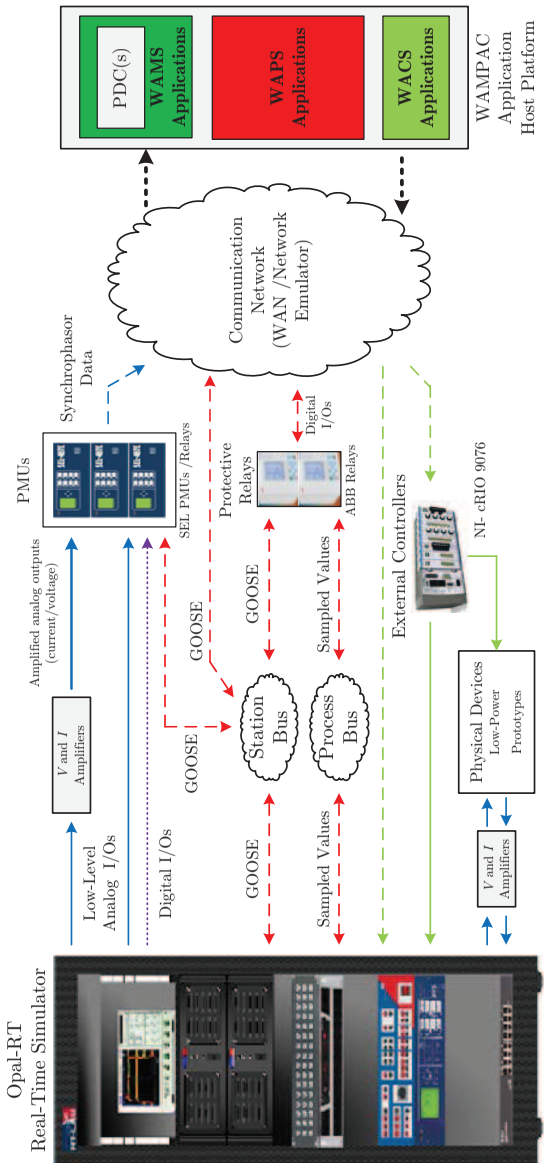

Note: Measurement and data streams are indicated, non-exclusively, as follows: blue for WAMS, red for WAPS, and green for WACS applications.

Solid lines indicate measurement streams, while dotted lines indicate digital data streams over Ethernet.

Figure 3.24: Overall Architecture of SmarTS Lab.

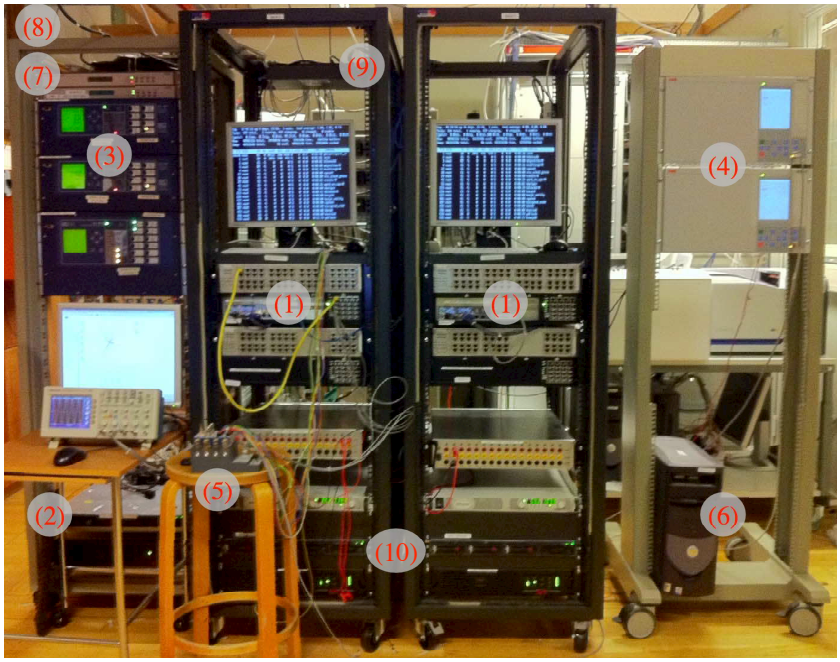

Figure 3.25: Hardware Implementation of SmarTS Lab as of Dec. 2011.

Table 3.1: RT Simulator Main Features

Features	Description
Number of Cores	2 HIL boxes each with 12 Intel i7 3.3 GHz cores
Analog Inputs	32 (± 10mA and ± 100V)
Analog Outputs	128 (± 10mA and ± 16V)
Digital Inputs	128 (± 4V to ± 30V and 6mA)
Digital Outputs	128 (± 4V to ± 30V, sink up to 100 mA current)
HVDC Interface	16 Digital outputs (250V DC and up to .125 A current)
Communication	IEC 61850-8-1 (GOOSE) and IEC 61850-9-2 Sampled Values through two separate Ethernet ports.

hardware components. (2) The WAMPAC application host platform includes the PDC and takes the form of either proprietary software solutions from Schweitzer Engineering Laboratories (SEL) and/or solutions built in-house [91].

The WAMPAC application host platform interfaces with the RT simulator through the following hardware components: (3) protection relays with embedded PMU functions

from Schweitzer Engineering Laboratories (SEL) [92], (4) line differential protection relays from ABB with Optical Ethernet Module (OEM) for station and process bus implementation [93], current and voltage amplifiers from Megger [94] (not shown), (5)compact Reconfigurable Input/Output (cRIO) real-time controller from National Instruments, (6) a PC with a communication networks emulator and (7) a GPS substation clock from Arbiter Model 1094B [95] fed by (8) a GPS antenna which provides time stamping to the PMUs and IEDs.

The IED's stream data over TCP/IP using a (9) network switch, which also allows users to transfer models to the real-time targets from four independent workstations (not shown). (10) Two servers allow access to the real-time simulator from other locations within KTH. There are additional devices that provide ancillary services for the facility which are not listed here.

3.3.3 Real-time simulator

It is costly to adopt a real power system for an experimental purposes, and PMU data from utilities is not always available. Thus, a development and testing operates that performs as close as possible to real existing networks is adopted for the experiments involving *real* PMU data. The RT simulators help to model power systems and then simulate them, with very high resolution and small time-steps, to accurately emulate the behaviour of actual power systems. Here, the eMEGAsim real-time digital simulator [90] was procured from Opal-RT and deployed in the lab. The major features of the simulator are shown in Table 3.1. With this configuration, the RT simulator allows for the simulation of large power grids while including detailed models of HVDC, FACTS, wind farms, etc., and hardware-in-the-loop interfacing of physical devices.

The test system as shown in Fig. 3.1 is also implemented in the RT simulator. The reason of having the test system in two test platforms, the positive-sequence-based (PSB) simulatior (DIgSILENT PowerFactory) and Real-time Hardware-In-Loop (RT-HIL), is to guarantee that the proposed algorithms will perform robustly when the "real" PMU data is involved. PSB simulations may exclude the effect of switching devices and events on measurements, ambient behavior, noise and outliers in actual PMU data, as it will be shown in Chapter 4.

3.3.4 Physical devices and their interface with the RT Simulator

The overall interconnection of the Opal-RT simulator with the PMU/relays and vendor softwares is shown in Fig. 6.3. The analog outputs of the simulator are low level voltage and current signals. These analog outputs of the simulator are connected to the current and voltage inputs of the amplifiers procured from Megger. The amplifiers step up the low level signals to the level acceptable to be fed to the protection relays and PMUs (i.e. 100 V and 1 A). These amplified three-phase voltage and current are directly fed to the current transformer (CT) and voltage transformer (VT) inputs of the PMUs and protection relays from SEL (SEL-421 distance relay and SEL-487E transformer differential protection

relay), ABB (two RED-670 Line Differential Relays) and Arbiter (Model 1133A Power Sentinel).

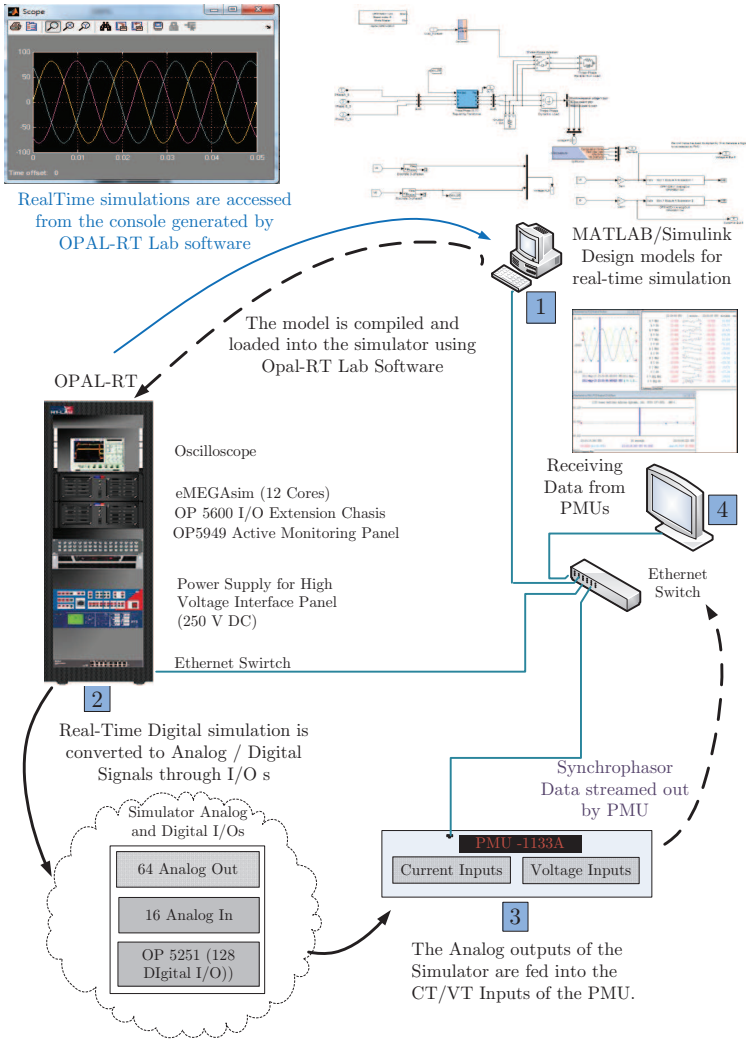

Figure 3.26: Model-to-Data Work-Flow for Generating Real-Time Data Streams

Vendor specific softwares such as SEL's AcSELerator Quickset, ABB's PCM 600 and Arbiter's Power Sentinel are used to configure the PMUs and protection relays to update CT and VT ratios, selecting measurements to be included in synchrophasor data streamed out of the PMUs, activating the protection functions (e.g., overcurrent, distance, etc.) and developing a substation architecture based on GOOSE messages. In this thesis, only one

aspect of the problem which is noise and outliers by having PMUs in the loop is considered. Several practical aspects such as problems in communications networks (e.g. package delay and loss) or impact of measurement channels (e.g. PTs, CTs, measurement cables) are not considered but will be investigated in future work.

The modeling platform for Opal-RT real-time simulator is MATLAB/ Simulink SimPowerSystems which can be modified using libraries provided by Opal-RT. The software interface of the Opal-RT simulator known as RT-Lab allows the users to build, compile and execute the MATLAB/Simulink SimPowerSystem models in real-time. This overall workflow to obtain data streams from building a model to receiving real-time data is shown also in Fig. 6.3. More detailed information about the SmarTS-Laboratory can be found in [96].

Chapter 4

Voltage Stability Monitoring using Sensitivities Computed from PMU data

This chapter describes the first approach to mitigate voltage instabilities. This first approach utilizes synchrophasors in order to determine when the system is going towards a voltage instability and also to trigger the operation of HVDCs to relieve the system's stress. Simultaneously with the activation of the HVDC controller input signals are selected among those available from the PMUs. The approach consists in using voltage sensitivities from synchrophasor data for voltage stability monitoring. In addition, a visualization approach that can be implemented in wide-area early warning systems uses these sensitivities. This chapter also proposes an algorithm that utilizes the computed voltage sensitivities to cooperate with VSC-HVDCs so that voltage instability can be avoided.

4.1 Wide-area voltage stability monitoring concepts

Voltage instability detection methods can be categorized in to the following branches: local [97, 98] versus wide-area measurement [99] or synchronized [100] versus non-synchronized [101] approaches. These categories aid in identifying how the accumulated measurement information is used. To have a complete system awareness, it appears that the entire power system state needs to be reconstructed from synchrophasor measurements and other data [102], or that different indices for different system components need to be computed to determine instabilities [100].

PMU data has been adopted to develop indicators to detect voltage instability type. However, the pre-processing method in order to compute accurate and robust indicators (if they are to be used for control room applications) is not well-established. For example, this issue is avoided in [103] by extracting the slope of the sensitivities instead of sensitivities themselves. To achieve this, a large parcel of data is needed, delaying the delivery of information to a wide-area early warning system. The pre-processing issue is partly addressed in [104] by using filtering to separate the quasi-steady state components of simulated data; however, the approach is limited because the simulated data does not contain

the correct features observed from PMU data and it is not capable to cater for inconsistencies and errors embedded in them. Hence, a filtering methodology for robust voltage sensitivity computation is proposed in Section 4.3.

It can be argued that wide-area early warning systems could contain monitoring tools that display voltage stability indicators; however, it is not clear how to present this information to operators so that it is easy to understand. Therefore, the ultimate goal of this thesis is to create voltage stability (VS) indicators by computing sensitivities and presenting them in ways that are simple to comprehend.

4.2 PV and QV sensitivities as VS indicators

The use of voltage sensitivities for voltage instability detection has been proposed in [103–106]. In this thesis a similar approach is adopted, with the main difference being that the Jacobian matrix directly from the measurements instead of matching these measurements to a Jacobian. Furthermore, the Jacobian utilized here varies from the standard power flow Jacobian in that it considers every measured branch individually. To this end, individual components of sensitivities are constructed from the power flow in each transmission line (one direction) instead of injected power flow of the bus (summation of power flow). Secondly, the lines' power flow are calculated solely based on measured voltage and current phasors. This means that the effects of shunt capacitances of the transmission line (in the case of medium and long lines) of the nominal π-model are also included.

The transmitted power on the line can be expressed as follows:

$$\begin{aligned} \overline{S}_{ik} &= V_i e^{j\delta_i} \{I_{ik} e^{j\delta_{ik}}\}^* \\ P_{ik} &= Re(\overline{S}_{ik}), \quad Q_{ik} = Im(\overline{S}_{ik}) \end{aligned} \tag{4.1}$$

where
V_i = voltage magnitude at Bus i.
I_{ik} = current magnitude from from Bus i to Bus k.
δ_i = voltage angle at Bus i.
$\delta_{ik} = \delta_i - \delta_k$.

$\overline{S}_{ik}$ = complex power transmitted from Bus i to Bus k.
P_{ik} = transmitted real power from Bus i to Bus k.
Q_{ik} = transmitted reactive power from Bus i to Bus k.

From (4.1) it follows that the real and reactive power flows through the transmission lines can be calculated directly regardless the system's model and parameters (differently from [104, 107]). Normally, sensitivites in the Jacobian matrix are constructed as a production of partial derivatives. However, the proposed sensitivites in this thesis are computed discretely as the ratio of differences in two consecutive computation points from measured voltages and powers which are constructed as follows:

$$\text{Sensitivities} \Rightarrow \begin{bmatrix} \delta_{P_{ik}}(t) & V_{P_{ik}}(t) \\ \delta_{Q_{ik}}(t) & V_{Q_{ik}}(t) \end{bmatrix} \tag{4.2}$$

where
$\delta_{P_{ik}}(t) = \delta_i(t) - \delta_i(t-1)/P_{ik}(t) - P_{ik}(t-1) = \Delta\delta_i/\Delta P_{ik}$
$V_{P_{ik}}(t) = V_i(t) - V_i(t-1)/P_{ik}(t) - P_{ik}(t-1) = \Delta V_i/\Delta P_{ik}$
Similar expressions can also be derived for $\delta_{Q_{ik}}$ and $V_{Q_{ik}}$.

In this thesis, only $\Delta V_i/\Delta P_{ik}$, and $\Delta V_i/\Delta Q_{ik}$ are studied and used as voltage instability indicators. Each individual component of the sensitivities is obtained from the PMU data. The values of these sensitivities can aid in assessing voltage instability with the considerations below.

1. The sensitivities are consistently at a low-positive value (or negative depending the current measurement direction) with the assumption of steady-state operation. This indicates that a system operates far away from a voltage instability condition.

2. The value of the sensitivities will increase positively (or negatively) when a system is stressed. This denotes a system is moving towards a "weak" operating condition; thus, this is a trend in the development of the voltage instability.

3. The value increases abruptly to very high positive (or negative) and switches sign in the case of a lack of reactive power support for $\Delta V_i/\Delta Q_{ik}$ or when the maximum power transfer is reached for $\Delta V_i/\Delta P_{ik}$. This depicts an unstable condition which consequently leads to voltage collapse.

4.3 Filtering methodology

The proposed filtering method used in this study is similar to the low pass part of the complementary filter in [108]. There are two restrictions that differentiate this filter from an ordinary low pass filter[1] which is affected by discrete events that occur in power systems. This filter screens out only high frequency noise. Its aim is to smooth all signals before computing voltage sensitivities. Figure 4.1 shows a block diagram of the processing method. It starts by taking raw data and applying a first-order high pass filter with cut-off frequency of 1.37 Hz. This cutoff frequency corresponds to the dominant oscillatory component in the system. Then, the original data is subtracted by the filtered data. By applying this subtraction, electromechanical oscillations, high frequency noise and large outliers are removed from the original signal, this is shown in Fig. 4.1 with a (i); signals from this step are termed *"Filtered"* signals.

An additional step is to apply a moving average (MA) window by computing the mean and standard deviation of the filtered signal. The size of the MA window is designed to

[1] 1) the high pass filter must have left-right symmetry (i.e., a zero or linear phase), and 2) the impulse must be added at the center of symmetry [109].

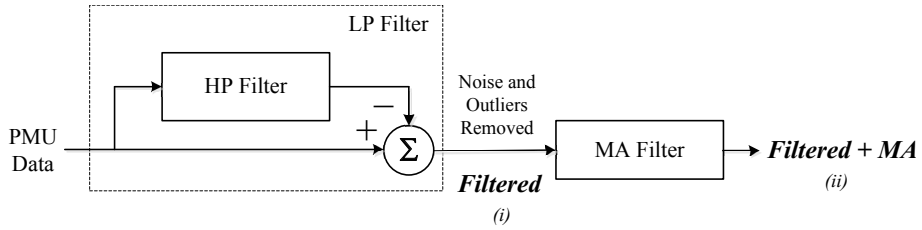

Figure 4.1: Proposed filtering approach for pre-processing data to compute voltage stability indicators.

cover the data which deviates from the mean value by three standard deviations of the filtered signal, which originally has the same size as the predefined finite-size window mentioned earlier. Then, this predefined finite-size of the MA window is decreased when MA algorithm detects the data exceeds the threshold standard deviation. This process is repeated over the entire data set. As denoted in Fig. 4.1 (*ii*), these signals are termed *"Filtered+MA"*. The MA aids to increase the smoothness of the computed sensitivities.

There are two ways to filter the signal which are *"post-event"* and *"near real-time"* approaches. In the *post-event* approach the time-synchronized data is gathered from different locations for a particular time range, and the entire set of data is filtered. Here the start-up and ending transients of the filters are minimized by matching the initial and final conditions. This is accomplished by reversing the filtered data sequence, and process the input data in both the forward and reverse directions. On the other hand, the *"near real-time"* approach processes the input data only in the forward direction. The start-up and ending transients of the filters for this approach can be eliminated by buffering data into a predefined finite-size window. The data buffer for eliminating the start-up transient can be constructed by creating parcels[2] which contains the steady state values of each variable[3]. Then, the data in the buffer is replaced with measurements, one sample at a time, always maintaining a finite-size window full. The filtering process is applied to each data window, which is updated with each new sample. Finally, the ending transient of the filter is eliminated by using the last measured samples in a data buffer to maintain the size of the data window (in a similar fashion as described for the other parcels used).

In this thesis, the proposed filtering method is validated by examining its performance under different types of voltage scenario. Numerical examples are given in Chapter 5, where the methodology is applied to both the DIgSILENT PowerFactory simulation (of 0.001 sec step-size) and the PMU measurement data (50 samples per second) from both RT-HIL simulations and the Norwegian grid.

[2]These parcels are vectors of data which contain in each entry the steady state values of its corresponding variable.

[3]When using models this steady state value can be obtained from the power flow solution.

4.4 Utilizing sensitivities for VSC-HVDC control to mitigate voltage instability

The $\Delta V_i/\Delta P_{ik}$ and $\Delta V_i/\Delta Q_{ik}$ sensitivities can be used to generate the early-warning and final alarm signals for system operators. These two signals are derived by comparing the computed $\Delta V_i/\Delta P_{ik}$ and $\Delta V_i/\Delta Q_{ik}$ sensitivities with the pre-defined early warning and final alarm thresholds. If the sensitivities (denoted as "**a**" in Fig. 4.2) are less than the the warning threshold (denoted as "**b**"), a system is in normal operating conditions. In case the value of sensitivities is greater than warning threshold but less than the alarm threshold (denoted as "**c**"), it indicates that a system operates in a weak condition. Finally, a system approaches endangered condition in case the sensitivities value is greater than the alarm thresholds. The logic behind warning and final alarm signals activation can be illustrated as shown in Fig. 4.2.

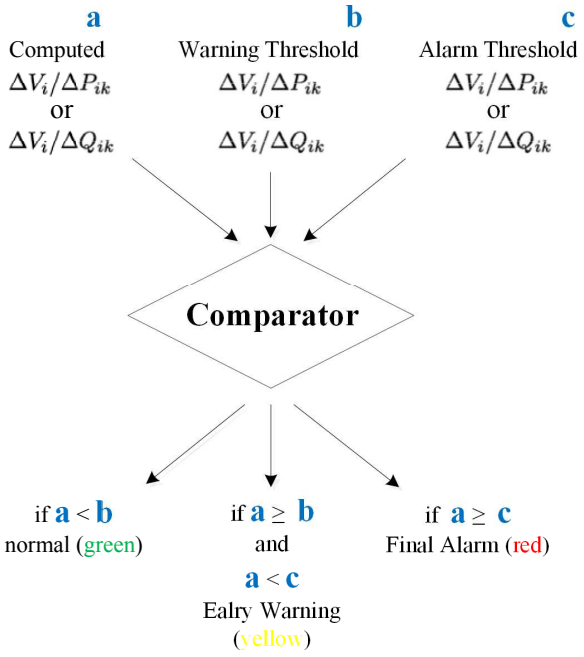

Figure 4.2: Generation of early warning and alarm signals

In order to mitigate voltage instabilities, an early warning signal described earlier can be adopted to trigger the change of power transfer through an VSC-HVDC and its control modes of operation. Fig. 4.3 shows a block diagram of the proposed method to adapt the HVDC control.

As seen from Fig. 4.3, the method starts by gathering synchronized voltage and current phasors from different locations. Then, these phasors are used to compute sensitivities as

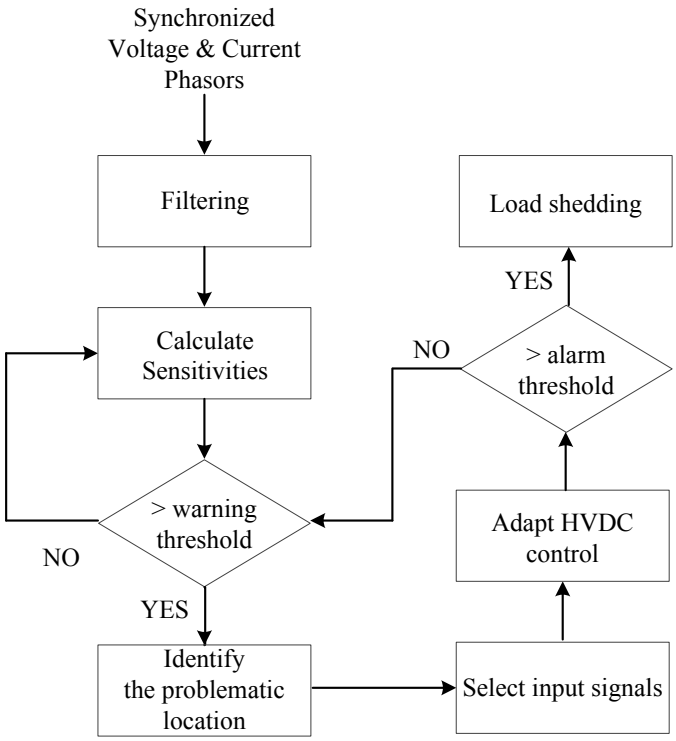

Figure 4.3: Proposed method to mitigate voltage instability

described in (4.1) and (4.2). Next, the computed sensitivities ($\Delta V_i/\Delta P_{ik}$ and $\Delta V_i/\Delta Q_{ik}$) are compared with pre-set values of early warning signals to determine the locations leading to voltage instability. After problematic locations have been found, system quantities are selected as input signals to change the control mode and/or operational reference of the VSC-HVDC. The VSC-HVDC that is used in this thesis is the built-in model available from the PowerFactory [84] software's library. The original model is modified by implementing an additional stabilizing control comprised by a PI-controller (indicated by dash box in Fig. 4.4) to change the active and reactive reference power of the VSC-HVDC. This allows the use of PMU signals as controller inputs.

In the case of reactive power ($\Delta V_i/\Delta Q_{ik}$ signal), the input signal of this PI-controller is the measured voltage level of the problematic location indicated by computed sensitivities while the voltage reference value (U_{ss} in Fig. 4.4a) is the voltage value when an early warning is triggered. In case of active power, the input signals are measured voltage angles at Bus i and k (which are selected w.r.t. the sensitivities $\Delta V_i/\Delta P_{ik}$), while the angle reference value (θ_{ss} in Fig. 4.4b) is the angle different between Bus i and Bus k when an early warning is triggered. The required controller input signals are assumed to be available from PMUs.

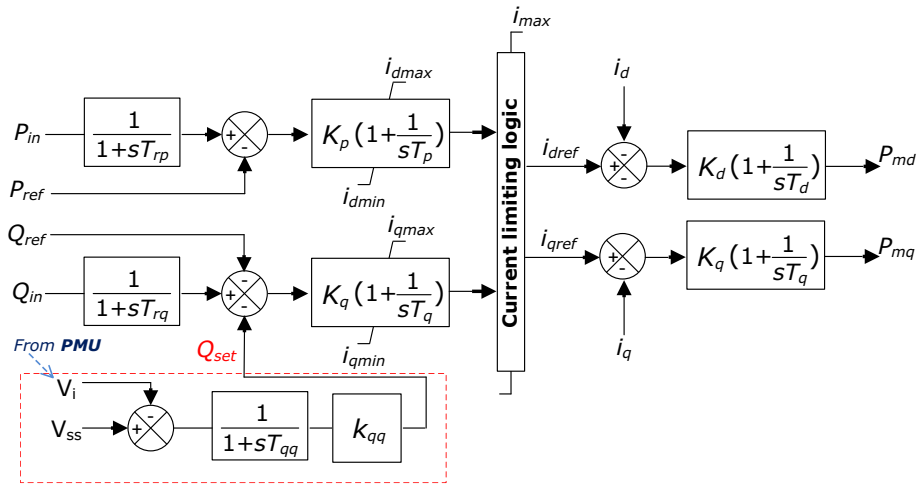

(a) HVDC Control Scheme activated by $\Delta V_i/\Delta Q_{ik}$ signal, control using PMU signal V_i

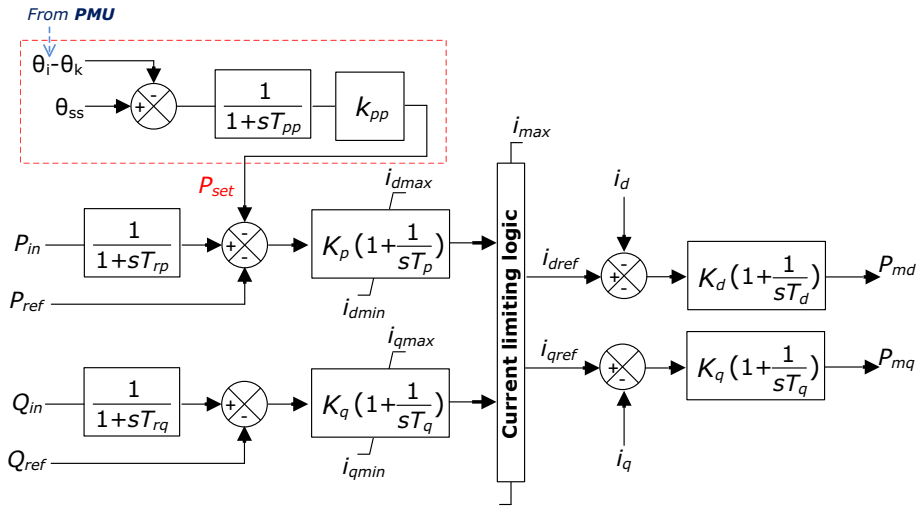

(b) HVDC Control Scheme activated by $\Delta V_i/\Delta P_{ik}$ signal, control using PMU signal θ_i and θ_k

Figure 4.4: VSC-HVDC Control Scheme activated by $\Delta V_i/\Delta Q_{ik}$ and $\Delta V_i/\Delta P_{ik}$ with PMU input signals

Finally, if sensitivities approach values near the final alarm threshold, a load shedding scheme has to be activated to disconnect loads. However, this thesis does not present the load shedding scheme. The proposed load shedding will be developed in future work. An example of load shedding strategies can be found in [110]. In addition, parameters for the PI-controller such as gain and time constant values are selected regardless of particular

response characteristics of the VSC-HVDC. Different controller parameters can provide different rise time, overshoot, time-to-peak, or steady-state error respecting the same physical limits of VSC-HVDC. This paper only focuses on how to utilize sensitivities in order to mitigate voltage instabilities. The important issue of control tuning will also be addressed in future work.

Chapter 5

Case Studies on Monitoring and Voltage Instability Mitigation using Sensitivities

This chapter provides numerical examples of how voltage sensitivities computed from synchrophasor data can be used to detect voltage instability. A visualization method is also demonstrated for wide-area voltage stability monitoring purposes. Moreover, this chapter shows how voltage instability can be achieved by coordinating synchrophasor-based sensitivities and the use of PMU measurements for VSC-HVDC control.

5.1 Case studies on voltage stability monitoring and detection

The test system described in Chapter 3 is modified (see Fig. 5.1) by combining transmission line L1-3 and L1-3b. A modification is done so that the total impedance of these lines equals to the same as in the original system.

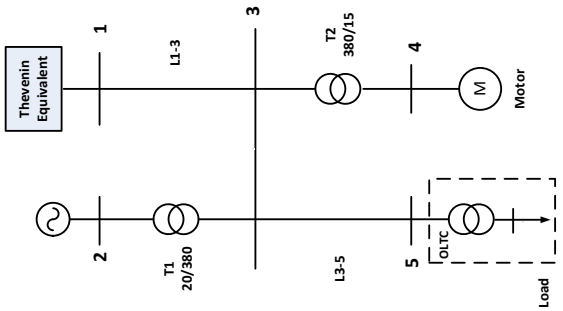

Figure 5.1: Test system used for generating voltage instability scenarios

The voltage instability scenario used for demonstration is implemented by increasing the load at Bus 5 of the test system shown in Fig. 5.1. Typical constant active and reactive

power models are used. The load is assumed to change as follows:

$$P_L = P_{Lo}(1 + \lambda) \tag{5.1}$$
$$Q_L = Q_{Lo}(1 + \lambda) \tag{5.2}$$

where P_{Lo} and Q_{Lo} are the initial base active and reactive powers, respectively, and λ is a varying parameter representing the loading factor.

5.1.1 Case 1: Load increase without OEL

Case 1.1: PSB simulation

As mentioned earlier, the load at Bus 5 is increased at $t = 70$ sec. The on-load tap changer (OLTC) tries to restore the voltage at the load bus within its deadband [81]. Since the load increases monotonically, the OLTC unsuccessfully attempts to restore the load bus voltage, until it reaches its lower limit. The load bus voltage then decreases stepwise accordingly and the system collapses at $t = 440$ sec (see Fig. 5.2).

The filtering approach and sensitivities computation (as described in Chapter 4) are applied in order to demonstrate advantages of the proposed method. Figure 5.2 and 5.3 show the difference between filtering and not filtering a voltage and the corresponding PV-curve at Bus 5, respectively. Figure 5.4 depicts the plot of a sensitivity ($\Delta V_5/\Delta P_{53}$) at Bus 5 that was obtained by using data from a DIgSILENT PowerFactory PSB simulation.

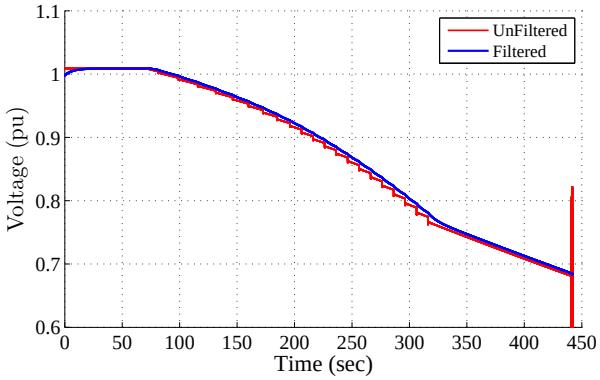

Figure 5.2: Filtered and Unfiltered Voltage at Bus 5 (PSB Simulation)

As mentioned in Chapter 4, the sensitivity ($\Delta V_i/\Delta P_{ik}$ in this case) can be used to generate an early warning alarm when its value changes from positive to negative; this occurs at $t = 400$ sec (while the system collapses at $t = 440$ sec). This early warning alarm can

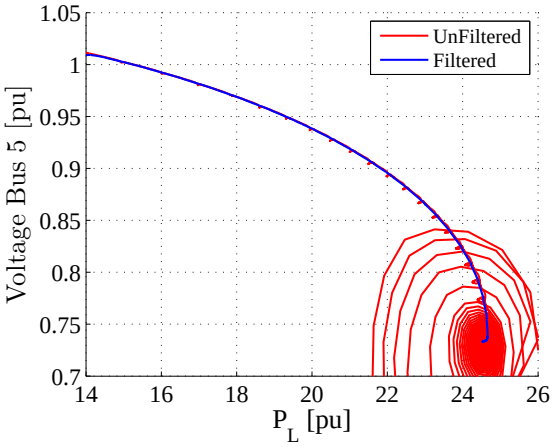

(a) PV-curve (Load Power vs Voltage Bus 5)

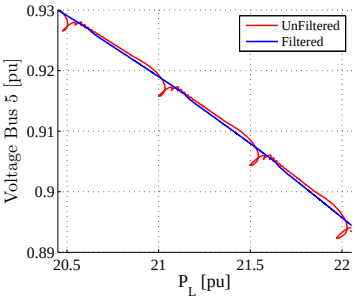

(b) Zoom of Fig. 5.3a

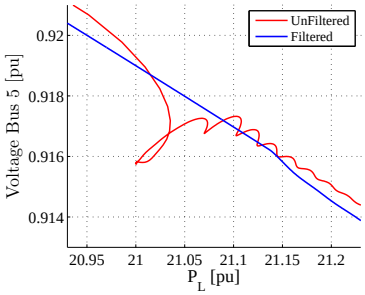

(c) Zoom of Fig. 5.3b

Figure 5.3: An example of filtered and unfiltered PV-curves.

be generated by setting a threshold value (e.g., $\Delta V_5/\Delta P_{53} = 0.08$); this allows detection before the sensitivity changes abruptly to a large positive value. This can be verified from Fig. 5.2. The spikes shown in green in Fig. 5.4 correspond to OLTC tap position changes. It can also be noted that the sensitivity calculated from the unfiltered data (green line) are vulnerable to OLTC tap switching and vary abruptly compared with those computed using data which has been filtered, or filtered + MA. Figure 5.4b shows that the "filtered+MA" approach provides a more robust result compared to the one without MA. However, these filtering methods (either with or without moving average window) introduce a small delay to the calculation ($\approx$ 5 sec for this experiment).

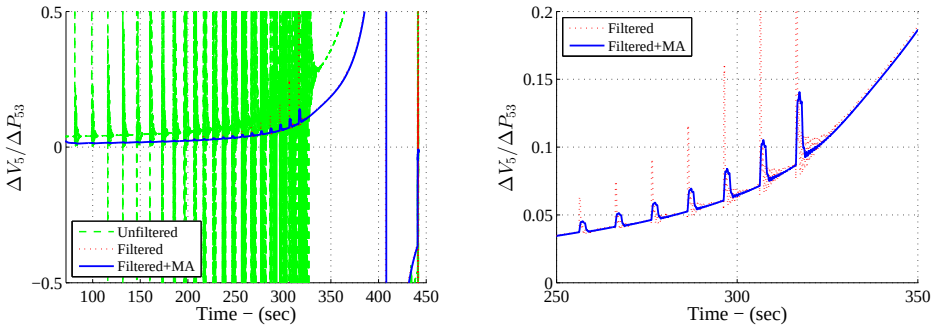

(a) $\Delta V_5/\Delta P_{53}$ (b) Zoom of Fig. 5.4 (without Unfiltered data plot)

Figure 5.4: Plot of calculated $\Delta V_5/\Delta P_{53}$ sensitivity at Bus 5 from filtered PSB simulation data.

Case 1.2: RT-HIL simulation

The same experiment is conducted in the laboratory using the RT-HIL approach, and the synchrophasors for Bus 5 are acquired. Figure 5.5 shows the voltage magnitude from the phasor streamed out from a SEL PMU. Note that the traces obtained from the PMU have significantly different characteristics than those from the PSB simulation (Fig. 5.2). Notice that Fig. 5.5 clearly contains not only electromechanical oscillations, but also noise, and outliers due to the switching of discrete devices whereas Fig. 5.2 does not contain most of these characteristics. To develop a robust wide-area monitoring application, these data features need to be considered.

Sensitivities computation results were obtained using PMU data, which are shown in Fig. 5.6. Here the spikes due to OLTC switching that appear in the computed sensitivities are much higher than those obtained using PSB simulation results. This is of natural occurrence with measurement devices when sampling a signal that has been subject to discrete switching. Moreover, there are other nuisances in the PMU data generated from the RT HIL simulator such as outliers and noise. The "filtering+MA" approach helps in dealing with these natural characteristics of measurement data.

In addition, the voltage when the system becomes unstable for Case **1.1** is lower as compared to Case **1.2**. This is because the load in Case **1.1** is modeled with a constant impedance characteristic which leads to the collapsing point not necessary to be at the tip of the PV-curve but it can be at very low voltage value [111] (see Fig. 5.3). The use of constant impedance load model will allow for simulation to reach the unstable branch of the PV-curve although this is not a feasible operating point in practice.

Meanwhile, the load in Case **1.2** is modeled with a constant power characteristic where the tip of the PV-curve represents both the maximum loadability and voltage instability limit [111]. The intention of having constant power load is to verify that the proposed sensitivities can detect a voltage collapse whether the voltage level is not at low values or

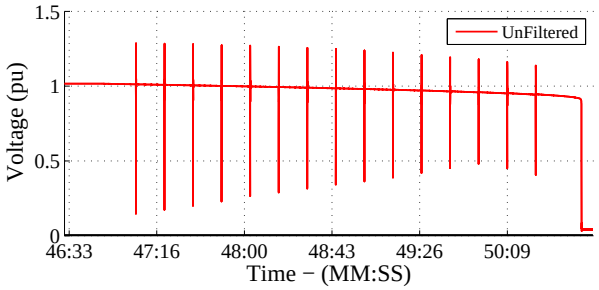

(a) Voltage Magnitude at Bus 5 - complete time span until collapse.

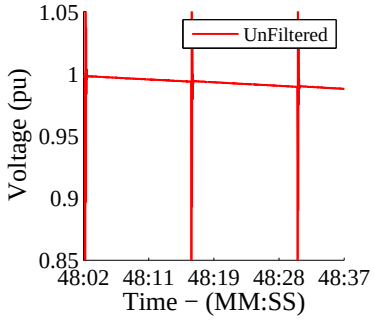

(b) Zoom of Fig. 5.5a

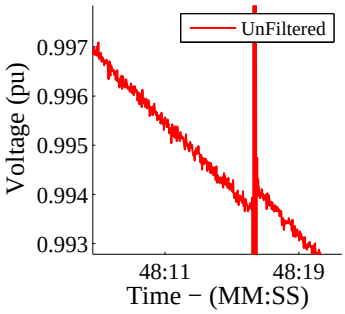

(c) Zoom of Fig. 5.5b

Figure 5.5: Voltage Magnitude at Bus 5 from PMU Measurements.

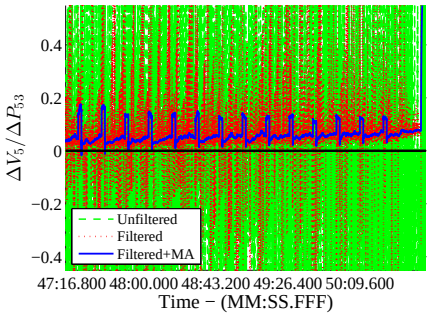

(a) Plot of $\Delta V_5/\Delta P_{53}$ sensitivity using PMU data.

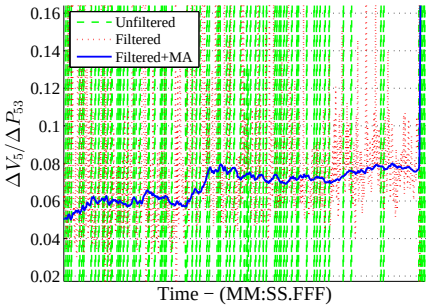

(b) Zoom of Fig. 5.6a when $\Delta V_5/\Delta P_{53}$ changes abruptly

Figure 5.6: $\Delta V_5/\Delta P_{53}$ sensitivity using PMU-data generated from the RT-HIL experiment.

if the lower part of the PV-curve does exist as with constant impedance loads. Therefore, sensitivities only increase abruptly to high positive but do not switch sign as in Case **1.1**.

5.1.2 Case 2: Load tripping with OEL limiter activated

In this test scenario, an Over Excitation limiter (OEL) is added to allow a generator to operate at high excitation levels for a sustained duration. An OEL is adopted to suppress the field current for cases when the temperature of the field winding exceeds the allowed level. The test system for this test scenario is the original system described in Chapter 3.

A voltage instability is created by tripping one of the parallel lines between Bus 1 and Bus 3. The generator at Bus 2 produces more power to compensate the power flow from the Thevenin equivalent due to disconnected line. As seen in Fig. 5.7, the OLTC also attempts to restore the load bus voltage; however, an OEL at the generator is activated (at "●"). Consequently, the generator voltage is no longer controlled and the voltage at Bus 5 drops steeply as shown in Fig. 5.7. Figure 5.8 also shows that the OLTC attempts to restore the load bus voltage to the reference level (represented by the vertical dash-dot line). However when OEL's limit is reached, the system's operating point jumps from one PV-curve (at "●") to another PV-curve ("♦") where there is no intersection between the PV-curve and the load, thus the system is unstable.

The $\Delta V_i/\Delta Q_{ik}$ (see Fig. 5.9) is of interest due to coupling between voltage and reactive power. After the OEL's limit is reached, it can be seen that the $\Delta V_5/\Delta Q_{53}$ increases sharply and switches from positive values to negative ones. This confirms the fact that a voltage instability has occured.

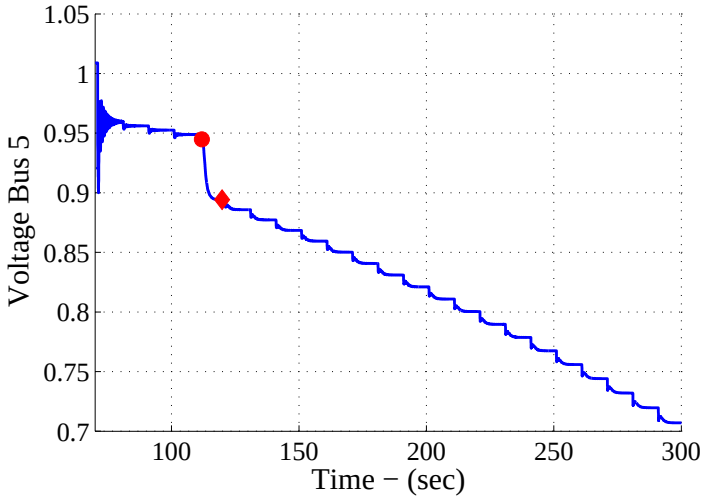

Figure 5.7: Voltage at Bus 5: OEL limiter activated

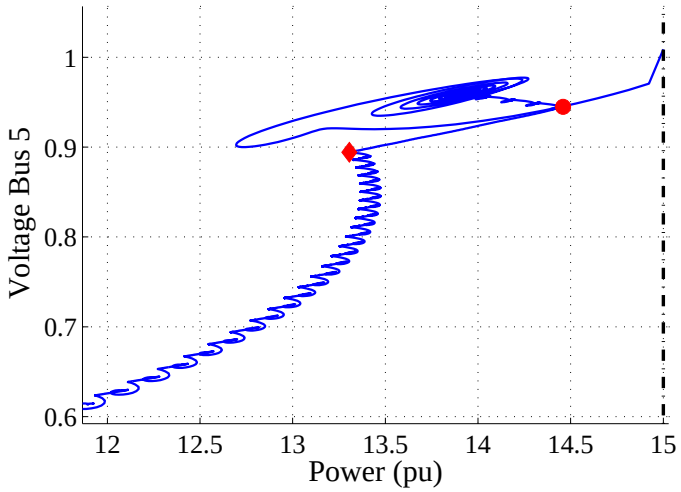

Figure 5.8: PV-curve: OEL limiter activated

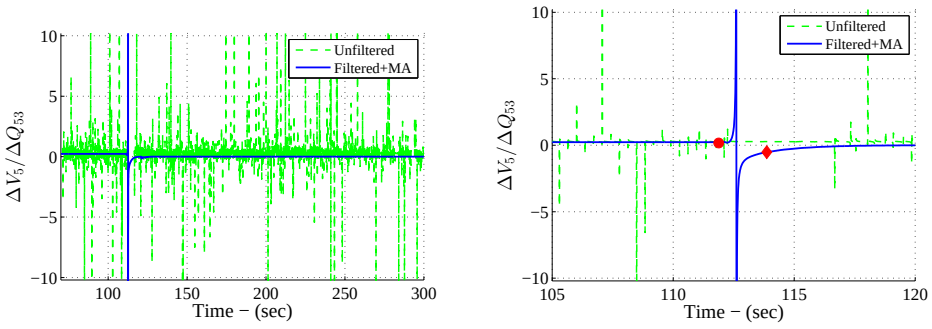

(a) Plot of calculated $\Delta V_5/\Delta Q_{53}$ sensitivity

(b) Zoom of Fig. 5.9a

Figure 5.9: $\Delta V_5/\Delta Q_{53}$ sensitivity: OEL limiter activated

5.1.3 Case 3: Real PMU data from the Norwegian Grid

In this case, the PMU-data from January 29, 2010 was gathered from three PMUs installed in the Norwegian Grid. Figure 5.10 shows the approximated location of PMUs installed at high voltage substations.

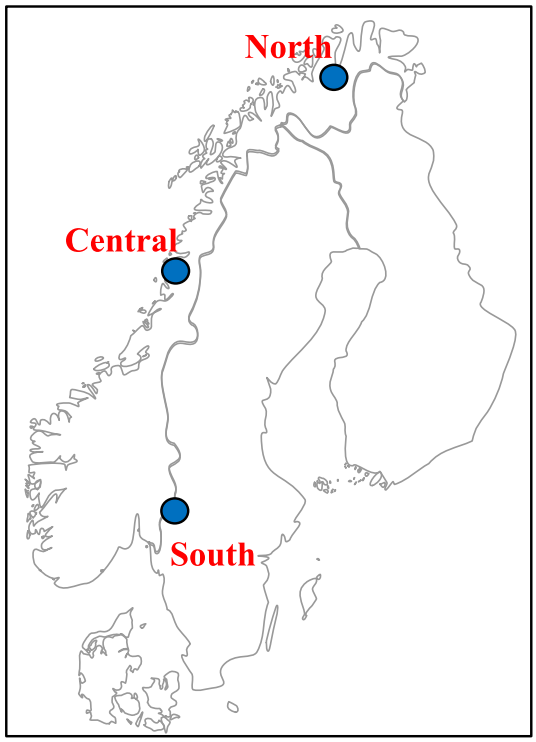

Figure 5.10: Norwegian transmission system and approximate PMU locations

Figure 5.11a shows measured voltage from three substations, and Fig. 5.11b depicts only the unfiltered and filtered voltage of the "North" substation.

As seen in Fig. 5.11b, the voltage at "North" substation started to drop at 16:07 hrs and one of the transmission line near the substation was disconnected at 16:10 hrs. The OLTC was activated to step up the voltage level at 16:12 hrs and 16:15 hrs, respectively. However, since the voltage was very low (0.93 pu approximately), a large industrial load which is at a distant location from the closet high voltage transmission substation, was manually disconnected to prevent a voltage collapse. Figure 5.12 shows the $\Delta V_i/\Delta Q_{ik}$[1] sensitivity calculated from PMU-data of the "North" substation can detect the line tripping (indicated by "**1**"), the two steps of OLTC's activation ("**2**" and "**3**"), and the load disconnection ("**4**").

[1] ΔQ_{ik} is calculated from the measured reactive power flows in the line towards the large industrial load.

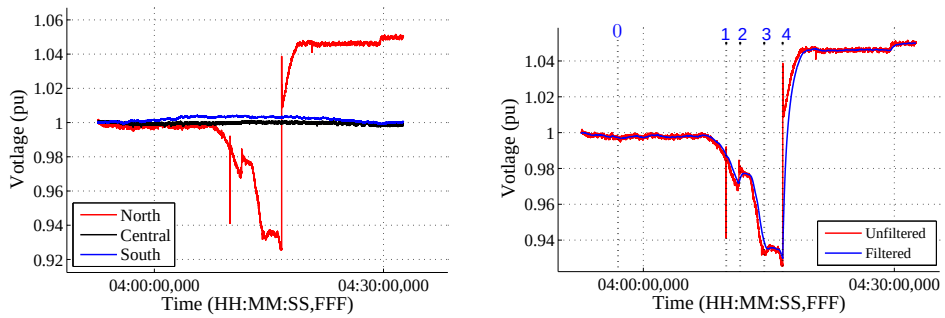

(a) Measured voltage from three high voltage substations (b) Unfiltered and Filtered voltage of the "North" substation

Figure 5.11: Measured voltage from Norwegian grid

The author suspects that the $\Delta V_i/\Delta Q_{ik}$ sensitivity would continue to increase steeply if the load was not shedded. In adddtion, it is worth noting that the sensitivity decreases after the load disconnection and it remains at positive value (higher than the pre-fault value at "**0**") which means that the system is stable.

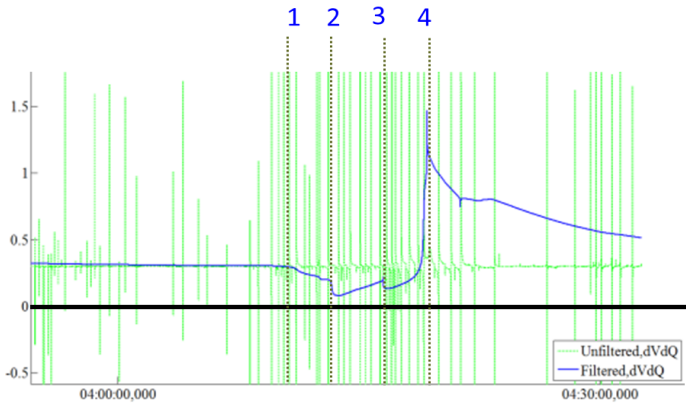

Figure 5.12: $\Delta V_i/\Delta Q_{ik}$ sensitivity calculated from PMU data of the "North" substation

The examples shown in this section show that the proposed sensitivities are accurate voltage instability indicators for PSB simulation, RT-HIL, and real PMU data cases. Since individual sensitivities are reconstructed from measurements, there are many advantages obtained from this proposed method. First, power system model or its topology changes do not need to be known. Second, for short-term dynamics such as generator control and limits, e.g. OEL, their actual control modes are not known by the methodology, however it

is possible to detect their change from the computed sensitivities. Also, the methodology is applicable for systems that are comprised of discrete switching components, e.g. OLTC, where unwanted noise and especially outliers will be produced in PMU measurements close to those components.

5.2 Visualization approach

For visualization purposes, the voltage and current phasors are gathered from different locations of the modified system shown in Fig. 5.1 using a PDC. Each incoming voltage and current phasors from different locations is filtered. Then, the active and reactive power flow of each line are calculated. Consequently sensitivities are computed as described in Chapter 4.

The computed sensitivities for each location are assembled in one display which maps their values to a contour overlaying the power system one-line diagram[2]. Figure 5.13 shows a screenshot of the voltage stability monitor tracking $\Delta V_5/\Delta P_{53}$ (Case **1.1** in Section 5.1). As shown in Fig. 5.13, the contour is on the left-hand side while the sensitivities are displayed in the middle; a vertical red line indicates the time instant for which the contour is being computed. The top-right-hand side is the PV-curve of a particular bus chosen (by previous stability studies). A red circle indicates the current operating condition, which has been computed from the PMU data. Vertical and horizontal yellow and red dash-dot lines indicate the distance to the maximum power transfer (active power margin) for the $\Delta V_i/\Delta P_{ik}$ thresholds that have been set by the user. These correspond to the "traffic signal" that is displayed on the bottom-right-hand side. The green light of this traffic signal indicates that the fact that the system is in a secure operating state while yellow and red refer to an insecure and an emergency state, respectively. Determination of the PV and QV curves and P & Q margins for each bus can be carried out off-line through continuation studies, or on-line as proposed in [112].

All of these quantities can be updated dynamically as the data is processed and passed to the display for visualization. Two thresholds for alarms are set at $\Delta V_5/\Delta P_{53} = 0.08$, for an early warning signal (yellow dash-dot line), and $\Delta V_5/\Delta P_{53} = 0.24$, for a final alarm (red dash-dot line). A similar screenshot of $\Delta V_5/\Delta Q_{53}$ (see Fig. 5.14) can be done in the similar way.

To explain how this wide-area early warning monitoring tool works, two screenshots of $\Delta V_5/\Delta Q_{53}$ (Case **1.1** in Section 5.1) at two different times (**I** at t = 240 sec and **II** at t = 360 sec) are captured and combined as shown in Fig. 5.15. The voltage instability scenario is implemented by increasing the load at Bus 5 as explained earlier. The load increase rises the value of the sensitivities. This in turn changes the colors of the contour map. This color corresponds to the sensitivity values. The selected QV-curve (of Bus 5, in this case) changes its value decreasingly when the load increases. Before the system collapses, an early warning signal can be generated by setting different threshold values. This signal can be generated when $\Delta V_5/\Delta Q_{53} = 0.2$ or a final alarm signal in case $\Delta V_5/\Delta Q_{53} = 0.6$. The traffic light in the monitor will change colors accordingly.

[2]Observe that this could also be done using a Geographical Information System (GIS).

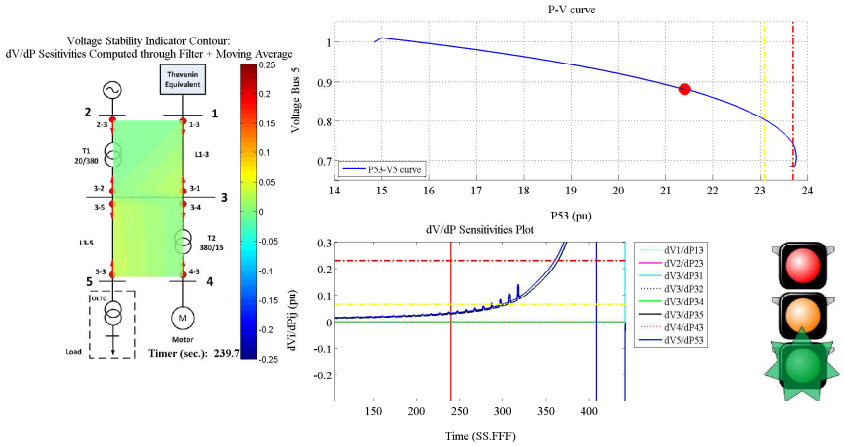

Figure 5.13: Screenshot of Voltage Stability Monitor: $\Delta V_5/\Delta P_{53}$ Sensitivities

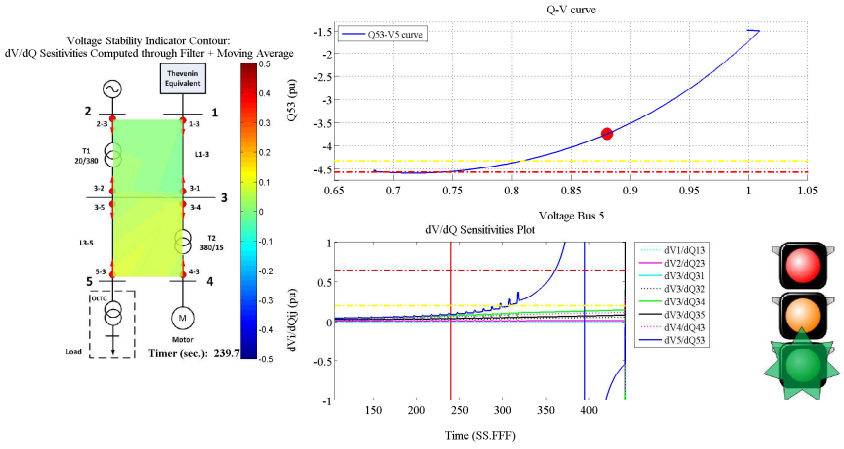

Figure 5.14: Screenshot of Voltage Stability Monitor: $\Delta V_5/\Delta Q_{53}$ Sensitivities

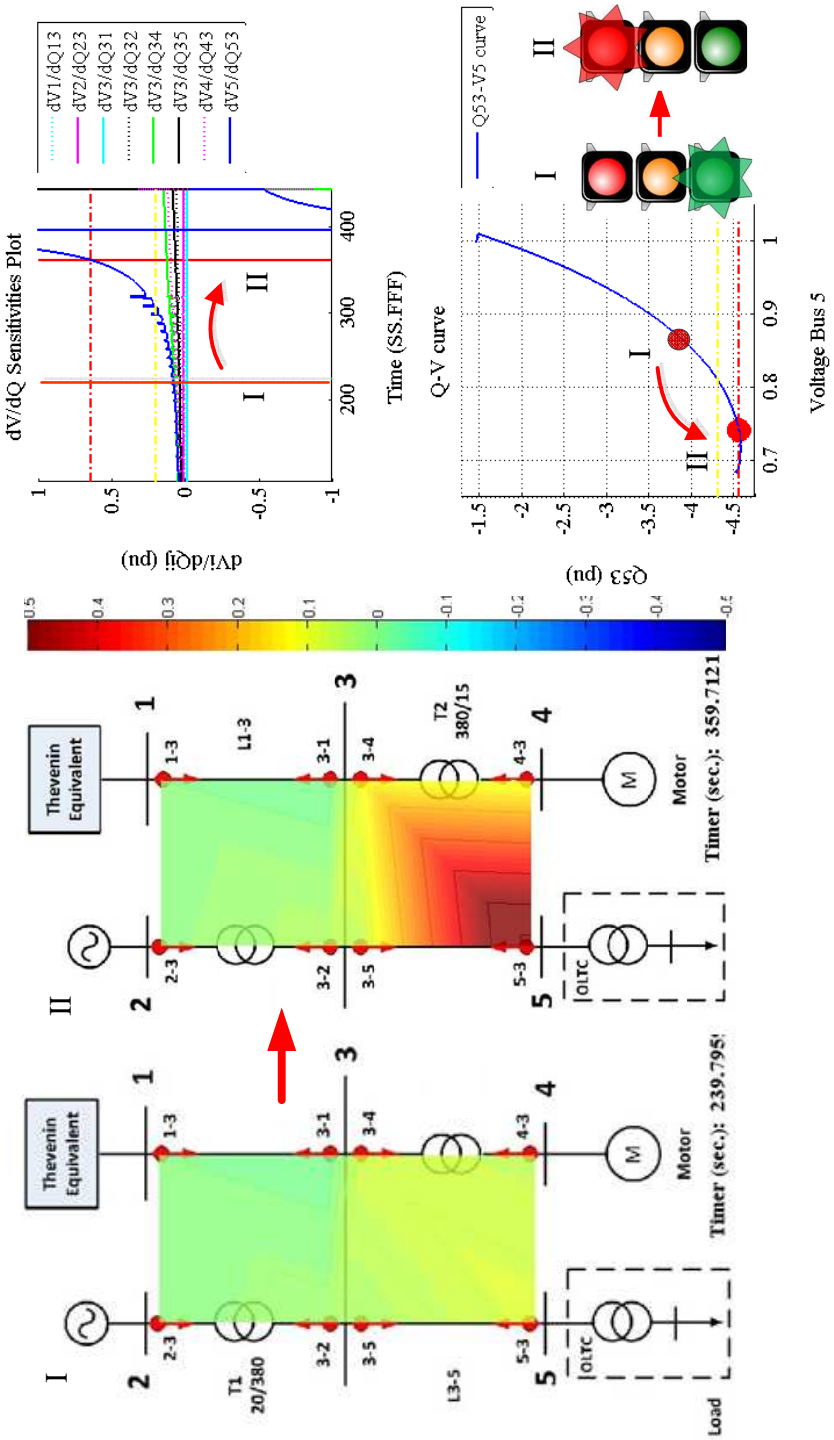

Figure 5.15: Transition of $\Delta V_5/\Delta Q_{53}$ sensitivities from t = 240 sec to t = 360 sec

5.3 Observations on the use of sensitivities for the activation of VSC-HVDC

Monitoring of both $\Delta V_i/\Delta Q_{ik}$ and $\Delta V_i/\Delta Q_{ik}$ are necessary since the bifurcation points of the PV-curve and QV-curve can occur at different times. This can be done by varying λ in (5.1) at a different rate. An example of increasing active and reactive loads with different λ rate (Case **1.1**) is shown in Fig. 5.16. It can be seen that $\Delta V_i/\Delta P_{ik}$ and $\Delta V_i/\Delta Q_{ik}$ do not switch from positive values to negative ones at the same time. This phenomena is confirmed by the PV and QV-curve plots shown in Fig. 5.17 where the QV-curve's bifurcation point is reached at $t = 235$ sec whereas it takes 35 sec more for the PV-curve's one.

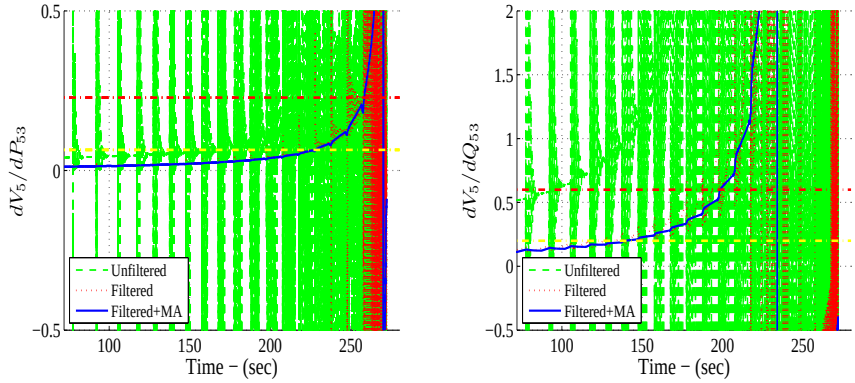

(a) dV_5/dP_{53} (b) dV_5/dQ_{53}

Figure 5.16: Plot of calculated $\Delta V_5/\Delta P_{53}$ and $\Delta V_5/\Delta Q_{53}$ sensitivities computed from filtered and unfiltered signals.

However, it is more important to mention that $\Delta V_5/\Delta P_{53}$ and $\Delta V_3/\Delta P_{35}$ sensitivities in case of active power, and only the $\Delta V_5/\Delta Q_{53}$ sensitivity in case of reactive power experience the abrupt change in their values as shown in Fig. 5.13 and Fig. 5.14, respectively. This means that the problematic location that tends toward voltage instability regarding reactive power is at point *5-3*, while points *3-5* and *5-3* shown in Fig. 5.1 need to be considered for active power issues. To avoid the repetition of results and present new experiments, the computed sensitivities at other locations are omitted.

Next, it is assumed that there is an VSC-HVDC installed between Bus 3 and Bus 5 (see Fig. 5.18), in order to mitigate voltage instability, an early warning signal can be adopted to trigger the change of power transfer though an VSC-HVDC as described in Chapter 4, and appropriate PMU signals are used as inputs to additional stabilizing controls. Different control modes of VSC-HVDC are tested and the benefits of using these controls are described in Section 5.4

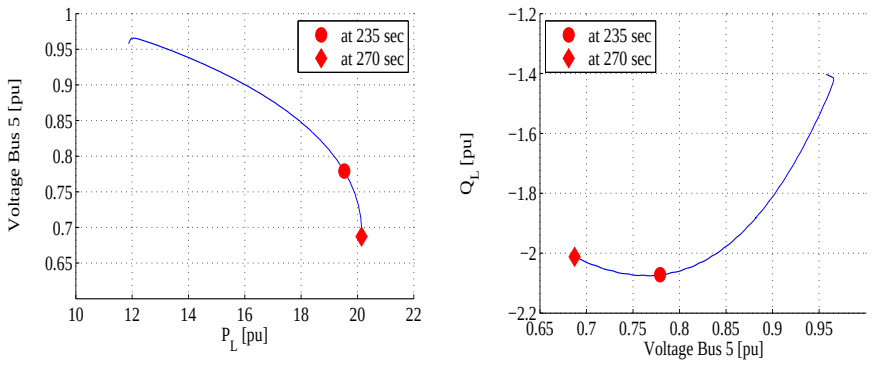

(a) *PV – curve* (b) *QV – curve*

Figure 5.17: Plot of calculated *PV – curve* and *QV – curve* calculated from filtered signals.

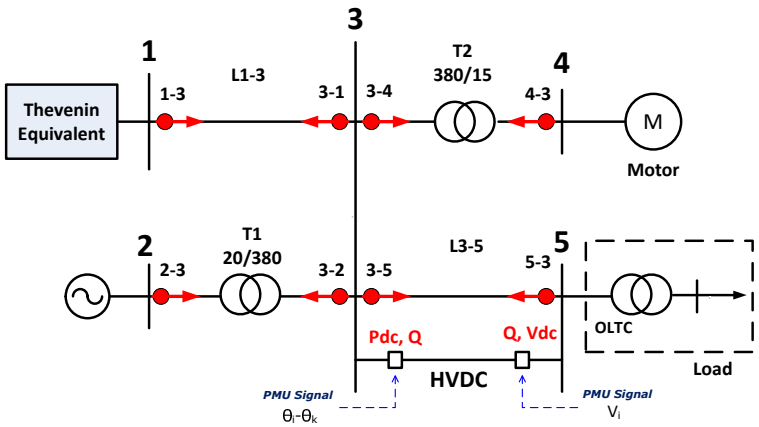

Figure 5.18: Test system with HVDC

5.4 Case studies on voltage instability mitigation

In this section, simulation results are presented to illustrate the test system's response with and without the inclusion of the proposed coordination method as shown in Fig. 4.3 in Chapter 4. In these simulations, load increases are used to produced a voltage instability (Case **1.1** in Section 5.1), different power responses supported by the VSC-HVDC, and also different control modes at the inverter side are considered. The control at the rectifier side is in $P_{dc} - Q$ mode where the active and reactive power are fixed at 400 MW and 10 MVar (where each converter size is 550 MVA), respectively. Meanwhile, the active and reactive load are 1500 MW and 150 MVar, and being increased (at $t = 1$ sec) as defined in (5.1) until test system experiences a voltage instability.

5.4.1 Case 1: $Q - V_{dc}$ control, Q ramp support

In this case, reactive power support at the inverter side is ramped up starting at $t = 147$ sec. The reactive power support is activated by sensitivity $\Delta V_5/\Delta Q_{53}$. This reactive power ramping is achieved through the control scheme shown in Fig. 4.4a.

The comparison of the resulting PV and QV-curves with and without reactive power ramping is shown in Fig. 5.19. Meanwhile, the comparison of voltage at Bus 5 between the two cases is shown in Fig. 5.20.

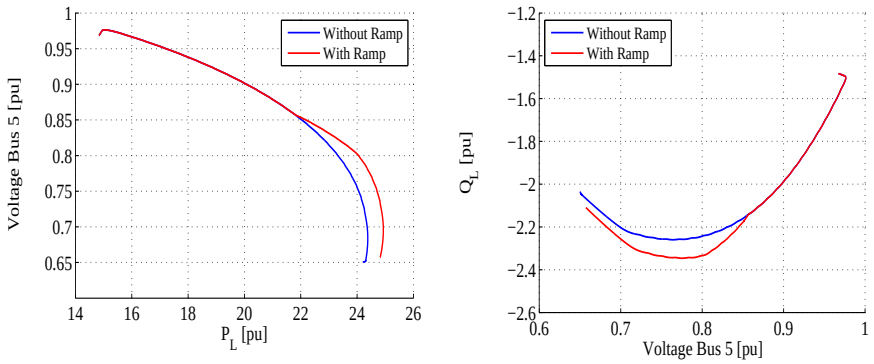

(a) *PV – curve* (b) *QV – curve*

Figure 5.19: PV-curve and QV-curve plots (Case 1)

As shown in Fig. 5.20, the reactive power that is ramped up by the VSC-HVDC supports a voltage drop caused by increasing load. This voltage support allows the system to operate 10 more seconds before a collapse.

For comparison, the following schemes have been considered to control the VSC-HVDC: reactive power (Case 1), active power (Case 2), and both active and reactive power (Case 3) are ramped in such a way that make a test system collapses at approximately

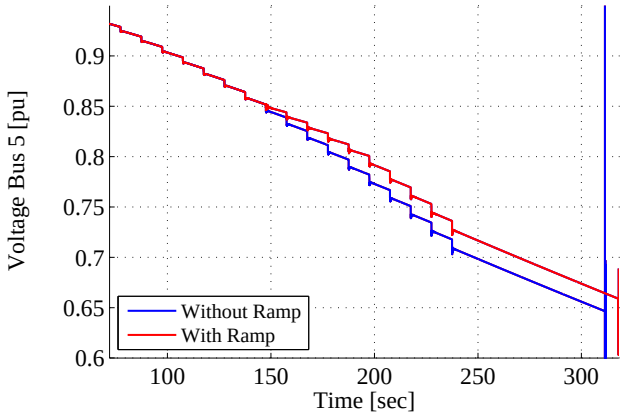

Figure 5.20: Voltage at Bus 5, comparison between cases with and without VSC-HVDC coordination (Case 1)

same point (see Fig. 5.20). Fig. 5.21 shows the delay of an abrupt change of sensitivities compared to the case without control.

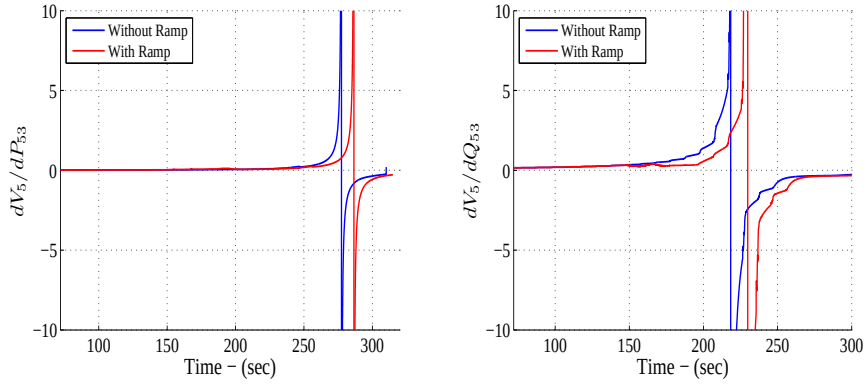

(a) $\Delta V_5/\Delta P_{53}$ (b) $\Delta V_5/\Delta Q_{53}$

Figure 5.21: $\Delta V_5/\Delta P_{53}$ and $\Delta V_5/\Delta Q_{53}$ sensitivities comparison between with and without VSC-HVDC coordination (Case 1)

5.4.2 Case 2: $Q - V_{dc}$ control, P_{dc} ramp support

This case is similar to Case 1, however despite the reactive power support at inverter side, active power is ramped up at rectifier side and transmitted through DC line. The active power ramping is controlled through the scheme shown in Fig. 4.4b. Meanwhile, Fig. 5.22 shows the comparison of PV-curve and QV-curve between with and without active power ramping.

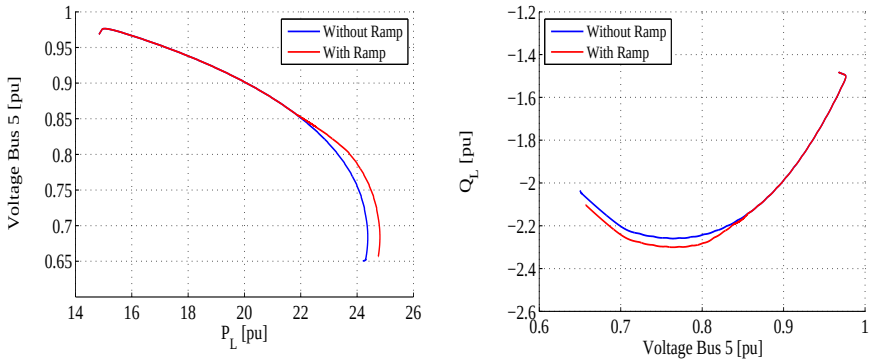

(a) *PV – curve* (b) *QV – curve*

Figure 5.22: PV-curve and QV-curve plots (Case 2)

The increase of active power load is allowed to flow through the VSC-HVDC, resulting in a decrease of active power transfer through the parallel AC transmission line, L3-5. By transmitting higher power through the VSC-HVDC, the system AC stress is relieved and the loadability is increased. The system's loadability represented by PV and QV-curves are greater than in the case without active power ramping.

5.4.3 Case 3: $Q - V_{dc}$ control, P_{dc} & Q ramp support

In this case, the active power support (P_{dc}) is ramped up by the rectifier while the reactive power Q is ramped up by the inverter. This means that we take advantage of the VSC-HVDC described in both Case 1 and Case 2 to extend the maximum transferable Power (MTP) point before the test system is confronted with the voltage instability. Fig. 5.23 shows the comparison of PV and QV-curves between only ramping Q (Case 1), only ramping P_{dc} (Case 2), and ramping P_{dc} & Q (Case 3). These associated PV and QV-curve shows three different ways to utilize the capacity of the VSC-HVDC. It can be seen that, ramping both active and reactive power by VSC-HVDC provides the best loadability in the system. Table 5.1 shows a comparison between all three control schemes.

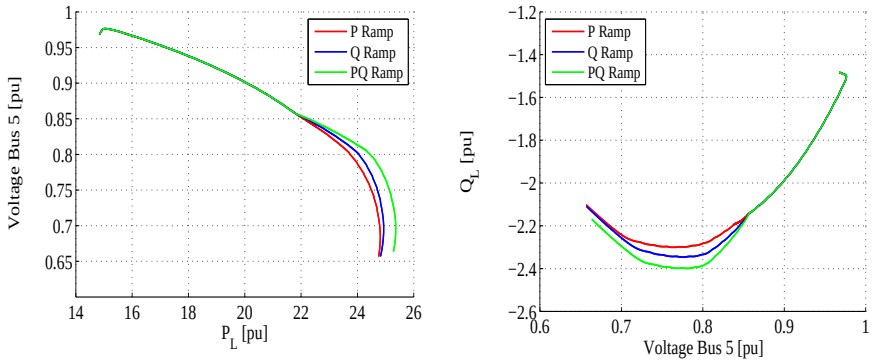

(a) *PV – curve* (b) *QV – curve*

Figure 5.23: Comparison of *PV – curve* and *QV – curve* plots between Case 1, 2, and 3

Table 5.1: Loadability of different control schemes

Control	MPT [p.u.]	Gain [p.u.]	Gain/Converter Size
No Control	24.38	-	-
P_{dc} Control	24.81	0.43	-21 %
Q Control	24.98	0.60	+9 %
P_{dc} & Q Control	25.36	0.98	+78 %

5.4.4 Case 4: $Q - V_{dc}$ control, P_{dc} step support

This case is similar to Case 2 in which the VSC-HVDC supporting only active power. However, instead of ramping the active power, the transmitted power is controlled through a step response. It is worth noting that since HVDC's operation depends on alarms that are set by the user, examples of stepping up DC power at different sensitivity values (which corresponds to different activation times) are important to analyse. Fig. 5.24 shows the upper half of PV curves considering the AC flows through line L3-5 vs. the voltage at Bus 3 and the DC active power increase in a step change from 400 MW to 550 MW at the HVDC.

As seen in Fig. 5.24, the closer the operating point to the stability boundary the higher the swings expressed through the size of the spiral trajectories. The reason for less damping when being closer to the stability boundary is that the synchronizing power goes down with decreasing stability margin. At the nose of the PV-curve this synchronizing power becomes zero, and it becomes negative when the nose of the PV-curve is surpassed. This happens simultaneously with the crossing of the maximum stable transmission angle. Then with

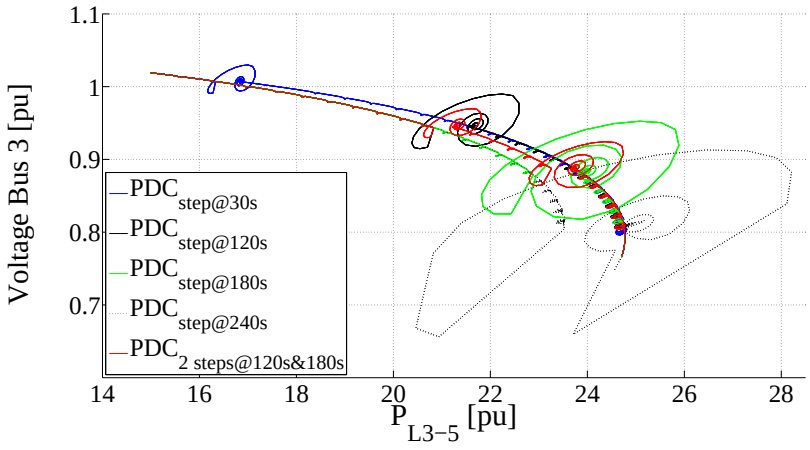

Figure 5.24: PV-curves from unfiltered data - Step DC

negative damping the system becomes electromechanically unstable [113].

It is worth noting that setting alarms also plays a vital role in finding new power system's equilibrium, i.e. operational point. Observe that an early adjustment of the DC transfer results in a shorter settling time, and that if adjustments are made latter, the use of 2 different stages in the transition can aid in reducing the overshoot and settling time required for finding a new equilibrium. Moreover, a step change of DC power creates oscillations in the system's response, thus the DC power should be gradually changed to prevent this undesired feature (as done in the previous examples by ramping P_{dc} and Q). For comparison, Fig. 5.25 shows the PV-curve from unfiltered data in case of no ramp, Q, and P_{dc} and Q ramp support.

In addition, the requirement of DC power step change which was mentioned earlier can occur when a specific load demand changes due to an hourly-block in the electricity market, regardless of the system's operating point at that moment. This power step could be applied without severe consequences if and only if the HVDC is VSC-type and a parallel AC line in Fig. 5.18 is a short line and of about the same length as the HVDC. However, if the HVDC is Classical-type and used to connect two grids which are, e.g., 1000 km apart, the HVDC itself is prone to voltage instability.

It is also important to note that the control mode of this VSC-HVDC is $P - Q$ control mode (i.e. the AC voltage control mode is not adopted) due to a specific active and reactive load demand whereas the use of AC voltage control mode (with a proper design) can be used to avoid voltage stability problem but not necessarily transmission angle instability [114]. The proposed HVDC stabilizing methods to prevent the voltage and transmission angle instabilities due to these operation condition will be described in Chapter 6.

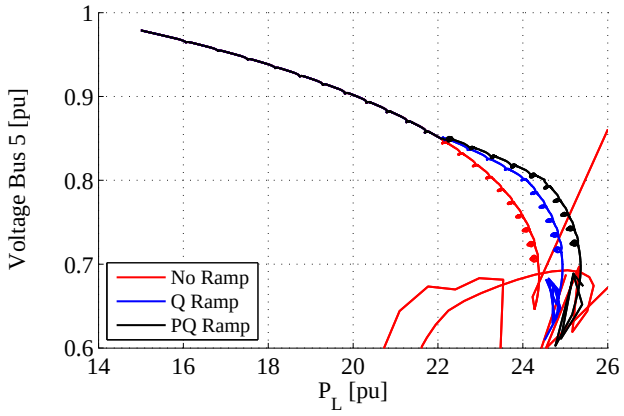

Figure 5.25: PV-curves from unfiltered data - no ramp, Q, and P_{dc} and Q ramp support

5.4.5 Case 5: P_{dc} & V_{ac} control at inverter

It has been noted before that Bus 5 experiences voltage stability issues, thus the control of inverter is changed from $Q - V_{dc}$ to $P_{dc} - V_{ac}$ mode to investigate control schemes' efficiency. However, in order to keep the active power on the AC side to be equal to the active power transmitted from the DC side (losses neglected), the control mode of the other side must regulate the DC voltage [115]. Therefore the control mode of the rectifier is changed to $V_{ac} - V_{dc}$ mode. Fig. 5.26 shows a comparison of the PV-curves between no ramping, PQ ramping (Case 3), and AC voltage control at Bus 5.

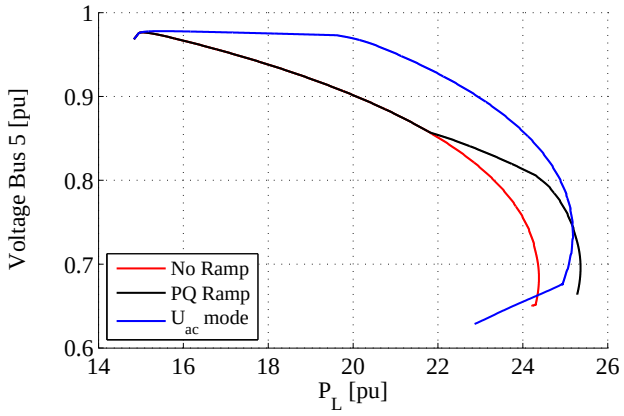

Figure 5.26: Comparison of PV-curves between different control modes

As shown in Fig. 5.26, the voltage at Bus 5 is kept constant in the case of AC voltage control. This is because reactive power is injected from the inverter of the VSC-HVDC. However the voltage cannot be held any longer when active load power increases to 20 p.u. due to the VSC-HVDC's inner current control reaching its limit. Consequently, voltage at Bus 5 starts declining until system collapse. It is worth noting that the proposed control scheme (ramping active and reactive power) provides a better result as can be seen from the MTP point between these two cases.

Chapter 6

Real-Time Implementation of HVDC Stabilizing Controls

This chapter describes the implementation of the Automatic Voltage Stability (AVS) and Automatic Power Order Reduction (APOR) which are special stabilizing controls that are used in the second approach to prevent voltage and angle instabilities when HVDCs are operated under undesired conditions. This approach ensures that HVDCs will operate securely when their transfer is pushed towards the maximum transferable power level. The AVS and APOR controls are implemented and their performances are tested using both an off-line and a real-time platform. This chapter focuses on the use of these stabilizing controls on classical HVDC systems.

6.1 The proposed Classical HVDC stabilizing methods

The idea behind the Automatic Voltage Stabilizer (AVS) originates from [116] where theoretical analysis and preliminary PSCAD/EMTDC simulations using a simpler HVDC model was conducted. The further development has been carried out on a CIGRÉ Benchmark [117] and proved that the proposed methodology is suitable in a real-time platform.

The AVS is based on an on-line steady state stability analysis using a dynamic stability limit detection method [118]. The PV-characteristic in Fig. 6.1 provides information about a generic AC transmission system with regards to voltage instability.

The uncontrolled AC voltage (V_{AC}) is at the receiving end of an AC transmission system. The voltage declines with increasing power up to the maximum transferable power (MTP) level, once the MTP-Point has been reached, it will decline with decreasing power. In general, this PV-curve holds also for an HVDC system being connected to an AC grid of moderate stiffness [119]. For the current control loop the upper branch is stable and the lower branch is unstable.

On the upper branch, DC current rises in proportion to the ordered DC power. If the MTP-Point is surpassed, the DC current continues to grow but the DC power declines. The conventional HVDC power controller is not able to detect this change, and the AC terminal

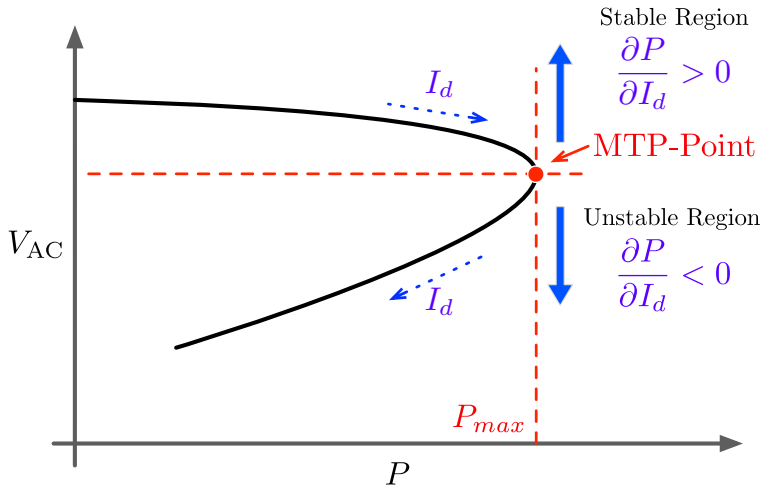

Figure 6.1: PV-curve and principle used in the stability limit detection method

voltage starts to collapse. The collapse can be halted through voltage dependent current order limitation (VDCOL) [120]. However, VDCOL does not recognize if the system has already passed the stability border and that HVDC operates on the lower branch of the PV-curve. The Automatic Voltage Stabilizer (AVS) [119, 114], on the other hand, does not experience this problem. Essential for a statement on steady state stability is the sign of the quotient $\partial P/\partial Id$. AVS uses this derivative sign to distinguish between the upper and lower branch of the PV-curve and use it as a signal to trigger its operation. Since $\partial P/\partial Id$ cannot be measured directly, it is determined by measuring the derivatives $\partial P/\partial t$ and $\partial I_d/\partial t$ with respect to time, and forming the product of these derivatives resulting in: $\partial P/\partial t \times \partial t/\partial I_d$. If only one of the derivatives with respect to time becomes negative, which indeed occurs when moving along the lower branch of the PV-curve, the resulting derivative becomes negative. If both derivatives with respect to time are either positive or negative (which happens when the operating point moves along the upper branch) the product is positive, so we know that the operating point is on the upper branch. Therefore, we can use this signal to switch on the AVS where the current level in the closed-loop current controller is adjustable so that the operating point is brought to the upper branch or revolve around the stability boundary which can be stopped by implementing the Automatic Power Order Reduction (APOR).

The benefit of the AVS and the APOR cover both long-term (e.g. slow changes of internal grid voltages) and especially short-term (e.g. lines disconnection or voltage reaches OEL limit) voltage instabilities. This short-term instability can occur when the system's operating point moves suddenly to the lower branch of the PV-curve as shown in Fig. 6.2 when one of the parallel line between Bus 1 and 3 (of the test system shown in Fig.3.1) is disconnected.

As seen from Fig 6.2 after one of the parallel lines is tripped, the system's equilibrium

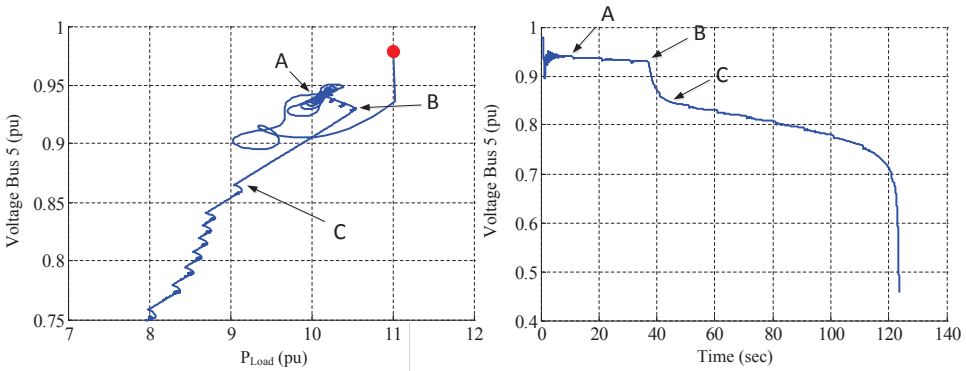

(a) PV-curve (b) Voltage

Figure 6.2: PV-Curve and Voltage - Line Trip Case

point moves from "red-dot" to point "A" to find a new equilibrium point. However, due to the operation of LTC that attempt to restore voltage at the lower voltage side of the transfer at the load bus, the voltage at higher side keeps decreasing. This triggers the OEL at the generator, thus generator voltage is no longer controlled. Consequently, this forces the system's operation point to jump from point "B" to point "C" which is the lower branch of the PV-curve. A similar process occurs with Classical HVDC working on a weak grid and transfer from DC voltage control to minimum extinction angle control [114].

This case is similar to **Case 2** described in Section 5.1.1 where the sensitivity changes abruptly, this implies that the change in control mode proposed in Section 4.4 will be exhausted quickly, and further measures are needed to avoid a system collapse. Therefore, the AVS and the APOR are necessary to avoid the voltage instability.

6.1.1 Benefits of Real-time simulation

The PSCAD digital simulator permits the set-up and simulation of truly complex power systems including power semiconductor equipment and necessary controls. The simulation time increases in proportion to configuration size and depends on the specific equipment needed. While for the comparison studies in this thesis PSCAD is sufficient, additional circuitry can from a certain amount on, increase computation time to unacceptable values. Further studies that consider the enhancement of the AC network model and the study of a three-terminal HVDC systems are planned. Thus, it is expedient to simulate the AVS with a real-time simulator (OPAL-RT simulator) and to get acquainted with its real-time features before considering more complex configurations. Both the PSCAD digital simulator and the OPAL-RT simulator contain an implementation of the CIGRÉ Benchmark Model for HVDC Controls, including the VDCOL function. The main tasks involved in the studies shown below include the implementation and verification of the automatic voltage stabilizer for both simulators and the performance evaluation of the VDCOL function.

Compared to analog simulators, digital Real-Time simulators use samples of the various system quantities and determine the next output of these quantities through some solution algorithm using previous outputs, previous inputs and the actual inputs. Due to the sampling period which has to cover the processing time of the samples as well as the time it needs to have the inputs stored in the computer memory and the outputs sent to the measuring terminals the notion of RT is important. The pre-determined time step used in our simulations is 50 μs, which allows us to sample up to 20 data points on a 1 kHz signal. With regard to firing signal generation and controls this is sufficient but regarding the exact determination of, e.g., lightning surge having a rise time of 1.2 μs this would not be sufficient. Usually, however, insulation coordination is not performed on a RT-simulator but on a Transient Digital Simulator as, e.g., PSCAD/EMTDC or EMTP-RV. It has to be noted: a the OPAL-RT real-time simulator permits calculations within any time frame, provided no real-time requirements have to be met.

A main reason for using a RT-simulator in the industry is to be able to connect control cubicles and test its hardware and software before shipping to site. In our case the pursued RT-simulation permitted to implement in a reasonable time frame a new stabilization method and to prepare a possible connection of real-time controls containing the stabilizer algorithm. Thus the results obtained are twofolds. First it is possible to operate the HVDC system at or close to the stability boundary without inducing voltage instability which is important in respect to building a smart power system. Secondly, connection points between main circuitry measurements and the controls are identified for later connection and tests of control cubicles.

6.2 Modelling Needs

6.2.1 CIGRÉ benchmark

The CIGRÉ Benchmark Model for HVDC Controls runs on a digital computer using an electromagnetic transient program. It permits to investigate steady state and dynamic control performance at weak AC grid conditions. The model contains a 12 pulse/ 500kVdc/ 1000MW mono-polar long distance transmission system including all necessary filter circuits and capacitor banks to provide proper operating voltage quality (Fig. 6.3). The grids are formed by static grid equivalents. Implemented in the model is constant extinction angle control but not the transition from DC voltage control to minimum extinction angle control as it is actually installed in DC transmission systems [121]. Therefore, for this study inverter controls were complemented by DC voltage control. The transfer from DC voltage to minimum extinction angle control is a rather problematic point on the power-voltage characteristic of the inverter [118, 122].

In actual systems either the valve side AC voltage or the extinction angle can be controlled via the converter transformer on-load tap changer. This improves stability conditions [122]. However in the CIGRÉ Benchmark Model no tap changer is foreseen and also for the present study no such equipment was added.

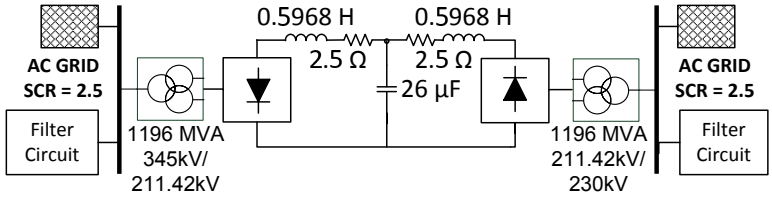

Figure 6.3: CIGRÉ Model

6.2.2 AVS implementation in PSCAD

The PV-curve provides analytical means to distinguish between the upper and the lower branch by determining the derivatives of the DC power with respect to the DC current (Fig. 6.1). Essential for a statement on steady state stability is the sign of the quotient $\partial P/\partial Id$.

As mentioned in Section 6.1, the derivatives product $\partial P/\partial t \times \partial t/\partial I_d$ can be used as a stabilizing signal for HVDC. This signal is named as "crit" (short-term of "critical point") in Fig. 6.4a. If the product "crit" becomes negative, this means that the operating point moves along the lower branch of the PV-curve.

The value of "crit" is passed to a hysteresis buffer that triggers a mono-flop which in turn sets the stability limit detection signal "slds" (short-term of "stability limit detection signal"). Fig. 6.4b illustrates how the "slds" generates a pulsed signal called "switchover" which operates finally the sign reversal switch.

Two clock signals, T1 and T2, are embedded in the circuit. With T1 the operating point is pushed back up, with T2 it falls back to the lower branch. The displayed principle ensures a safe oscillation around the MTP-Point.

Fig. 6.4c depicts the effect of the switchover signal. The two time-based switches can be disregarded. They are necessary to power up the system to nominal conditions without AVS control.

If the AVS is switched on ("Stabilization at Limit" in upper position), the feedback sign of the closed-loop current controller is switched between plus and minus depending on the switchover signal. A negative sign will change the current from increase to decrease. This leads the operating point back to the upper branch and then, since the "crit" value becomes positive, the sign is switched back to positive. In this way the operating point will revolve around the stability boundary.

Instead of bounding the operating point around the stability border, the power order can automatically be reduced at the first occurrence of the stability limit detection signal (slds) (Fig. 6.4d). This signal triggers a mono-flop that in turn operates a switch which reduces the power order by a defined value. In [118] this is a value adapting itself to the MTP level, but this value is fixed for the test purpose in this thesis.

Fig. 6.4d shows that VDCOL is DC based. This is indeed a limitation due to the fact that the AC voltage declines always earlier than the DC voltage [123]. However, for a weak AC grid with an SCR of around two there is only a very small AC voltage decline before

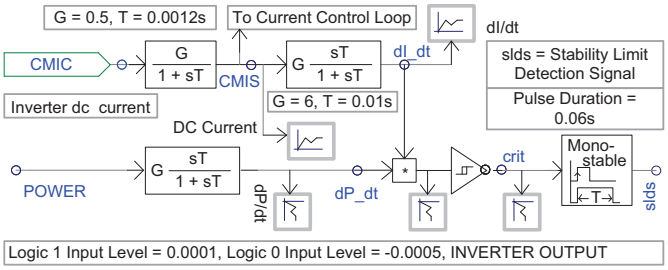

(a) Automatic Voltage Stabilizer (AVS)

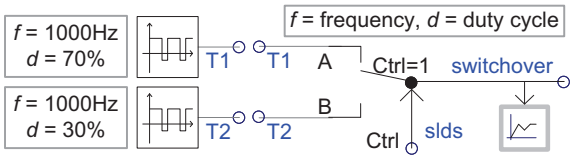

(b) Switchover Signal Generation

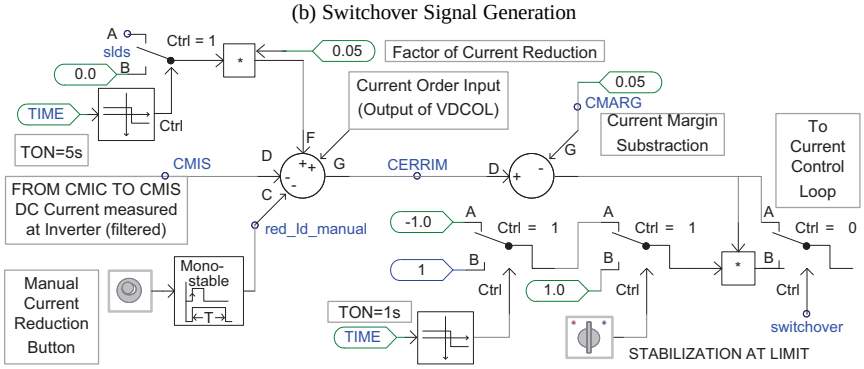

(c) AVS Implemented in Closed Loop Control

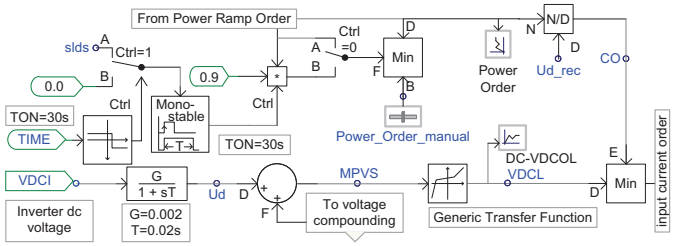

(d) Power Reduction Mechanism

Figure 6.4: PSCAD/EMTDC AVS Implementation

the voltage collapses. That is, the difference whether using AC VDCOL or DC VDCOL is only marginal and not decisive for the functioning and the performance of VDCOL at weak grid conditions. If needed, the change to AC voltage dependent VDCOL can be easily implemented.

6.2.3 Real-time AVS model implementation

Figure 6.5 illustrates the AVS mechanism implemented for Real-Time Simulation.

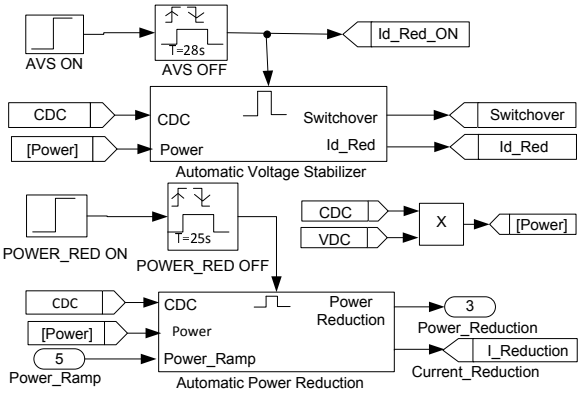

(a) AVS Implementation

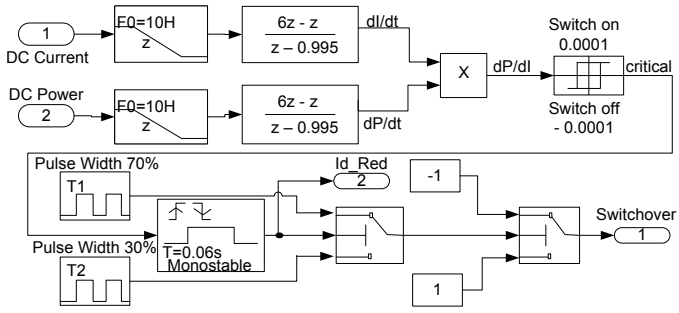

(b) AVS Stabilizer Subsystem

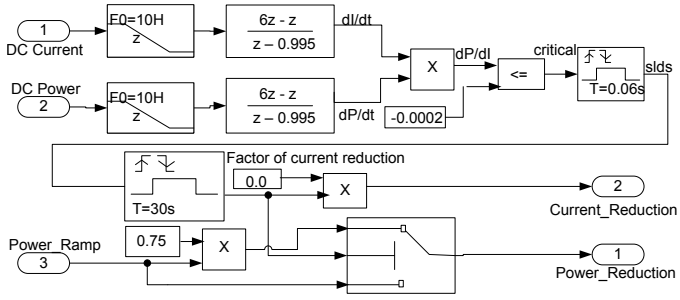

(c) Power Reduction Subsystem

Figure 6.5: AVS Implementation for Real-Time Simulation

The AVS was implemented within the inverter control subsystem of the original CIGRÉ model. This modeled needed proper tuning of parameters prior to the implementations of

the AVS. Figure 6.5a depicts the details of the AVS which was embedded. The measured DC current (CDC) and DC voltage (VDC) are multiplied to get the power transmitted over the DC link. The subsystems for the stabilizer (Fig. 6.5a and 6.5b) and the automatic power reducer (Fig. 6.5c) are equipped with a switch to set them active or inactive.

The stabilizer is switched on after 35 seconds and stays active for 30 seconds, while the automatic power reducer is switched on at 67 seconds and remains active for 28 seconds. When the stabilizer is switched on, the "*Id_Red_ON*" function is set on too.

To avoid an operation at the stability boundary with the accompanying swings around the MTP point a power order reduction triggered by the aforementioned "slds" signal is necessary. Inspite of generating the "switchover" signal as mentioned in Section 6.2.2, this "slds" signal can be generated by using a "monostable flip-flop" block (Fig. 6.5c).

Chapter 7

Case Studies of utilizing the Real-Time HVDC Stabilizing Controls

This chapter provides numerical examples of how the AVS and APOR can prevent voltage and transmission angle instabilities when HVDCs operate in some undesired conditions[1].

7.1 VDCOL characteristics

Classical HVDC is normally equipped with Voltage Dependent Current Order Limitation (VDCOL) on both rectifier and inverter. This VDCOL automatically reduces the reference DC current set-point when DC voltage decreases caused by, for example faults on the DC link. Thus, the reactive power demand on an AC network is reduced in favor to recover from a fault [124]. In general, the VDCOL on Classical HVDC is tuned with sufficient high short circuit ratio (SCR), for example SCR = 3.3 in this study. This is because there is a protection mechanism against voltage instability and at the same time, there is no unnecessary power curtailment if the voltage declines within the normal voltage band.

There are incidents that the SCR becomes lower, e.g. AC line disconnection (the SCR value changes from 3.3 to 1.9, in this study) which results to an inappropriate VDCOL setting. In other words, the VDCOL function would not reliably prevent the operating point from jumping to the lower unstable PV-curve. In other words, the calibration of the VDCOL characteristic based on SCR = 3.3 is no longer appropriate for the weaker grid. However, if the VDCOL would be tuned for a SCR = 1.9 another problem would occur which is the power would unnecessarily be curtailed at a normal operating conditions with only slightly decreased AC voltage. Moreover, it is not possible to discriminate between a normal voltage level and a voltage level indicating approaching instability.

The characteristic permits DC current overload of 1.2 at 0.9 p.u. DC voltage holding for the characteristic implemented in PSCAD controls. This is either a temporary overload or can even be continuous overload depending on the prevailing ambient temperature.

[1]The acronym SPS indicates the results were obtained using the OPAT-RT real-time simulator, while PSCAD indicates the use of PSCAD/EMTDC off-line simulator.

The parameters given in Fig. 7.1a show that the VDCOL calibration values differ between PSCAD and SimPower Systems (SPS). Accordingly the VDCOL characteristics are somewhat different as depicted in Fig. 7.1a.

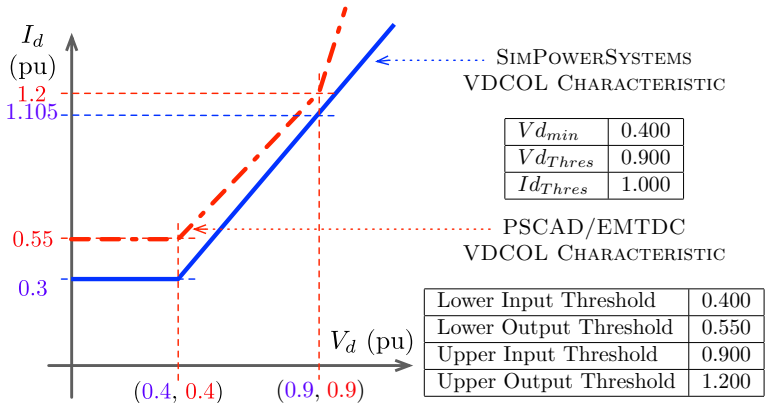

Vd_{min}	0.400
Vd_{Thres}	0.900
Id_{Thres}	1.000

Lower Input Threshold	0.400
Lower Output Threshold	0.550
Upper Input Threshold	0.900
Upper Output Threshold	1.200

(a) VDCOL Characteristics

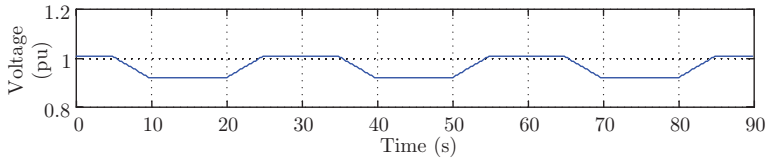

(b) Internal Grid Voltage - SPS

Figure 7.1: VDCOL characteristics and Internal Grid Voltage

Fig. 7.1b shows a controlled variation of the internal grid voltage to test the behavior of VDCOL, AVS and the AVS with automatic power reduction in the listed order. In PSCAD simulation the variation of the internal grid voltage can be accomplished manually or via an automatic ramp. Manual ramping is not possible with SPS due to time lags between the monitoring console and the real-time target, automatic ramping is used.

7.2 Case 1: Weak AC Grid on Rectifier Side

In this scenario the SCR at the rectifier is 1.9 while the SCR at the inverter is 2.5. Fig. 7.2a shows the response of the AC terminal voltage of the rectifier as a result of a variation of the internal grid voltage as shown in Fig. 7.1b.

Only the VDCOL is activated during t = 10-20 sec, which makes voltage drop to approximately above 0.8 p.u. The AVS is activated between t = 40-50 sec, which retains the voltage level around 0.9 p.u. The AVS with automatic power reduction is activated at t = 70-80 sec. The AC voltage is kept above 0.9 p.u. Fig. 7.2b illustrates the comparison of the DC quantities for the three different control methods.

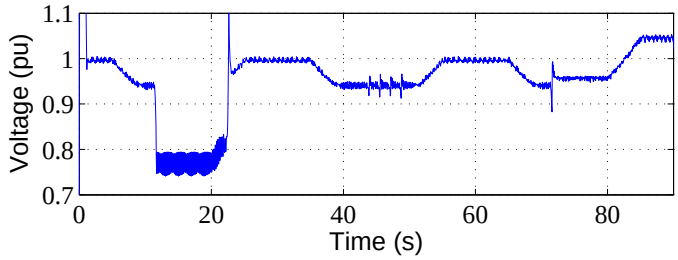

(a) AC Terminal Voltage

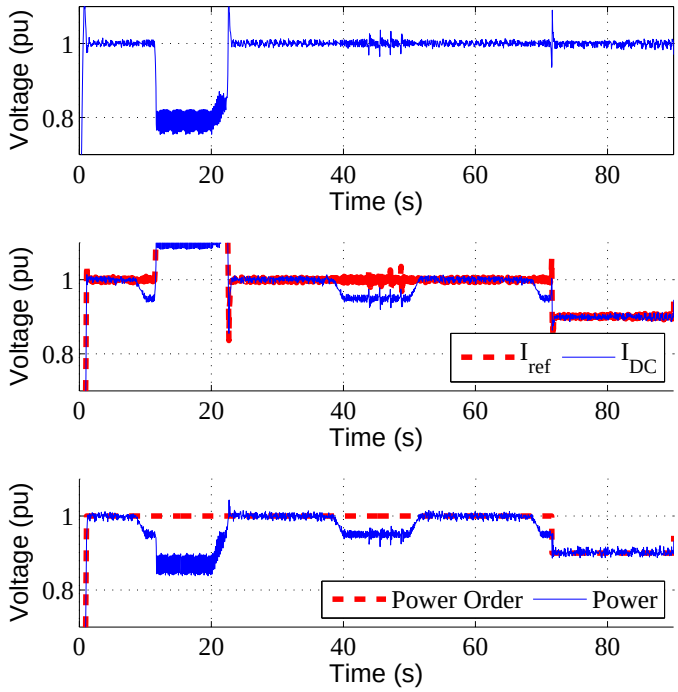

(b) Rectifier Oscillograms

Figure 7.2: Weak AC Grid on Rectifier Side (SPS)

It is clear that without AVS, the operating point at VDCOL operation slides to the lower branch of the PV-curve. The operation of AVS without the power order reduction yields stable swings around stability limit and this swing can be removed by applying the automatic power order reduction.

Fig. 7.3a and 7.3b depict the similar test on the PSCAD digital simulator. According

to Fig. 7.2a to 7.3b the AVS implementation on both simulators provide similar responses. While the oscillating operating point will not be acceptable for a longer time it provides the proof that the system is actually kept around the stability boundary. Setting the power order to a lower value as soon as these swings occur, either manually or automatically, yields a stable system.

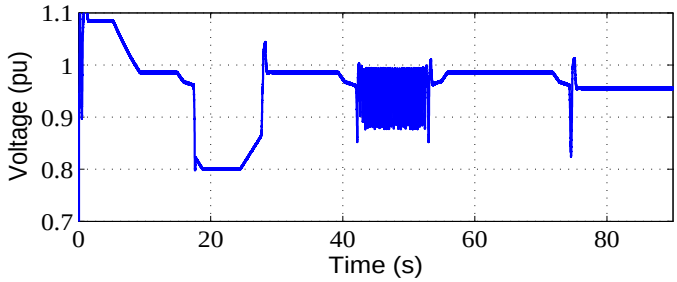

(a) AC Terminal Voltage

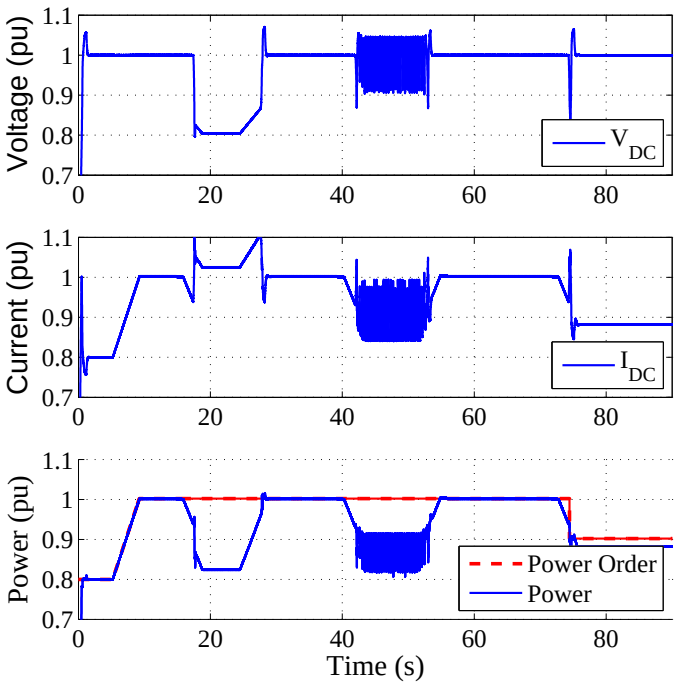

(b) Rectifier Oscillograms

Figure 7.3: Weak AC Grid on Rectifier Side (PSCAD)

7.3 Case 2: Weak AC Grid on Inverter Side

The internal grid voltage shown in Fig. 7.1b is applied at the inverter. The SCR values are 2.5 at both rectifier and inverter sides. In this scenario only VDCOL and AVS with the automatic power reduction are tested. Only the VDCOL is activated during t = 10-20 sec, the commutation failure occurs as shown in Fig. 7.4. In contrast to VDCOL, the operation of AVS, at t = 40-50 sec, results to only a voltage dip and prevents the commutation failure. Similar simulation results were obtained from the PSCAD simulation are not shown here.

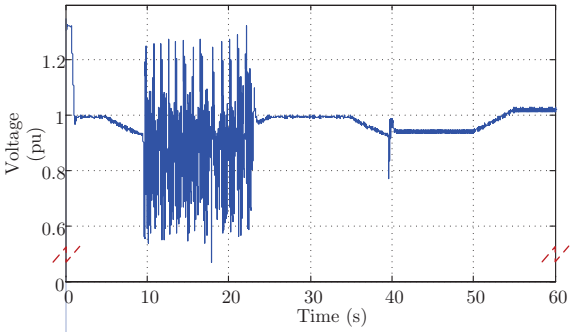

Figure 7.4: AC Terminal Voltage Inverter (SPS)

7.4 Case 3: Performance with embedded induction machine

The performance of AVS is further tested with the induction machine connected at the rectifier. The test system is modified as shown in Fig. 7.9.

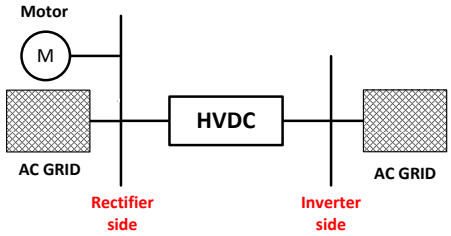

Figure 7.5: CIGRÉ benchmark with induction machine

In this scenario the SCR at the rectifier is set to 1.9 while the SCR at the inverter is set to 3.3. In contrast to the previous scenarios, the DC power is decreased to 0.8 p.u (taking into account the demand of an induction machine). The total power transfer on the AC line before the test is approximately same level as previous scenarios. The AC terminal voltage of the rectifier shows a steep decline with solely VDCOL in operation (t = 10-30 sec), dropping to 0.6 p.u. (Fig. 7.6a).

This low voltage level caused by the reactive power demand of the induction machine is pulling the AC voltage further down. In real operation this would be prevented by tripping

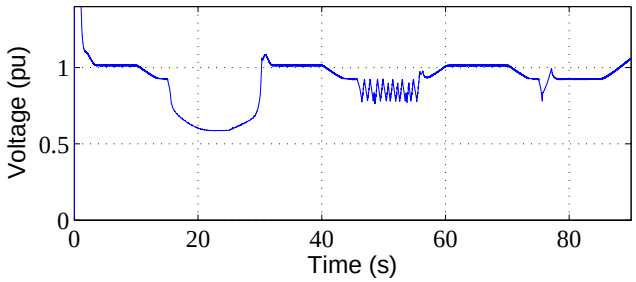

(a) AC Terminal Voltage at the Rectifier

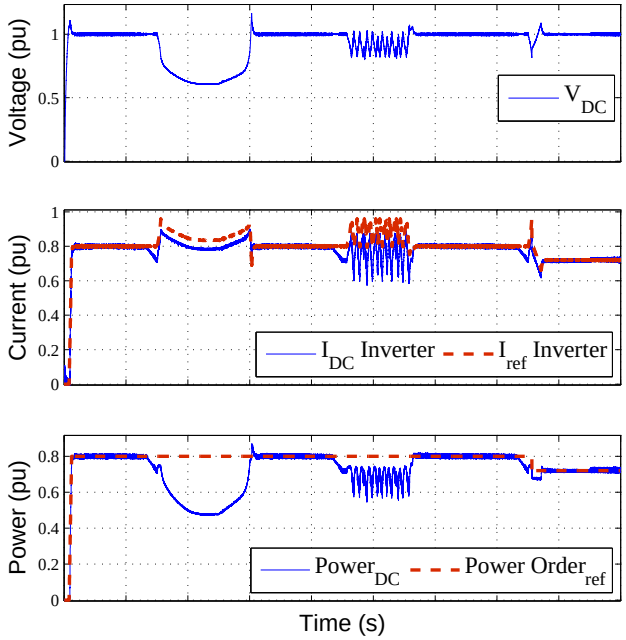

(b) Rectifier Oscillograms

Figure 7.6: Performance with induction machine (SPS)

the machines but it has to be recognized that before this happens the Vac versus Q behavior of both the machines and the converter station determine in combination the slide towards the lower branch of the PV-curve and the converter might have already surpassed the nose of the PV-curve before the machines trip.

Fig. 7.6b shows that DC power decreases despite the DC current increase, this is a clear indication that the MTP-Point is surpassed. As in the previous test, the AVS and the AVS with the Automatic Power Order Reduction (APOR) are applied at t = 40-60 sec and 70-90 sec, respectively, where both of them prevent system collapse.

Fig. 7.7a to 7.7b illustrate the similar response obtained from the PSCAD digital simulator. Fig. 7.8 shows the response of the induction machine. VDCOL cannot stop the AC grid voltage decline. The induction machine is sent over the pull-out slip causing further voltage decrease. AVS prevents this phenomenon either by keeping the operating point revolving around the maximum power point or by applying automatic power order reduction.

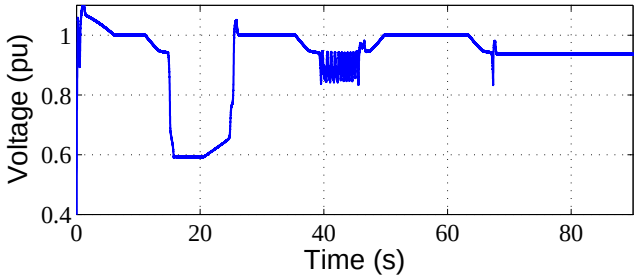

(a) AC Terminal Voltage

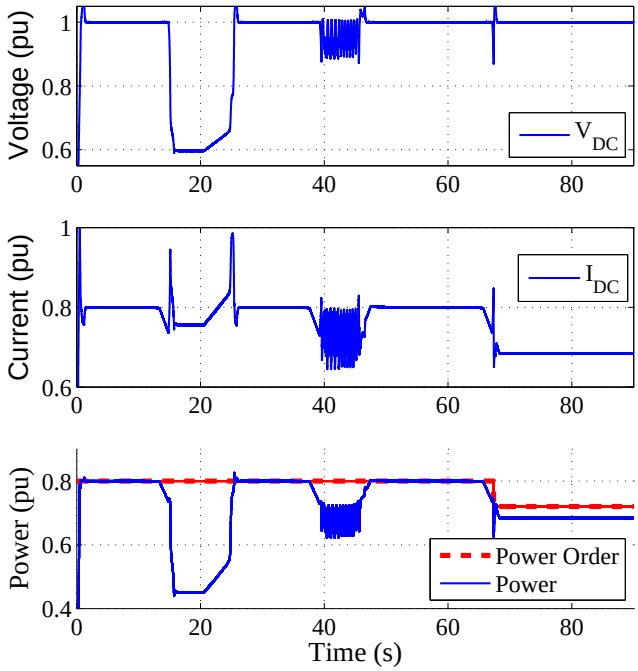

(b) Rectifier Oscillograms

Figure 7.7: Performance with induction machine (PSCAD)

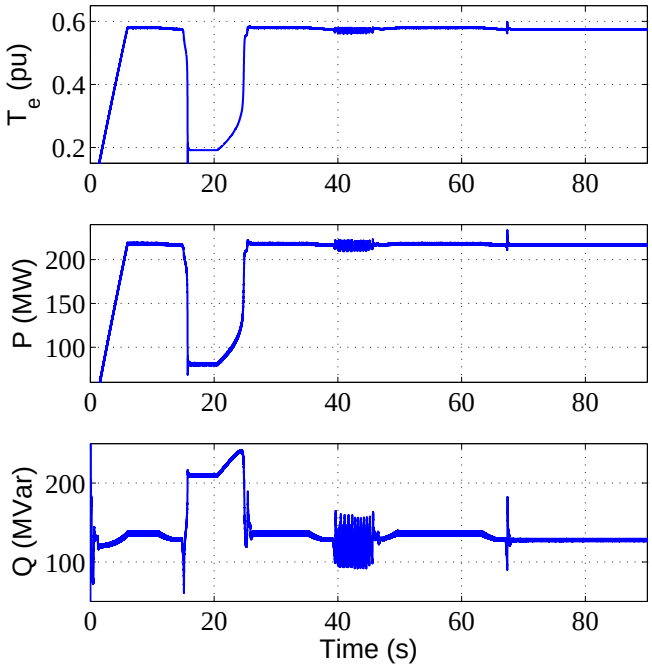

Figure 7.8: PSCAD Oscillograms for the induction machine

7.5 Case 4: Synchronous generator represents as AC grid

This case is similar to **Case 1** described in Section 7.2, however the AC grid (which is modelled as a static voltage source) in Fig. 7.5 is replaced by a synchronous generator. The test system is modified as shown in Fig. 7.9

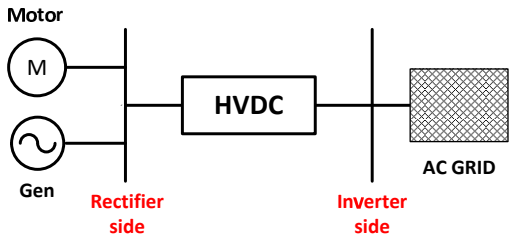

Figure 7.9: Modified version of Fig. 7.5

Fig. 7.10 shows the oscillograms of the HVDC with the operation of the VDCOL and the AVS. The SCR value is decreased from 3.3 to 1.9 at t = = 8 sec, thus this results in a sudden voltage decline. Only the VDCOL is activated during t = 8-15 sec, which makes the voltage drop to 0.75 p.u.

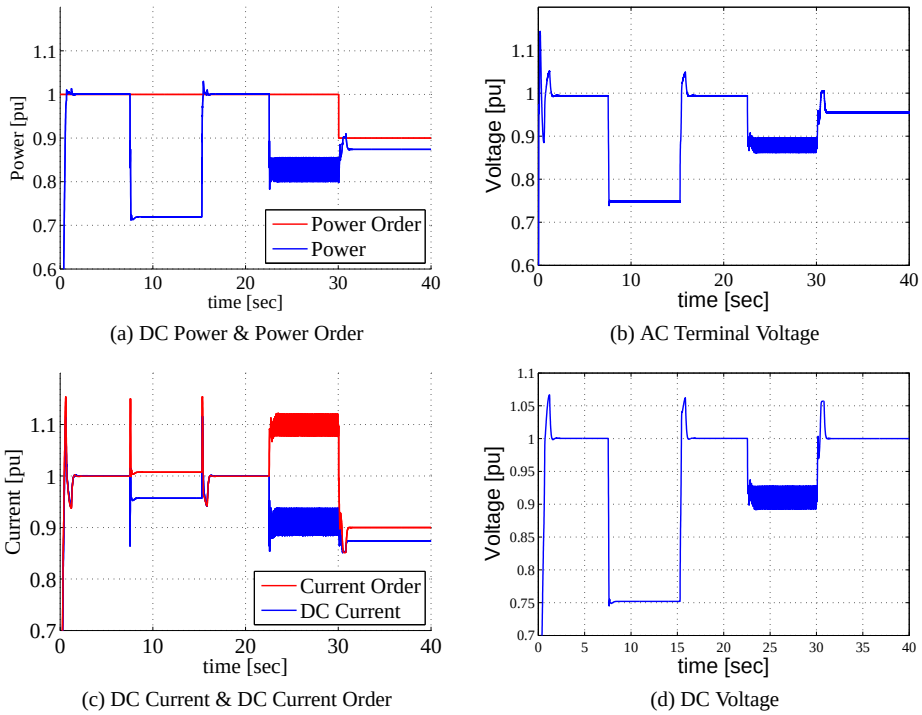

(a) DC Power & Power Order

(b) AC Terminal Voltage

(c) DC Current & DC Current Order

(d) DC Voltage

Figure 7.10: Rectifier Oscillograms - HVDC with the AVS (SPS)

Then the experiment is repeated by increasing and decreasing at t = 16 and 22 sec, respectively. However, in this case, the AVS is activated between t = 22-30 sec, which retains the voltage level above 0.9 p.u. In order to increase the voltage level, the power reduction is activated at t = 30 sec. Consequently, this brings the voltage back to 0.95 p.u. It is demonstrated that for the reduction of the SCR as given above the VDCOL cannot stop the shift over the nose of the PV-curve.

AVS operation makes the operating point revolve around the nose of the PV-curve. This nose determines the maximum transferable power. Of course, this kind of operation with periodically changing P- and Q-values is not desirable for a longer time. Therefore, the power can be reduced manually by the operator or automatically using APOR (which is done manually at 30 sec).

The next experiment is conducted for the HVDC with the operation of the VDCOL

and the APOR. It can be seen in Fig. 7.11, as compared to the VDCOL function, APOR keeps the DC voltage and power on a higher level and the DC current on a lower level. The obtained results are similar to the HVDC with the AVS (see Fig. 7.10) however since the power order is reduced by APOR, thus the operating point is not revolving around the stability boundary but brought to the upper branch of PV-curve.

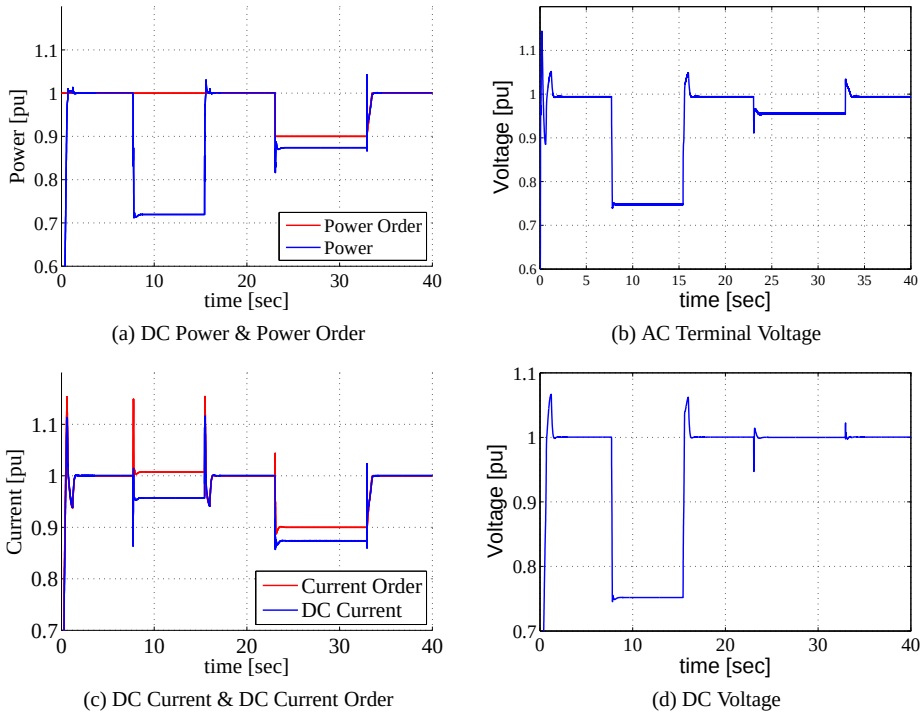

(a) DC Power & Power Order

(b) AC Terminal Voltage

(c) DC Current & DC Current Order

(d) DC Voltage

Figure 7.11: Rectifier Oscillograms - HVDC with the APOR (SPS)

7.6 Case 5: Two-area AC system

In this case, a HVDC with the operation of the VDCOL and the APOR in a two-area AC transmission system is investigated. Fig. 7.12 shows the equivalent of two-area AC system which is connected at the rectifier side of the HVDC system. This two-area AC transmission system consists of a 500 MVA (local) generator and an 380 MVA induction machine in one area while another area is modeled as 1200 MVA (remote) generator. The local generator controls the AC terminal voltage of the rectifier as long as its excitation limit is not reached. The remote generator runs on proportional/integral speed control, the local generator on proportional speed control with an initial power ramp.

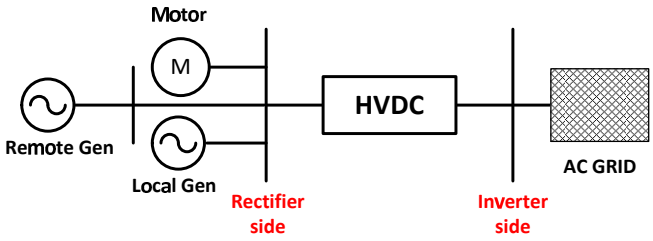

Figure 7.12: Two-area AC system

The comparison study of HVDC with and without APOR is conducted by increasing the power consumption of the induction machine. As seen in Fig. 7.13, the active load of the induction machine is ramped up starting at t = 10 sec. In response to the AC terminal voltage decline the APOR mechanism is becoming active at t = 15 sec, which results in a small oscillation in the induction machine's electrical torque, afterwards this torque is held constant until the active power of the induction machine is ramped down from t = 25 sec on. The same experiment is repeated at t = 40 sec, with only VDCOL being active. It can be seen that VDCOL cannot prevent stalling of the induction machine.

Fig 7.14 shows the oscillograms of the HVDC rectifier side. APOR, becoming active at t = 15 sec, aids HVDC to hold a constant DC voltage by changing the power order which leads to a decrease of DC current. The reactive power consumption of the rectifier is decreased and also the reactive power demand of the AC line between the remote and local bus becomes smaller. This relieves the local generator from reactive power demand thus permitting the local generator to control again the AC terminal voltage.

Moreover, oscillations in generators' torque, transmission angle and power angle cannot be prevented by VDCOL when the nose of the PV-curve is surpassed (see Fig. 7.15 and 7.16 from t = 45 sec on). These oscillations are resulted from DC power swings caused through unstable converter controls on the lower branch of the PV-curve.

Finally, it is not solely the HVDC's converter that pull an AC voltage down but also the induction machine. When the load is increased, the machine's slip also increases to create sufficient torque to turn the load. This implies that the machine's rotor speed is decreased. Thus, an induction machine requires higher voltage to permit faster changes to the current and magnetic field in its coils so that the rotor can have faster rotation. Therefore, it can be concluded that the induction machine might confront the stall phenomena when it runs at certain load level. Fig. 7.17 depicts the torque versus slip of the induction machine. It can be seen that, at t = 10-18 sec, the APOR decreases the machine's slip by reduction power order whereas the slip keeps increasing (until it is stalled) in case of the HVDC operates without the APOR (see Fig. 7.17b).

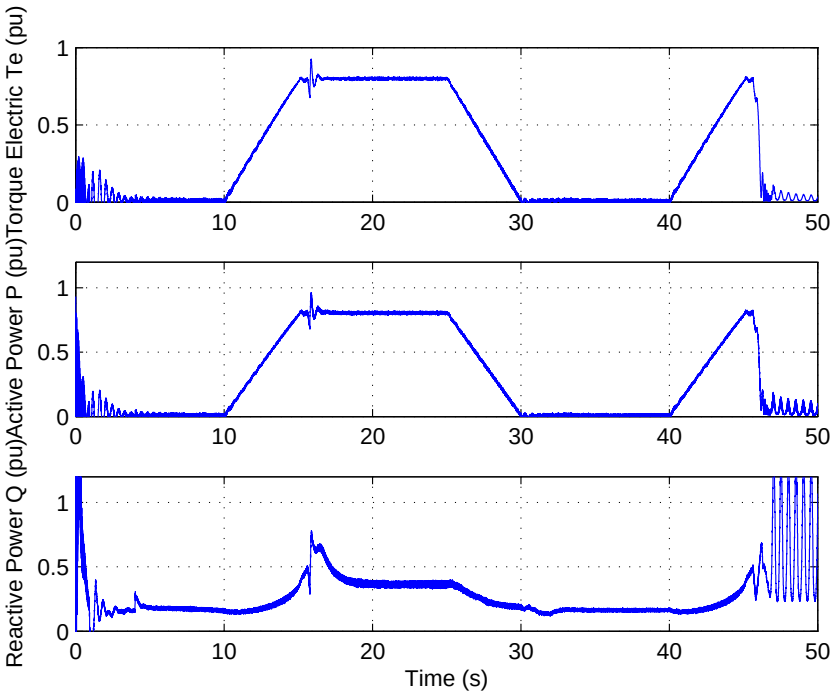

Figure 7.13: Induction machine Oscillograms (SPS)

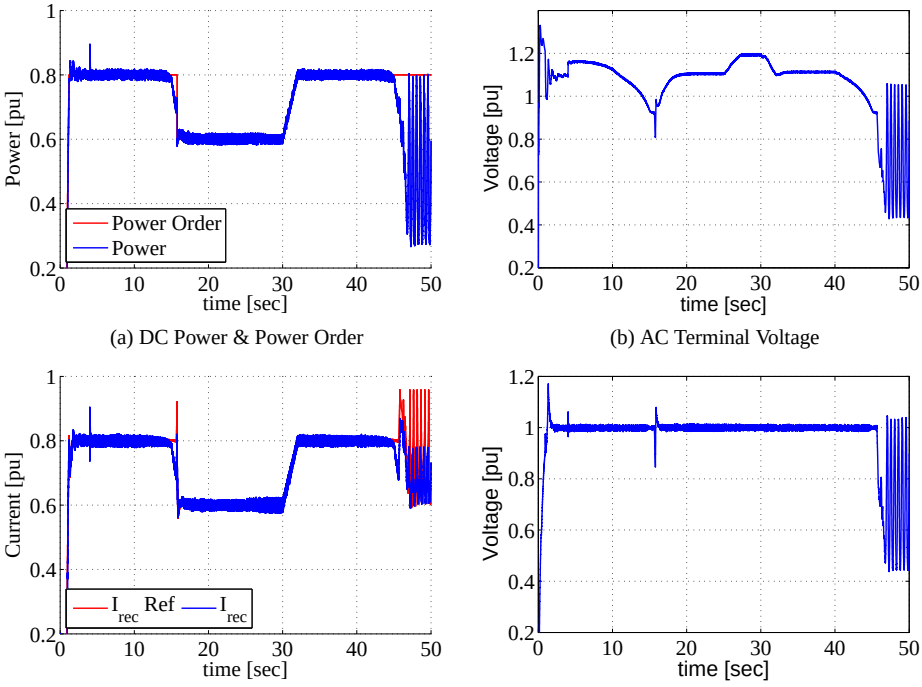

(a) DC Power & Power Order

(b) AC Terminal Voltage

(c) DC Current & DC Current Order

(d) DC Voltage

Figure 7.14: Rectifier Oscillograms - HVDC with the APOR (SPS)

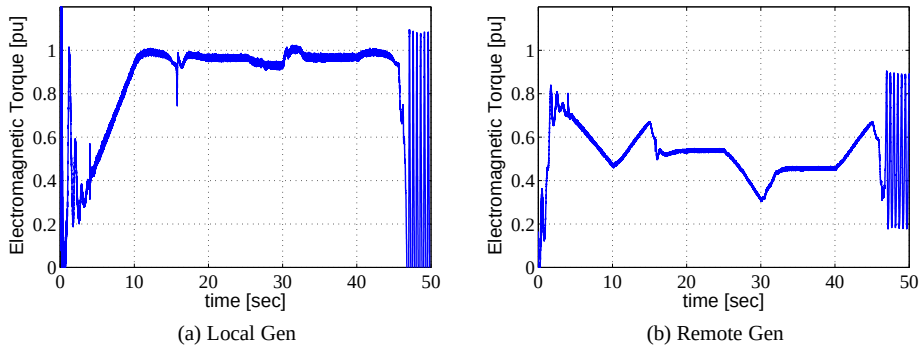

(a) Local Gen

(b) Remote Gen

Figure 7.15: Generators Torque

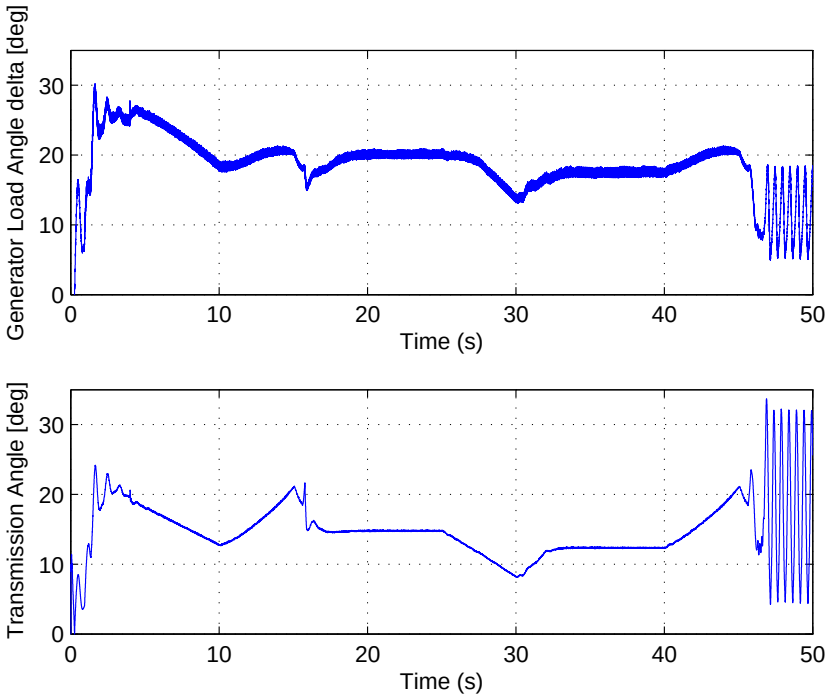

Figure 7.16: Angles Remote Generator (SPS)

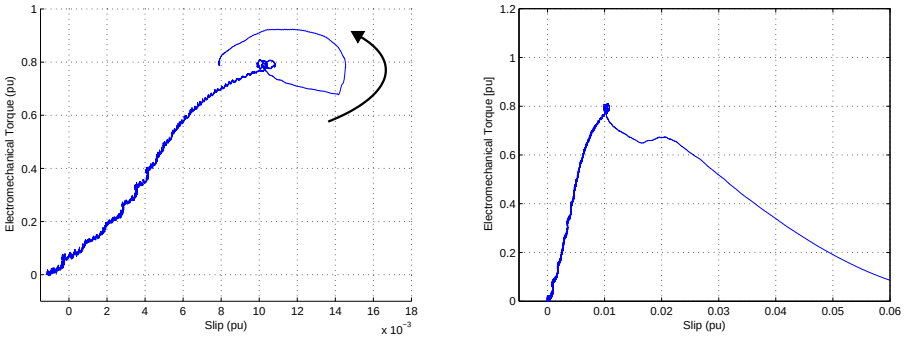

(a) 10-18s (b) 38-48s

Figure 7.17: Torque versus Slip (SPS)

Chapter 8

Closure

8.1 Conclusions

Protective relays have a major role to play in the development of future renewable and sustainable power deliver networks. However, to properly include them in the development of these future systems a broad understanding of their current capabilities, industrial implementation, and future potential is necessary. To bring this understanding under a comprehensive perspective, this thesis has presented an overview of available capabilities from the different relay types of the four most common vendors in the market, including the current availability of PMU functionalities. This includes information about measurements used and performed by the relays, the available capabilities within the relay to perform calculations, PMU functionalities, communication features, and the communication network and mechanisms used by the relays to send out any available information. Moreover, a comparison between different communication protocols which considers various architecture aspects and configuration, are presented — here the objective is to provide general information about each protocol. Protocol selection depends mainly on application specific requirements and functions to be carried out. In addition, the mediums' advantages and disadvantages (shown in Table 2.2) and communication delays (shown in Table 2.5) have to be weighed and chosen based on the required control dynamics and operating economics of the power system. An important fact that makes this a difficult process is that there are contradictory statements concerning the time-duration of different delays involved in delivering phasor data. This is important because protective relays are now providing synchrophasor capabilities and being used in WAMPAC, hence experimental studies are necessary to clarify these contradictions.

This thesis has described an approach for using voltage sensitivities computed from synchrophasor data, and a visualization approach that can be implemented for wide-area voltage stability monitoring to be used in wide-area early warning systems. If implemented for control room use, this monitoring tool can be used by system operators in order to track the state of a power system during normal and severe operating conditions. The idea behind this approach is to ease system operators' tasks by automatically generating early

warning signals before a collapse occurs. To achieve this, sensitivities calculated from PMU data are utilized as stability indicators. Different system conditions are determined by the sensitivities which need to be computed from filtered synchrophasor measurement data. The filtering approach has a large impact in sorting out unwanted electromechanical oscillations, noise and outliers before computing the sensitivities. Both visualization and filtering approaches are validated by using positive-sequence simulations, PMU-data from a real-time hardware-in-the-loop laboratory, and PMU data from a real transmission system (the Norwegian power grid).

The most important lesson to share from this experience is that any PMU data application for WAMPAC, and especially early warning systems, must be thoroughly tested with *actual* PMU measurements to guarantee its robustness. The effects of inherent data characteristics will require algorithms to cater for relevant features which are simply not present from traditional positive-sequence simulations. To this end the use of a real-time hardware-in-the-loop laboratory has been shown to be very advantageous.

To utilize the computed sensitivities for mitigating voltage instabilities, several control schemes are developed for an VSC-HVDC which operates in parallel with an AC transmission line. The controls are implemented additionally to the standard control schemes of VSC-HVDC in order to change its operating set point by using signals from PMUs as input signals to control VSC-HVDC's converters. Simulations of different controls confirm the benefits of using these controls in a VSC-HVDC connected in parallel with an AC line for voltage support and better power flow management, with implicit considerations of the VSC-HVDC's size.

There are however conditions where the determination of sensitivities is not sufficient because their magnitudes do not permit a conclusive interpretation regarding the stability margin. This is, e.g. the case, if stiffness changes in a non-foreseeable manner (i.e.further studies on the threshold values (in Section 4.1) are necessary) or if at a given low stiffness HVDC controls cause discontinuities in sensitivity values. Then no safe indication of an impending voltage collapse via sensitivity calculation and their interpretation is possible. The latter being particularly the case when controllers hit suddenly unpredicted control limits, e.g. firing angle limits at rectifier operation or extinction angle at inverter operation. The present state of art to determine sensitivities on-line and to use them in real-time for grids including Classical HVDC and VSC-HVDC is not yet advanced enough to ensure stability for obscured conditions. Further research is necessary combining sensitivity determination and HVDC system modeling to obtain continuously information on the distance to the stability boundary under inclusion of structural grid and load flow changes as well as internal grid and HVDC control limits.

Besides the voltage stability problem Classical HVDC systems are prone to electromechanical oscillations when embedded in AC systems with multiple-areas. Both voltage and electromechanical stability are presently not reliably ensured via the existing VDCOL function in HVDC. Therefore, a real-time/on-line method was developed, implemented and tested in a CIGRÉ Benchmark model for HVDC controls. The obtained Automatic Voltage Stabilizer and the Automatic Power Order Reducer operate independently or in combination in stand-alone or to back-up non-reliably working stabilizing methods and implementations. The use of real-time simulators for this type of study has not only the ben-

efit of allowing for faster computation times under inclusion of detailed controls, but also for the consideration of complex scenarios with multi-area AC grids and superimposed DC grids, distributed generation from renewable energy resources and bulk power transmission via AC and DC transmission systems.

8.2 Future Work

There are several issues that must be further addressed for implementing a wide-area voltage stability monitoring, including but not limited to: optimal filter design for sensitivity computations, base-lining for determining thresholds for different voltage instability indicators, and the consideration of hybrid AC/DC transmission system operation and related sensitivity computations. The ultimate goal is not only to have real-time visualization of power systems and early warnings, but also to use these sensitivities to real-time govern existing controllers in the power system before the PMU data is centralized in the control room. Therefore, the real-time tuning parameters of the additional controller described in Section 4.4 to cope with different time span of several voltage instability types as mentioned in Chapter 3 must be tested and validated. In other words, the additional controller should automatically adapt to mitigate all range of voltage instabilities that are generated by certain controls such as over and/or under-excitation limiters. In addition, a study on the load shedding proposed in the voltage instability mitigation method described in Section 4.4 when sensitivities reach final alarms can be further addressed. Although the manual load disconnection (as shown in Section 5.1.3) prevent system collapses, however the outcome might not be the most preferable in economic terms. One of the ideas for minimizing the amount of load shedding is to use second-order approximations to approximate the bifurcation point of the system when they are parameterized by loading [125].

The next steps planned for is the application of the automatic voltage stabilizer to the VSC-HVDC transmission system connecting weak AC grids. Already available results show the viability of the AVS for transmission angle stabilization. Transmission angle stability is of significance for our electric power systems being under continued development and construction in the years to come. Phasor Measurements Units used in WAMPAC systems can be used to support stable operation by monitoring of the proposed sensitivities in a WAMPAC application, but as to the results provided in this thesis, they do not provide complete security since threshold values of angles where instability occurs show a high degree of uncertainty. Further work on sensitivities computation considering hybrid AC/DC transmission computation is needed. However, currently the AVS/APOR closes this gap by becoming active if WAMPAC application fails to recognize an impending stability problem.

Regarding the AVS and the APOR, the next step is planned these stability mechanisms on the VSC-HVDC transmission system connecting weak AC grids. The controls of VSC-HVDC are relatively simpler as compared to Classical HVDC controls. However the interconnections with weak AC grids, especially operating in parallel to static generation has not received sufficient attention. Moreover, the proposed stability mechanisms should be tested their performance when HVDCs are operated in connection with renewable energy

systems such as offshore wind power park or photovoltaic plants. In order to obtain realistic results (as seen from simulation point of view), it requires the proper modeling of wind (or solar) generation. Therefore, various generator types, for example Double Fed Induction Generator (DFIG) or Full Converter Units with permanent magnet generator should be modelled sufficiently to present different generation patterns (as for instance shown in [126]). This means that the performance of the AVS/APOR will be evaluated considering the power transmission fluctuation of different turbine types. Moreover, a widespread use of storage devices can be taken into consideration to operate in connection with AVS/APOR. Hence, the stability studies that combine the operation of these two components can be carried out. This includes the determination of maximum transferable power level or evaluation of the mechanical stress relief on wind turbine generators when they are subjected to AC lines disconnection.

Appendix A

A.1 Initial condition settings for the voltage instability scenarios

A.1.1 Short-term voltage instability

For both Case 1 and 2

```
bus 1        :        V= 1.0400 pu    0.00 deg        395.20 kV
        > 1-3                      P=  400.0    Q=  107.1      > 3
        > 1-3b                     P=  400.0    Q=  107.1      > 3
    gener 1                        P=  800.0    Q=  214.1     Vimp= 1.0400

bus 2        :        V= 1.0000 pu   -9.35 deg         20.00 kV
        > 2-3                      P=  300.0    Q=  212.9      > 3
    gener 2                        P=  300.0    Q=  212.9     Vimp= 1.0000

bus 3        :        V= 1.0058 pu  -12.20 deg        382.21 kV
        > 1-3                      P= -400.0    Q=  -19.5      > 1
        > 1-3b                     P= -400.0    Q=  -19.5      > 1
        > 2-3                      P= -300.0    Q= -191.2      > 2
        > 3-4                      P=  600.0    Q=  140.0      > 4
        > 3-5                      P=  500.0    Q=   90.2      > 5

bus 4        :        V= 0.9930 pu  -15.87 deg         14.90 kV
        > 3-4                      P= -600.0    Q= -100.0      > 3
    gener 4                        P= -600.0    Q= -100.0     Vimp= 0.0000

bus 5        :        V= 1.0024 pu  -13.34 deg        380.92 kV
        > 3-5                      P= -500.0    Q=  -80.0      > 3
     load                          P=  500.0    Q=   80.0
```

A.1.2 Long-term voltage instability

Case 1: Load at Bus 5= 1200 MW and 0 MVar

```
bus 1        :        V= 1.0800 pu    0.00 deg        410.40 kV
        > 1-3                    P=  450.0    Q=  117.6      > 3
        > 1-3b                   P=  450.0    Q=  117.6      > 3
    gener 1                      P=  900.0    Q=  235.2     Vimp= 1.0800

bus 2        :        V= 1.0100 pu  -10.01 deg         20.20 kV
        > 2-3                    P=  300.0    Q=   36.9      > 3
    gener 2                      P=  300.0    Q=   36.9     Vimp= 1.0100

bus 3        :        V= 1.0455 pu  -12.72 deg        397.29 kV
        > 1-3                    P= -450.0    Q=  -15.1      > 1
        > 1-3b                   P= -450.0    Q=  -15.1      > 1
        > 2-3                    P= -300.0    Q=  -22.6      > 2
        > 3-4                    P=    0.0    Q=    0.0      > 4
        > 3-5                    P= 1200.0    Q=   52.8      > 5

bus 4        :        V= 1.0053 pu  -12.72 deg         15.08 kV
        > 3-4                    P=    0.0    Q=    0.0      > 3
    gener 4                      P=    0.0    Q=    0.0     Vimp= 0.0000

bus 5        :        V= 1.0445 pu  -15.24 deg        396.90 kV
        > 3-5                    P=-1200.0    Q=    0.0      > 3
     load                        P= 1200.0    Q=    0.0
```

Case 1: Load at Bus 5= 1500 MW and 150 MVar

```
bus 1        :        V= 1.0800 pu    0.00 deg        410.40 kV
        > 1-3                    P=  600.0    Q=  216.7      > 3
        > 1-3b                   P=  600.0    Q=  216.7      > 3
    gener 1                      P= 1200.0    Q=  433.5     Vimp= 1.0800

bus 2        :        V= 1.0100 pu  -14.79 deg         20.20 kV
        > 2-3                    P=  300.0    Q=  212.6      > 3
    gener 2                      P=  300.0    Q=  212.6     Vimp= 1.0100

bus 3        :        V= 1.0166 pu  -17.58 deg        386.30 kV
        > 1-3                    P= -600.0    Q=  -23.9      > 1
        > 1-3b                   P= -600.0    Q=  -23.9      > 1
        > 2-3                    P= -300.0    Q= -191.4      > 2
        > 3-4                    P=    0.0    Q=    0.0      > 4
        > 3-5                    P= 1500.0    Q=  239.3      > 5

bus 4        :        V= 0.9966 pu  -17.58 deg         14.95 kV
        > 3-4                    P=    0.0    Q=    0.0      > 3
    gener 4                      P=    0.0    Q=    0.0     Vimp= 0.0000
```

```
bus 5        :        V= 1.0089 pu  -20.93 deg        383.37 kV
        > 3-5                     P=-1500.0    Q= -150.0      > 3
     load                         P= 1500.0    Q=  150.0
```

Case 2: Higher Power generation

```
bus 1        :        V= 1.0800 pu    0.00 deg        410.40 kV
        > 1-3                     P=  525.0    Q=  186.5      > 3
        > 1-3b                    P=  525.0    Q=  186.5      > 3
    gener 1                       P= 1050.0    Q=  373.0     Vimp= 1.0800

bus 2        :        V= 1.0100 pu  -11.10 deg         20.20 kV
        > 2-3                     P=  450.0    Q=  197.6      > 3
    gener 2                       P=  450.0    Q=  197.6     Vimp= 1.0100

bus 3        :        V= 1.0205 pu  -15.26 deg        387.81 kV
        > 1-3                     P= -525.0    Q=  -39.5      > 1
        > 1-3b                    P= -525.0    Q=  -39.5      > 1
        > 2-3                     P= -450.0    Q= -159.7      > 2
        > 3-4                     P=    0.0    Q=    0.0      > 4
        > 3-5                     P= 1500.0    Q=  238.6      > 5

bus 4        :        V= 1.0005 pu  -15.26 deg         15.01 kV
        > 3-4                     P=    0.0    Q=    0.0      > 3
    gener 4                       P=    0.0    Q=    0.0     Vimp= 0.0000

bus 5        :        V= 1.0129 pu  -18.59 deg        384.90 kV
        > 3-5                     P=-1500.0    Q= -150.0      > 3
     load                         P= 1500.0    Q=  150.0
```

Case 3: Higher Motor load

```
bus 1        :        V= 1.0800 pu    0.00 deg        410.40 kV
        > 1-3                     P=  600.0    Q=  226.7      > 3
        > 1-3b                    P=  600.0    Q=  226.7      > 3
    gener 1                       P= 1200.0    Q=  453.3     Vimp= 1.0800

bus 2        :        V= 1.0000 pu  -14.84 deg         20.00 kV
        > 2-3                     P=  300.0    Q=  177.3      > 3
    gener 2                       P=  300.0    Q=  177.3     Vimp= 1.0000

bus 3        :        V= 1.0117 pu  -17.67 deg        384.45 kV
        > 1-3                     P= -600.0    Q=  -31.8      > 1
        > 1-3b                    P= -600.0    Q=  -31.8      > 1
        > 2-3                     P= -300.0    Q= -157.9      > 2
        > 3-4                     P=  600.0    Q=  139.5      > 4
        > 3-5                     P=  900.0    Q=   81.9      > 5
```

```
bus 4        :       V= 0.9990 pu  -21.30 deg         14.99 kV
        > 3-4                     P= -600.0    Q= -100.0      > 3
    gener 4                       P= -600.0    Q= -100.0     Vimp= 0.0000

bus 5        :       V= 1.0091 pu  -19.69 deg        383.46 kV
        > 3-5                     P= -900.0    Q=  -50.0      > 3
     load                         P=  900.0    Q=   50.0
```

Bibliography

[1] “"Three Gorges dam" website,” Available online: http://www.ctgpc.com/.

[2] “Statnett Grid Development Plan 2008-2025,” Available online: http://www.statnett.no/Documents/Kraftsystemet/Nettutviklingsplaner/.

[3] “Statoil Snøhvit LGN project,” Available online: http://www.statoil.com/en/OurOperations/ExplorationProd/ncs/snoehvit/Pages/default.aspx.

[4] A. Leirbukt, Ø. Breidablik, J. Gjerde, P. Korba, K. Uhlen, and L. Vormedal, “Deployment of a SCADA integrated wide area monitoring system,” in *IEEE/PES Transmission and Distribution Conference and Exposition: Latin America*, 2008.

[5] K. Uhlen, L.Warland, J. Gjerde, O. Breidablik, M. Uusitalo, A. Leirbukt, and P. Korba, “Monitoring amplitude, frequency and damping of power system oscillations with PMU measurements,” in *IEEE Power and Energy Society General Meeting*, 2008.

[6] V. Terzija, G. Valverde, D. Cai, P. Regulski, V. Madani, J. Fitch, S. Skok, M. Begovic, and A. Phadke, “Wide-Area Monitoring, Protection, and Control of Future Electric Power Networks,” *Proceedings of the IEEE*, vol. 99, no. 1, pp. 80 –93, jan. 2011.

[7] R. Best, D. Morrow, D. Laverty, and P. Crossley, “Synchrophasor Broadcast Over Internet Protocol for Distributed Generator Synchronization,” *IEEE Transactions on Power Delivery*, vol. 25, no. 4, pp. 2835 –2841, oct. 2010.

[8] D. Laverty, D. Morrow, R. Best, and P. Crossley, “Internet based phasor measurement system for phase control of synchronous islands,” in *IEEE Power and Energy Society General Meeting*, 2008.

[9] ——, “Differential ROCOF relay for Loss-of-Mains protection of Renewable Generation using phasor measurement over Internet Protocol,” in *Integration of Wide-Scale Renewable Resources Into the Power Delivery System, 2009 CIGRE/IEEE PES Joint Symposium*, july 2009.

[10] A. Ishibashi, M. Imai, K. Omata, S. Sato, T. Takagi, Y. Nakachi, and S. Ogawa, "New type of islanding detection system for distributed generation based on voltage angle difference between utility network and distributed generation site," in *IEE International Conference on Developments in Power System Protection*, vol. 2, april 2004, pp. 542 – 545 Vol.2.

[11] A. Oudalov, "Coordinated control of multiple facts devices in an electric power system," Ph.D. dissertation, EPF Lausanne, 2003.

[12] H. Ma, M. Crow, and B. Chowdhury, "Cascading line outage prevention with multiple upfcs," in *39th North American Power Symposium, 2007. NAPS '07. 39th North American*, December 2007, pp. 273–278.

[13] H. F. Wang, "Interactions and Co-Ordination of Multiple-Function FACTS Controllers," *European Transactions on Electrical Power*, vol. 11, pp. 7 – 15, 2007.

[14] L. Zhang, L. Harnefors, and P. Rey, "Power System Reliability and Transfer Capability Improvement by VSC-HVdc," in *CIGRÉ Regional Meeting*, June 2007.

[15] J. Pan, R. Nuqui, K. Srivastava, P. Holmberg, and Y. Hafner, "AC Grid with Embedded VSC-HVDC for Secure and Efficient Power Delivery," in *IEEE Energy 2030 Conference*, 2008.

[16] B. Rawn, P. Lehn, and M. Maggiore, "A Control Methodology to Mitigate the Grid Impact of Wind Turbines," *IEEE Transactions on Energy Conversion*, vol. 22, pp. 431 – 438, 2007.

[17] V. Akhmatov and P. Eriksen, "A Large Wind Power System in Almost Island Operation – A Danish Case Study," *IEEE Transactions on Power System*, vol. 22, pp. 937 – 943, 2007.

[18] A. Mills, M. Ahlstrom, M. Brower, A. Ellis, R. George, T. Hoff, B. Kroposki, C. Lenox, N. Miller, J. Stein, and Y. Wan, "Understanding Variability and Uncertainty of Photovoltaics for Integration with the Electric Power System," Berkeley National Laboratory, Tech. Rep., 2009.

[19] M. Nijhuis, B. Rawn, and M. Gibescu, "Classification technique to quantify the significance of partly cloudy conditions for reserve requirements due to PV plants," in *IEEE Trondheim PowerTech* , 2011.

[20] A. Abdel-Majeed, R. Viereck, F. Oechsle, M. Braun, and S. Tenbohlen, "Effects of Distributed Generators from Renewable Energy on the Protection System in Distribution Networks," in *46th International Universities' Power Engineering Conference (UPEC)*, 2011.

[21] F. Dai, "Impacts of Distributed Generation on Protection and Autoreclosing of Distribution Networks," in *10th IET International Conference on Developments in Power System Protection (DPSP 2010)*, 2010.

[22] S. Kwon, C. Shin, and W. Jung, "Evaluation of protection coordination with distributed generation in distribution networks," in *10th IET International Conference on Developments in Power System Protection (DPSP 2010)*, 2010.

[23] IEEE Power System Relay Committee, "Impact of distributed resources on distribution relay protection," Tech. Rep., 2004.

[24] A. Phadke and N. Hadjsaid, "Measurements for Adaptive Protection and Control in a Competitive Market," in *the 33rd Annual Hawaii International Conference on System Sciences*, 2000.

[25] J. De La Ree, V. Centeno, J. S. Thorp and A. G. Phadke, "Synchronized Phasor Measurement Applications in Power Systems," *IEEE Transactions on Smart Grid*, vol. 1, pp. 20 – 27, 2010.

[26] A.G. Phadke, J.S. Thorp, and S.H. Horowitz, "Study of Adaptive Transmission System Protection and Control," Oak Ridge National Laboratory, Tech. Rep., 1988.

[27] E. O. Schweitzer, D. E. Whitehead, A. Guzman, Y. Gong, and M. Donolo, "Advanced real-time synchrophasor applications," in *35th Annual Western Protective Relay Conference*, 2008.

[28] E. Schweitzer, D. Whitehead, and G. Zweigle, "Real-world synchrophasor solutions," in *IEEE Power and Energy Society General Meeting*, 2009.

[29] K. Shah, E. Detjen, and A. Phadke, "Feasibility of adaptive distribution protection system using computer overcurrent relaying concept," *IEEE Transactions on Industry Applications*, vol. 24, pp. 792–797, October 1988.

[30] J. Eisman, G. Gomez, and J. Torres, "Applied adaptive protection practices based on data transmission between relays," CIGRÉ Paper 34–207, Tech. Rep., 1995.

[31] R. Leelaruji, L. Vanfretti, *et al*, "Coordination of protection and VSC-HVDC systems for mitigating cascading failures," in *2010 International Conference on Power System Technology (POWERCON)*, oct. 2010.

[32] J. L. Blackburn, *Protective Relaying: Principles and Applications*, M. O. Thurston and W. Middendorf, Eds. Marcel Dekker, Inc., 1987.

[33] General Electric. G-60 Generator Protection Relay. [Online]. Available: http://tinyurl.com/3cezbub

[34] ——. T-60 Transformer Protection Relay. [Online]. Available: http://tinyurl.com/3avwcnk

[35] ——. MIFII Digital Feeder Relay. [Online]. Available: http://tinyurl.com/42vhs7a

[36] ——. D60 Line Distance Protection System. [Online]. Available: http://tinyurl.com/3kvkca3

[37] ——. MIV Voltage/Frequency M Family Relay. [Online]. Available: http://tinyurl.com/3dxrqo6

[38] Schweitzer Engineering Laboratories, Inc. SEL-700G Generator Protection Relay. [Online]. Available: http://tinyurl.com/3q9ceob

[39] ——. SEL-487E Transformer Protection Relay. [Online]. Available: http://tinyurl.com/3wp48tu

[40] ——. SEL-551C Overcurrent/Reclosing Relay. [Online]. Available: http://tinyurl.com/3q75ghp

[41] ——. Legacy SEL-311A Phase and Ground Distance Relay . [Online]. Available: http://tinyurl.com/3snoxe7

[42] ——. SEL-387E Current Differential and Voltage Relay. [Online]. Available: http://tinyurl.com/3oqvv2e

[43] GEC ALSTHOM T&D Protection & Control LIMITED. Micom Alstom P-345 Generator Protection Relay. [Online]. Available: http://tinyurl.com/4x9szsc

[44] ——. Micom Alstom P-645 Transformer Protection & Control. [Online]. Available: http://tinyurl.com/3u5t7fa

[45] ——. Micom Alstom P-145 Feeder Protection Relay. [Online]. Available: http://tinyurl.com/435ry3o

[46] ——. Micom Alstom P-441 Numerical Distance Protection. [Online]. Available: http://tinyurl.com/3qj54ph

[47] ——. Micom Alstom P-923 Voltage and Frequency Relays. [Online]. Available: http://tinyurl.com/3qoaljs

[48] ABB. Generator Protection REG 670. [Online]. Available: http://tinyurl.com/3q9yx6m

[49] ——. Transformer Terminal RET 545. [Online]. Available: http://tinyurl.com/3hq9p4f

[50] ——. Feeder Terminal REF 545. [Online]. Available: http://tinyurl.com/3pwvumk

[51] ——. Line Distance Protection REL 512. [Online]. Available: http://tinyurl.com/44usqjk

[52] ——. Motor Protection REM 545. [Online]. Available: http://tinyurl.com/3potmdf

[53] ——. PCM600, Protection and Control IED Manager, Brochure. [Online]. Available: http://tinyurl.com/3gclk7k

[54] ——. CAP 505 Relay Product Engineering Tools, Relay Product Engineering Tool Quick Start Referen. [Online]. Available: http://tinyurl.com/3f2z5rt

[55] *C37.118.2-2011 - IEEE Standard for Synchrophasor Data Transfer for Power Systems*, IEEE Power and Energy Society Std., 2011.

[56] IEEE Power System Relaying Committee Working Group H9 , "Digital Communications for Relay Protection," Tech. Rep., 2002.

[57] D. G. Fink and H. Beaty, *Standard Handbook for Electrical Engineers (15th Edition)*. McGraw-Hill, 2006.

[58] C. Strauss, *Practical Electrical Network Automation and Communication Systems*. Elsevier, 2003.

[59] J. Beaupre, M. Lehoux, and P.-A. Berger, "Advanced monitoring technologies for substations," in *2000 IEEE ESMO - 2000 IEEE 9th International Conference*, August 2000, pp. 287–292.

[60] E. Schweitzer and D. Whitehead, "Real-Time Power System Control Using Synchrophasors," in *61st Annual Conference for Protective Relay Engineers*, 2008, pp. 78–88.

[61] MODICON, Inc., Industrial Automation Systems. Modicon Modbus Protocol Reference Guide. [Online]. Available: http://tinyurl.com/3do3ya4

[62] RuggedCom Industrial Strength Networks. IEEE 1588 Precision Time Synchronization Solution for Electric Utilities. [Online]. Available: http://tinyurl.com/3sfz3q6

[63] Tyco Electronics UK Limited Crompton Instruments. RS485 & Modbus Protocol Guide. [Online]. Available: http://tinyurl.com/3k2thp3

[64] Triangle MicroWorks, Inc. Modbus and DNP3 Communication Protocols. [Online]. Available: http://tinyurl.com/3u57t5k

[65] GEC ALSTHOM T&D Protection & Control LIMITED. K-Bus Interface Guide. [Online]. Available: http://tinyurl.com/3ul4z4j

[66] ABB Substation Automation. SPA-Bus communication Protocol V2.5 – Technical Description. [Online]. Available: http://tinyurl.com/3tsfgv9

[67] SIEMENS. IEC 61850 V Legacy Protocols. [Online]. Available: http://tinyurl.com/3ks55hl

[68] Kalkitech intelligent energy systems. IEC 61850. [Online]. Available: http://tinyurl.com/3dxgslz

[69] LonMark International. Introduction to LON-Setting the Standards for Open Control Systems. [Online]. Available: http://tinyurl.com/3my8kdx

[70] B. Naduvathuparambil, M. C. Valenti, and A. Feliachi, "Communication Delays in Wide Area Measurement Systems," in *Proceedings of the Thirty-Fourth Southeastern Symposium on System Theory*, March 2002, pp. 118–122.

[71] P. Dutta and P. D. Gupta, "Microprocessor-based UHS relaying for distance protection using advanced generation signal processing," *IEEE Transactions on Power Delivery*, vol. 3, pp. 1121–1128, July 1992.

[72] M. Kim, M. Damborg, J. Huang, and S. Venkata, "Wide-Area Adaptive Protection Using Distributed Control and High-Speed Communications," in *Power Systems Computation Conference (PSCC)*, June 2002.

[73] C. Martinez, M. Parashar, J. Dyer, and J. Coroas, "Phasor Data Requirements for Real Time Wide-Area Monitoring," Consortium for Electric Reliability Technology Solutions – CERTS, Tech. Rep., 2005.

[74] M. Chenine, K. Zhu, and L. Nordstrom, "Survey on priorities and communication requirements for PMU-based applications in the Nordic Region," in *IEEE Bucharest PowerTech*, 2009.

[75] C. D. Vournas, E. G. Potamianakis, C. Moors, and T. V. Cutsem, "An Educational Simulation Tool for Power System Control and Stability," *IEEE Transactions on Power Systems*, vol. 19, no. 1, pp. 48–55, Feb 2004.

[76] A. Murdoch, G. Boukarim, M. D'Antonio, and J. Zeleznik, "Use of the latest 421.5 standards for modeling today's excitation systems," in *IEEE Power Engineering Society General Meeting*, 2005.

[77] Digital Excitation Task Force of the Equipment Working Group, "Computer Models for Representation of Digital-Based Excitation Systems," *IEEE Transactions on Energy Conversion*, vol. 11, pp. 607–615, 1996.

[78] *IEEE Recommended Practice for Excitation System Models for Power System Stability Studies*, IEEE Standard 421.5-2005 Std.

[79] IEEE Committee Report, "Dynamic Models for Steam and Hydro Turbines in Power System Studies," *IEEE Transactions on Power Apparatus and Systems*, vol. PAS-92, pp. 1904–1915, 1973.

[80] IEEE Task Force on Excitation Limiters, "Recommended models for overexcitation limiting devices," *IEEE Transactions on Energy Conversion*, vol. 10, pp. 706–713, 1995.

[81] T. Van Custom and C. Vournas, *Voltage Stability of Electric Power Systems*. Kluwer Academic Publisher, 1998.

[82] *CIGRE Task Force 38-02-10. Modelling of voltage collapse including dynamic phenomena*, CIGRE Publication Std., 1993.

[83] P. Sauer and M. Pai, "A comparison of discrete vs. continuous dynamic models of tap-changing-under-load transformers," in *NSF/ECC Workshop on Bulk power System Voltage Phenomena - III : Voltage Stability, Security and Control*, 1994.

[84] "Digsilent powerfactory version 14." [Online]. Available: http://www.digsilent.de/

[85] R. Leelaruji and L. Vanfretti, "All-in-one test system modelling and simulation for multiple instability scenarios," KTH, Royal Institute of Technology, Internal Report, April 2011.

[86] ——, "Detailed Modelling, Implementation and Simulation of an 'All-in-one' Stability Test System including Power System Protective Devices," *Simulation Modelling Practice and Theory, Elsevier,*, vol. 23, pp. 36–59, 2012.

[87] P. Kundur, J. Paserba, V. Ajjarapu, G. Andersson, A. Bose, C. Canizares, N. Hatziargyriou, D. Hill, A. Stankovic, C. Taylor, T. Van Cutsem, and V. Vittal, "Definition and classification of power system stability IEEE/CIGRE joint task force on stability terms and definitions," *IEEE Transactions on Power Systems*, vol. 19, no. 3, pp. 1387 – 1401, aug. 2004.

[88] C. Taylor, D. Erickson, K. Martin, R. Wilson, and V. Venkatasubramanian, "WACS-Wide-Area Stability and Voltage Control System: R&D and Online Demonstration," *Proceedings of the IEEE*, vol. 93, no. 5, pp. 892 –906, may 2005.

[89] K. Uhlen, L. Vanfretti, M. de Oliveira, A. Leirbukt, V. Aarstrand, and J. O. Gjerde, "Wide-Area Power Oscillation Damper Implementation and Testing in the Norwegian Transmission Network," in *IEEE Power and Energy Society General Meeting*, july 2012.

[90] "eMEGAsim PowerGrid Real-Time Digital Hardware in the Loop Simulator Opal RT," Available online: http://www.opal-rt.com/.

[91] L. Vanfretti1, V. Aarstrand, M. S. Almas, V. Peric and J.. Gjerde, "A Software Development Toolkit for Real-Time Synchrophasor Applications," in *submitted to IEEE PES PowerTech 2013*, 2012.

[92] "Protection Relays by Schweitzer Engineering Laboratories," Available online: http://www.selinc.com/protection/.

[93] "Line Differential Relay RED-670 by ABB," Available online: http://www.abb.com/relion.

[94] "Current and Voltage Amplifiers by Megger," Available online: http://www.megger.com/cae/story/Index.php?ID=527.

[95] "GPS Substation Clock by Arbiter," Available online: http://www.arbiter.com/.

[96] L. Vanfretti *et al*, "SmarTS Lab — A Laboratory for Developing Applications for WAMPAC Systems," in *IEEE Power and Energy Society General Meeting*, july 2012.

[97] K. Vu, M. Begovic, D. Novosel, and M. Saha, "Use of local measurements to estimate voltage-stability margin," *IEEE Transactions on Power Systems*, vol. 14, pp. 1029 – 1035, 1999.

[98] I. Smon and G. Verbic and F. Gubina, "Local Voltage-Stability Index Using Tellegen's Theorem," *IEEE Transactions on Power Systems*, vol. 21, pp. 1267–1275, 2006.

[99] C. D. Vournas and N. G. Sakellaridis, "Tracking Maximum Loadability Conditions in Power Systems," in *2007 iREP Symposium Bulk Power System Dynamics and Control - VII. Revitalizing Operational Reliability*, 2007.

[100] B. Milosevic and M. Begovic, "Voltage-stability protection and control using a wide-area network of phasor measurements," *IEEE Transactions on Power Systems*, vol. 18, pp. 121–127, 2003.

[101] L. Bao, Z. Huang, and W. Xu, "Online Voltage Stability Monitoring Using Var Reserves," *IEEE Transactions on Power Systems*, vol. 18, pp. 1461–1469, 2003.

[102] M. Glavic and T. Van Cutsem, "Investigating state reconstruction from scarce synchronized phasor measurements," in *2011 IEEE Trondheim PowerTech*, 2011.

[103] Venkatasubramanian, V. and Xing Liu and Guoping Liu and Qiang Zhang and Sherwood, M., "Overview of wide-area stability monitoring algorithms in power systems using synchrophasors," in *American Control Conference (ACC), 2011*, 29 2011-july 1 2011, pp. 4172 –4176.

[104] M. Glavic and T. Van Cutsem, "Wide-Area Detection of Voltage Instability From Synchronized Phasor Measurements. Part I: Principle," *IEEE Transactions on Power Systems*, vol. 24, pp. 1408 – 1416, 2009.

[105] T. Van Cutsem, "An approach to corrective control of voltage instability using simulation and sensitivity," *IEEE Transactions on Power Systems*, vol. 2, pp. 616–622, 1995.

[106] M. Begovic and A. G. Phadke, "Control of voltage stability using sensitivity analysis," *IEEE Transactions on Power Systems*, vol. 7, pp. 114–123, 1992.

[107] M. Glavic and T. Van Cutsem,, "Wide-Area Detection of Voltage Instability From Synchronized Phasor Measurements. Part II: Simulation Results," *IEEE Transactions on Power Systems*, vol. 24, pp. 1417 – 1425, 2009.

[108] W. Higgins, "A Comparison of Complementary and Kalman Filtering," *IEEE Transactions on Aeospace and Electronic Systems*, vol. AES-11, pp. 321–325, 1975.

[109] Steven W. Smith, *The Scientist and Engineer's Guide to Digital Signal Processing*. California Technical Pub, 1997.

[110] C. Taylor, "Concepts of undervoltage load shedding for voltage stability," *IEEE Transactions on Power Delivery*, vol. 7, pp. 480 – 488, April 1992.

[111] S. Corsi and G. Taranto, "Voltage instability - the different shapes of the "Nose"," in *Bulk Power System Dynamics and Control - VII. Revitalizing Operational Reliability, (iREP Symposium)*, 2007.

[112] M. Parniani, J. Chow, L. Vanfretti, B. Bhargava, and A. Salazar, "Voltage Stability Analysis of a Multiple-Infeed Load Center Using Phasor Measurement Data," in *2006 IEEE PES Power Systems Conference and Exposition, 2006 (PSCE '06)*, Nov 2006, pp. 1299 –1305.

[113] O. I. Elgerd, *Electric Energy Systems Theory: An Introduction*, 2nd ed. McGraw-Hill Education - Europe, 1998.

[114] W. Kuehn, A. Hammad, G. Güth, P. Neidhart, "Design and Control Strategies of HVDC-Schemes for AC Voltage Control and Stabilization," in *International Conference on DC Power Transmission*, 1984.

[115] C. Du, "VSC-HVDC for Industrail Power Systems," Ph.D. dissertation, Chalmers University of Technology, 2007.

[116] W. Kuehn, "Method and Apparatus for Automatic Network Stabilization in Electric Power Supply Systems using at least one converter," US Patent App. Pub. No.: US 2012/0112713 A1, Pub., May 2012.

[117] M. O. Faruque, Y. Zhang, and V. Dinavah, "Detailed Modeling of CIGRÉ HVDC Benchmark System Using PSCAD/EMTDC and PSB/SIMULINK," *IEEE Transaction on Power Delivery*, vol. 21, pp. 378 – 387, 2006.

[118] W. Kuehn, "Real-time method to prevent voltage collapse and power instability of HVDC systems," in *IEEE PES ISGT Europe*, 2010, pp. 1 – 8.

[119] P.C.S. Krishnaya, R.J. Piwko, T.L. Weaver, M.P. Bahrman, A.E. Hammad, "DC Transmission Terminating at Low Short Circuit Ratio Locations," *IEEE Transactions on Power Delivery*, vol. PWRD-1, 1986.

[120] V. K. Sood, *HVDC and FACTS Controllers Applications of Static Converters in Power Systems*, M. Pai, Ed. Kluwer Academic Publisher, 2004.

[121] R. Bunch and D. Kosterev, "Design and implementation of AC voltage dependent current order limiter at Pacific HVDC Intertie," *IEEE Transactions on Power Delivery*, vol. 15, pp. 293–299, 2000.

[122] W. Kuehn, "Control and Stability of Power Inverters Feeding Renewable Power to Weak AC Grids with No or Low Mechanical Inertia," in *IEEE PES PSCE09*, 2009.

[123] ——, "Method and Apparatus for Automatic Network Stabilization in Electric Power Supply Systems using at least one converter," Tech. Rep. WO/2010/119136, October 2010.

[124] J. Arrillaga, *High Voltage Direct Current Transmission*. Institution of Electrical Engineers, 1998.

[125] I. D. S. Greene and F. L. Alvarado, "Sensitivity of the loading margin to voltage collapse with respect to arbitrary parameters," *IEEE Transactions on Power Systems*, vol. 12, pp. 262–272, 1997.

[126] B. Rawn, M. Gibescu, and W. Kling, "Availability of Kinetic Energy from Wind Turbines: A Static Analysis Method," in *IEEE Power Engineering Society General Meeting*, 2010.